An Analysis on Material Constants Estimation for the Low Characteristic Impedance Piezoceramic Pz37HD using Measurements and FEM Modeling.

by
Philip Trætteberg

Master Thesis in Physics,
Acoustics

Department of Physics and Technology
University of Bergen

January 21, 2022

Abstract

The area of application for piezoceramic transducers are ever expanding, and so is the need for better modeling them. This thesis looks at the possibility of estimating parameters used for such models through FEM simulations and curve-fitting with measurements.

Acknowledgements

I would like to thank my supervisors Per Lunde, Magne Vestrheim and Mathias Sæther for their guidance and encouraging words throughout my masters.

Contents

Chapter 1

Introduction

University of Bergen's (UiB) acoustics department have performed extensive research and experimenting with high acoustic/characteristic impedance piezoceramics such as Vernitron's PZT-5A and Ferroperm's Pz27. The ever advancing use of piezoceramics in acoustic resonance technology poses the need of high precision models and simulations for these transduceconstructions.

FEMP allows one to model complex transducer constructions in both vacuum and fluid. Another, albeit lesser use of FEM, is in estimating the very input parameters used for the modeling. To be precise, the material constants and their associated loss coefficients. Previously this has been done for fine-adjusting the material constants to better fit measurements with great success [7, 19, 16, 3], which raises the question if FEM could be used as an independent method for estimating the material constants by itself. A thorough analysis documenting each material constants impact on the output simulations from FEMP has been done by Fardal [7], which worked as a guideline for the "trial and error"-process Lohne and Knappskog used to fine-adjust the material constants for Pz27 in their master thesis' [19, 16]. The material data set went through a final iteration in Aanes' Ph.D. [3] which now serves as the baseline material data set for Pz27 at UiB.

In this thesis similar analysis' conducted for PZT-5A by Fardal in the past are replicated for Pz37HD. The thought behind it being such an analysis can serve as a similar guide for Pz37HD and other like-behaved materials, as the work Fardal did for PZT-5A was. The possibility for a systematic method for fine-adjusting the material constants have been also been considered.

Chapter 2 introduces the theory behind a piezoelectric resonator in vacuuum, as well as material constant calculations following known standards as IEEE1987. Chapter 3 and 4 addresses the measurement and simulation setup. In chapter 5 results from a simulation analysis is presented and compared with work previously done at UiB.

Chapter 2

Theory

This chapter introduces notations and definitions used in this thesis. Equations for describing a piezoelectric resonator are given in Section 2.2. Material constants calculations are found in Section 2.4.

2.1 Fundamental Theory and Terminology

In order to clearly describe vibrational mode affiliation the following notation have been adopted in this thesis

$$f_i^{\text{MODE}}$$

where

i = s,p	:	where $i = s$ denotes series resonance, and $i = p$ parallel resonance [13].
MODE	:	Mode of vibration, e.g. the first radial mode $R1$, or the second thickness extensional mode $TE1$.

The resonance frequencies are defined as in Sherrit et al [22, 23]:

- maximum of the real part of the admittance over the angular frequency Y/ω for the series resonances f_s.
- maximum of the real part of the impedance times the angular frequency $Z \cdot \omega$ for the parallel resonances f_p.

These definitions differ from the IEEE definitions [13] by either dividing or multiplying with the angular frequency ω to counteract the effects of ω outside the brackets in Equation 2.20 for the admittance Y, and in Equation 2.41 for the impedance $Z(\omega)$. Evaluating the resulting expressions at their maximums are stated as being more mathematically correct [23].

2.2 Linear Theory of Piezoelectricity

This section introduces the linear relations that describes a piezoelectric resonator. The equation of motion for the piezoelectric element with no external forces acting

upon it can be expressed as [13, 17]

$$T_{ij,j} = \rho \ddot{u}_i, \qquad i, j = 1, 2, 3 \tag{2.1}$$

where $T_{ij,j}$ is the spatial derivative in j-direction of the mechanical tension, ρ is the density of the piezoelectric element, and $\ddot{u}_i$ is the twice temporal derivative of the displacement in i-direction. Assuming a time-harmonic solution for the displacement, that is $u_i = u_0 e^{i\omega t}$ where u_0 is some arbitrary displacement amplitude, $\omega = 2\pi f$ the angular frequency, and t time, Equation 2.1 can be rewritten as [13, 17]

$$T_{ij,j} = -\omega^2 \rho u_i \tag{2.2}$$

To describe the electrical effects acting on the piezoelectric element the quasi-electrostatic approximation is usually sufficient, meaning the magnetic effects are negligible in comparison [13]. As a result the curl of the electric field vector $\mathbf{E}$ must fulfill

$$\nabla \times \mathbf{E} = 0 \qquad \rightarrow \qquad \mathbf{E} = -\nabla \phi \tag{2.3}$$

or expressed as in [13]:

$$E_i = -\phi_{,i} \tag{2.4}$$

where $\phi_{,i}$ is the derivative of a scalar electric potential ϕ in i-direction. The i-component of the electric displacement D can be expressed as [13]

$$D_i = \varepsilon_0 E_i + P_i \tag{2.5}$$

where $\varepsilon_0 = 8.854 \cdot 10^{-12} F/m$ is the permittivity in vacuum, and E_i and P_i are the i-components of the electric field, and polarization in the material respectively. From Ampére's modified 2nd Law [18]

$$\nabla \times \mathbf{H} = \frac{\delta \mathbf{D}}{\delta t} + \mathbf{J_f} \tag{2.6}$$

where $\mathbf{H}$ is the magnetic field, and $\mathbf{J_f}$ is the current density of free charges in the element. The continuity equation , applied here it reads the net influx of electric charges must equal the rate for which the free-charge density ρ_f increase in the element [15]:

$$\nabla \cdot \mathbf{J_f} + \frac{\delta \rho_f}{\delta t} = 0 \tag{2.7}$$

Inserting Equation 2.7 into Equation 2.6, and looking at the gradient of it all gives

$$\nabla \cdot \nabla \times \mathbf{H} = 0 \tag{2.8}$$

which implies

$$\nabla \cdot \frac{\delta D}{\delta t} = -\nabla \cdot \mathbf{J} = \frac{\delta \rho_f}{\delta t} \tag{2.9}$$

Integrating both sides over time t gives

$$\nabla \cdot \mathbf{D} = \rho_f = 0 \tag{2.10}$$

since the density of free charges ρ_f in the material is assumed to be small [13, 25]. The following set of constitutional equations describing a piezoelectric body in vacuum can be derived [13]

$$T_p = c_{pq}^E S_q - e_{jp} E_j \tag{2.11}$$
$$D_i = e_{iq} S_q + \varepsilon_{ij}^S E_j \tag{2.12}$$

where compressed notation p, q is used for the mechanical tensors [25]

$$i, j = 1, 2, 3$$
$$p, q = 1, 2, ..., 6$$

and

T_p	:	Mechanical stress $[N/m^2]$
S_q	:	Mechanical strain
E_j	:	Electric field strength $[V/m]$
D_i	:	Electric flux density $[C/m^2]$
c_{pq}^E	:	Elastic stiffness constant at constant electric field $[N/m^2]$
$e_{jp/iq}$	:	Piezoelectric/coupling constant $[C/m^2]$
ε_{ij}^S	:	Dielectric constant at constant mechanical strain $[F/m]$

2.3 Losses in Piezoelectric Materials

In piezoelectric materials 3 types of losses are to be considered: mechanical relaxation, dielectric dissipation and imperfect conversion of piezoelectric energy. Each of these can be included through the use of complex material constants [10, 24]

$$\hat{c}_{pq}^E = c_{pq}^{E'} + i c_{pq}^{E''} = c_{pq}^{E'} \left(1 + i \frac{1}{Q_{pq}^{c^E}} \right) \tag{2.13}$$
$$\hat{e}_{jp} = e_{jp}^{'} + i e_{jp}^{''} = e_{jp}^{'} \left(1 + i \frac{1}{Q_{jp}^{e}} \right) \tag{2.14}$$
$$\hat{\varepsilon}_{ij}^S = \varepsilon_{ij}^{S'} + i \varepsilon_{ij}^{S''} = \varepsilon_{ij}^{S'} \left(1 - i \frac{1}{Q_{ij}^{\varepsilon^S}} \right) \tag{2.15}$$

where $i, j = 1, 2, 3$ and $p, q = 1, 2, ..., 6$. A hat $\hat{}$ denotes a complex valued quantity, a prime $'$ the real component, and double prime $''$ the imaginary component of the quantity. The Quality Factors (Q-factors) are related to the loss tangents as following

$$\tan\delta_{pq}^{c^E} = \frac{1}{Q_{pq}^{c^E}} = \frac{c_{pq}^{E''}}{c_{pq}^{E'}} \tag{2.16}$$

$$\tan\delta_{jp}^{e} = \frac{1}{Q_{jp}^{e}} = \frac{e_{jp}^{''}}{e_{jp}^{'}} \tag{2.17}$$

$$\tan\delta_{ij}^{\varepsilon^S} = \frac{1}{Q_{ij}^{\varepsilon^S}} = \frac{\varepsilon_{ij}^{S''}}{\varepsilon_{ij}^{S'}} \tag{2.18}$$

$$\tag{2.19}$$

where i, j, p, q may take on the same values as before. Holland [10] derived a set of constraints for the imaginary parts of the material constants having basis in that the power dissipation of a passive material must always be positive. This can be used to affirm that the estimated set of material constants are valid in the physical sense.

2.4 Methods for Calculating Real Material Constants

This section contains methods for determining material constants through measurements on thin disc-shaped piezoelectric elements, following the now withdrawn Institute of Electrical and Electronics Engineers' (IEEE) Standard on Piezoelectricity [11].

To determine a full set of material constants with these methods additional elements of different dimensions and polarizations are required [13]. A method for estimating 5 additional material constants, not relying on said additional elements, is described in Section 2.4.4.

In Table 2.2 at the end of this section is an overview over calculable material constants in this section, and which parameters are included in their respective equations.

2.4.1 Radial Mode Model

The admittance Y of an infinitely thin radial resonator can be expressed as [13].

$$Y(\omega) = i\omega\varepsilon_{33}^{T}\frac{\pi a^2}{t}\left[1-k_p^2\right]\left[\frac{\mathfrak{J}(\eta)-1+\frac{\sigma^p+k_p^2}{1-k_p^2}}{\mathfrak{J}(\eta)-1+\sigma^p}\right] \tag{2.20}$$

where Onoe's function $\mathfrak{J}$ is given as [22, 4]

$$\mathfrak{J}(\eta) = \frac{\eta J_0(\eta)}{J_1(\eta)} \tag{2.21}$$

$$\eta = \frac{2\pi f a}{v^p} \tag{2.22}$$

and

J_0: Bessel function of the first kind, zeroth order.
J_1: Bessel function of the first kind, first order.
v^p: Planar sound velocity.

Expressions for the first two series resonances, corresponding to radial modes R1 and R2, can be derived from Equation 2.20 by evaluating Y at $Y \to i\infty$:

$$\Im\left(\eta_1^{\mathrm{R1}}\right) - 1 + \sigma^p = 0, \qquad \eta_1^{\mathrm{R1}} = \frac{2\pi f_s^{\mathrm{R1}} a}{v^p} \tag{2.23}$$

$$\Im\left(\eta_1^{(R2)}\right) - 1 + \sigma^p = 0, \qquad \eta_1^{(R2)} = \frac{2\pi f_s^{(R2)} a}{v^p} \tag{2.24}$$

The planar Poisson's ratio σ^p and the first root of Onoe's equation η_1^{R1} can be approximated by a third- and fourth order polynomial respectively [22]

$$\eta_1^{\mathrm{R1}} = a_0 + a_1 r_s + a_2 r_s^2 + a_3 r_s^3 \tag{2.25}$$

$$\sigma^p = b_0 + b_1 r_s + b_2 r_s^2 + b_3 r_s^3 + b_4 r_s^4 \tag{2.26}$$

$$r_s = \frac{f_s^{(R2)}}{f_s^{\mathrm{R1}}} \tag{2.27}$$

where the a_n- and b_n-coefficients are given in Table 2.1.

n	a_n	b_n
0	11.2924	97.527023
1	−7.63859	−126.91730
2	2.13559	63.400384
3	−0.215782	−14.340444
4		1.2312109

Table 2.1: Coefficients for the polynomial fit of $\eta_1^{(R1)}$ and σ^p estimated through a least squares method [22].

Equations 2.23 and 2.24 can be expressed as the following relation

$$\eta_1^{(R2)} = \eta_1^{\mathrm{R1}} \frac{f_s^{(R2)}}{f_s^{\mathrm{R1}}} \tag{2.28}$$

which removes the need of v^p to calculate η_1^{R2}. With Equation 2.25 and 2.26 the following material constants can be calculated [12, 22]

$$c_{11}^{p} = \frac{\left(2\pi f_s^{(R1)} a\right)^2 \rho}{\left(\eta_1^{(R1)}\right)^2} \tag{2.29}$$

$$s_{11}^{E} = \frac{1}{c_{11}^{p}\left(1-\left(\sigma^{p}\right)^2\right)} \tag{2.30}$$

$$s_{12}^{E} = -\sigma^{p} s_{11}^{E} \tag{2.31}$$

$$\left(k^{p}\right)^2 = \frac{1-\sigma^{p}-\Im\left(\eta_2^{(R1)}\right)}{2} \tag{2.32}$$

where

$$\eta_p^{\mathrm{R1}} = \eta_s^{\mathrm{R1}} \frac{f_p^{\mathrm{R2}}}{f_s^{\mathrm{R1}}} \tag{2.33}$$

$$Y_T = i\omega C_0^T \text{ for } f \to 0 \tag{2.34}$$

where the blocked conductance can be expressed as [25]

$$C_0^T = \frac{B_T}{\omega} \quad \text{for} \quad f \leq 0.01 f_s^{\mathrm{R1}} \tag{2.35}$$

and the Relative dielectric constant at constant mechanical stress can be expressed as [25]

$$\varepsilon_{33}^{T} = \frac{B_T \cdot t}{\omega \varepsilon_0 \pi a^2} \tag{2.36}$$

where t is thickness of the transducer, and $A = \frac{\pi D^2}{4}$ surface area of the transducers sides in contact with the electrodes, and B_T is the susceptance at constant mechanical stress.

This is best determined at frequencies $f \leq 0.01 \times f_s^{\mathrm{R1}}$ given a DT-ratio of higher than 10 [12].

Using the previously determined ε_{33}^{T} from Equation 2.36 the following material constants can be calculated [22, 13, 19]

$$\varepsilon_{33}^{p} = \frac{\varepsilon_{33}^{T}}{1+\frac{2\left(k^{p}\right)^2}{1+\sigma^{p}}} \tag{2.37}$$

$$k_p^2 = 1 - \frac{\varepsilon_{33}^{p}}{\varepsilon_{33}^{T}} \tag{2.38}$$

$$k_{31}^2 = k_p^2 \left(\frac{1-\sigma^{p}}{2}\right) \tag{2.39}$$

$$d_{31} = k_{31}\sqrt{\varepsilon_{33}^{T} s_{11}^{E}} = k_p \sqrt{\frac{1-\sigma^{p}}{2} \varepsilon_{33}^{T} s_{11}^{E}} \tag{2.40}$$

2.4.2 Thickness Mode Model

The impedance Z of a piezoelectric thickness resonator is given by [13]

$$Z(\omega) = \frac{1}{i\omega C_0^S}\left[1 - k_t^2 \frac{\tan(x)}{x}\right] \tag{2.41}$$

where

$$x = \frac{\omega t}{2v^D} = \frac{\pi f t}{v^D}$$

and

$C_0^S = \frac{\varepsilon_{33}^S \pi a^2}{t}$	: Capacitance at constant mechanical strain S.
k_t	: Thickness coupling factor.
v^D	: Sound velocity in thickness direction

An expression for v^D can be derived by evaluating Equation 2.41 at its parallel resonances, which corresponds to Z's maxima [13]. This is the case when $tan(x) =\rightarrow \infty$ which, for the first order resonance, is

$$x_p^{\mathrm{TE1}} = \frac{\pi t f_p^{\mathrm{TE1}}}{v^D} = \frac{\pi}{2} \tag{2.42}$$

$$v^D = 2t f_p^{\mathrm{TE1}} \tag{2.43}$$

An expression for k_t can be derived by evaluating Equation 2.41 at its series resonance, which corresponds to $Z \rightarrow 0$ [13]. For the first order resonance this is the case when

$$1 - k_t^2 \frac{\tan(x_1^{\mathrm{TE1}})}{x_1^{\mathrm{TE1}}} = 0, \quad \text{or}$$

$$k_t^2 = \frac{x_1^{\mathrm{TE1}}}{\tan(x_1^{\mathrm{TE1}})} \tag{2.44}$$

where

$$x_1^{\mathrm{TE1}} = \frac{\pi t}{v^D} f_s^{\mathrm{TE1}} \tag{2.45}$$

Substituting Equation 2.43 into 2.44 the coupling factor k_t can be rewritten as [13, 19]

$$k_t^2 = \frac{\pi f_s^{\mathrm{TE1}}}{2 f_p^{\mathrm{TE1}}} \tan\left(\frac{\pi\left(f_p^{\mathrm{TE1}} - f_s^{\mathrm{TE1}}\right)}{2 f_p^{\mathrm{TE1}}}\right) \tag{2.46}$$

which can be used to find the elastic stiffness constant c_{33}^E [13]

$$c_{33}^E = 4\rho\left(1 - k_t^2\right)\left(f_p^{\mathrm{TE1}} t\right)^2 \tag{2.47}$$

2.4.3 Combination of Constants from the Radial- and Thickness Models

Using both material constants from Section 2.4.1 and 2.4.2 additional material constants can be calculated [25, 19].

$$c_{33}^{D} = c_{33}^{E}\left(1 - k_t^2\right)^{-1} \tag{2.48}$$
$$\varepsilon_{33}^{S} = \varepsilon_{33}^{T}\left(1 - k_t^2\right)\left(1 - k_p^2\right) \tag{2.49}$$
$$e_{33} = k_t\sqrt{\varepsilon_{33}^{S} c_{33}^{D}} \tag{2.50}$$

To determine the rest measurements on elements of other dimensions and poling than a disc are necessary [13, 4]. A bar excited and polarized in the length direction, and a bar polarized in the length direction, but with the electrodes on two opposite sides.

2.4.4 Lohne's Method

Lohne [19] describes a method for which the material constants c_{11}^{E}, c_{12}^{E} and c_{13}^{E} can be calculated given an already known e_{31}, as well as previous constants calculated in Sections 2.4.1 - 2.4.3.

Firstly the two elastic compliance factors s_{13}^{E} and s_{33}^{E} are estimated [14, 20]

$$s_{13}^{E} = \frac{d_{31} - e_{31}\left(s_{11}^{E} + s_{12}^{E}\right)}{e_{33}} \tag{2.51}$$
$$s_{33}^{E} = \frac{\varepsilon_{33}^{T} - \varepsilon_{33}^{S} - 2e_{31}^{2}\left(s_{11}^{E} + s_{12}^{E}\right) - 4e_{31}e_{33}s_{13}^{E}}{e_{33}^{2}} \tag{2.52}$$

Which can be further used to express the elastic stiffness constants c_{11}^{E}, c_{12}^{E} and c_{13}^{E}:

$$c_{11}^{E} = \frac{s_{11}^{E}s_{33}^{E} - \left(s_{13}^{E}\right)^2}{\left(s_{11}^{E} - s_{12}^{E}\right)\left[s_{33}^{E}\left(s_{11}^{E} + s_{12}^{E}\right) - 2\left(s_{13}^{E}\right)^2\right]} \tag{2.53}$$
$$c_{12}^{E} = \frac{-s_{12}^{E}s_{33}^{E} + \left(s_{13}^{E}\right)^2}{\left(s_{11}^{E} - s_{12}^{E}\right)\left[s_{33}^{E}\left(s_{11}^{E} + s_{12}^{E}\right) - 2\left(s_{13}^{E}\right)^2\right]} \tag{2.54}$$
$$c_{13}^{E} = \frac{-s_{13}^{E}}{s_{33}^{E}\left(s_{11}^{E} + s_{12}^{E}\right) - 2\left(s_{13}^{E}\right)^2} \tag{2.55}$$

Material Constant	Measurables	Primary Formula	Secondary Formulas
c_{33}^D : elastic stiffness constants at constants electric displacement		2.48	2.47, 2.46
c_{11}^E : elastic stiffness constants at constant electric field		2.53	2.30, 2.52, 2.51, 2.31
c_{12}^E : elastic stiffness constants at constant electric field		2.54	2.30, 2.52, 2.51, 2.31
c_{13}^E : elastic stiffness constants at constant electric field		2.55	2.30, 2.52, 2.51, 2.31
c_{33}^E : elastic stiffness constants at constant electric field	$t, \rho, f_p^{\mathrm{TE1}}$	2.47	2.46
c_{11}^p : planar elastic stiffness constant	$f_s^{\mathrm{R1}}, a, \rho,$	2.29	2.25
d_{31} : piezoelectric strain constant		2.40	2.39, 2.36, 2.30
e_{33} : piezoelectric constant		2.50	2.46, 2.49, 2.48
ε_{33}^p : relative planar dielectric constants		2.37	2.36, 2.32, 2.26
ε_{33}^S : relative dielectric constants at constant mechanical strain		2.49	2.36, 2.46, 2.38
ε_{33}^T : relative dielectric constants at constant mechanical stress	t, a	2.36	2.35
η_s^{R1} : root of Onoe's equation		2.25	2.27
η_p^{R1} : root of Onoe's equation	$f_p^{\mathrm{R1}}, f_s^{\mathrm{R1}}$	2.33	2.25
k_{31} : transverse coupling coefficient		2.39	2.38, 2.26
k^p : planar radial coupling coefficient		2.32	2.26, 2.21, 2.33
k_p : planar coupling coefficient		2.38	2.36, 2.37
k_t : thickness coupling coefficient	$f_s^{\mathrm{TE1}}, f_p^{\mathrm{TE1}}$	2.46	
r_s : ratio of series resonances	$f_s^{\mathrm{R2}}, f_s^{\mathrm{R1}}$	2.27	
σ^p : planar Poisson's Ratio		2.26	2.27
s_{11}^E : elastic compliance constant at constants electric field		2.30	2.29, 2.26
s_{12}^E : elastic compliance constant at constants electric field		2.31	2.30, 2.26
s_{13}^E : elastic compliance constant at constant electric field		2.51	2.40, 2.30, 2.31, 2.50
s_{33}^E : elastic compliance constant at constant electric field		2.52	2.36, 2.49, 2.30, 2.31, 2.51, 2.50
v^D : sound velocity in thickness direction	t, f_p^{TE1}	2.43	

Table 2.2: Summary of the calculated material constants and quantities used in their calculations in Section 2.4. Secondary formulas are material constants appearing in the current primary formula. Constants necessary for FEMP: $c_{11}^E, c_{12}^E, c_{13}^E, c_{33}^E, c_{44}^E, e_{31}, e_{33}, e_{15}, \varepsilon_{11}^S$, and ε_{33}^S. Constants that are calculable from measurements on a disc: $\sigma^p, c_{11}^p, s_{11}^E.s_{12}^E, d_{31}, \varepsilon_{33}^T, \varepsilon_{33}^p, k^p, k_p, k_{31}, c_{33}^E, v^D, k_t, e_{33}, \varepsilon_{33}^S$ and c_{33}^D. Constants **not** calculable from measurements on a disc [13]: $c_{11}^E, c_{12}^E, c_{13}^E, c_{44}^E, e_{31}, \varepsilon_{11}^S, s_{13}^E$ and s_{33}^E. All of the listed material quantities are necessary to calculate the FEMP constants using methods described in Section 2.4.

2.5 Methods for Calculating Complex Material Constants

Losses in the piezoelectric medium may be accounted for by using complex material constants. Section 2.5.1 describes one such method by utilizing complex valued resonance frequencies.

Another method for estimating complex material constants has been considered [6, 5], but not tested due to the model performing seemingly worse than Sherrit's Model at modes with multiple pronounced resonance peaks when tested for a bar-shaped element [4].

2.5.1 Sherrit's Method

The methods described in Section 2.4 for calculating material constants do not account for the imaginary parts of said constants. Sherrit et al. [22, 23] describes a method for estimating these imaginary parts through complex frequencies calculated at series- and parallel resonances:

$$\hat{f}_s^{\mathrm{R1}} = f_s^{\mathrm{R1}} \left[1 - i \frac{f_{1,\text{-3dB}}^{\mathrm{R1}} - f_{1,\text{+3dB}}^{\mathrm{R1}}}{f_s^{\mathrm{R1}}} \right]^{-\frac{1}{2}}$$

$$\hat{f}_s^{\mathrm{R2}} = f_s^{\mathrm{R2}} \left[1 - i \frac{f_{1,\text{-3dB}}^{\mathrm{R2}} - f_{1,\text{+3dB}}^{\mathrm{R2}}}{f_s^{\mathrm{R2}}} \right]^{-\frac{1}{2}}$$

$$\hat{f}_p^{\mathrm{R1}} = f_p^{\mathrm{R1}} \left[1 - i \frac{f_{2,\text{-3dB}}^{\mathrm{R1}} - f_{2,\text{+3dB}}^{\mathrm{R1}}}{f_p^{\mathrm{R1}}} \right]^{-\frac{1}{2}}$$

where $\hat{}$ indicates a complex valued quantity. The frequencies are defined accordingly [22]

f_s^{R1} : real frequency at R1 defined as the maximum for the real part of $Y(\omega)/\omega$
f_s^{R2} : real frequency at R2 defined as the maximum for the real part of $Y(\omega)/\omega$
f_p^{R1} : real frequency at R1 defined as the maximum for the real part of $\omega Z(\omega)$
$f_{i,\pm\text{3dB}}^{\mathrm{MODE}}$: half band frequency for either series- or parallel resonance $i = s, p$ respectively.

The complex frequencies can be inserted directly into Equations 2.23 - 2.28, 2.27 - 2.29, 2.35, and **??** - 2.47. Meaning the same expressions for calculating real material constants can be used for calculating the complex material constants, with the exception that complex frequencies are used.

Complex frequencies associated with the TE1-mode can be defined in a similar fashion [23]:

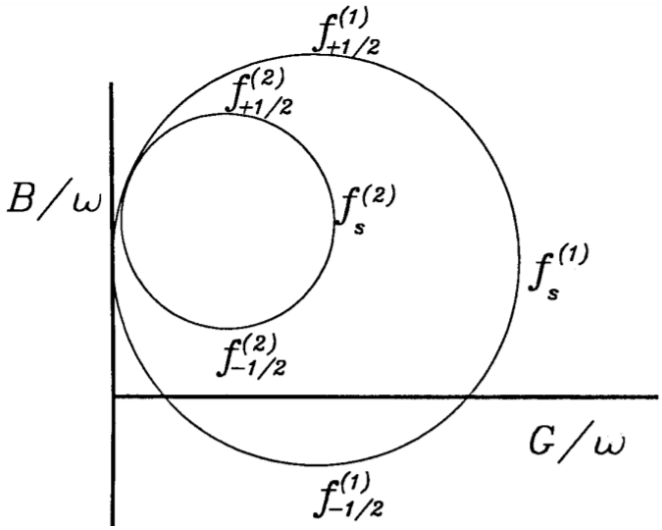

Figure 2.1: Modified locus diagram for the series resonances from [22]. Here $f^{(1)}_{+1/2}$ corresponds to $f^{\mathrm{R1}}_{s,+3\mathrm{dB}}$.

$$\hat{f}_s^{(TE1)} = f_s^{(TE1)} \left[1 - i \frac{f_{1,\text{-3dB}}^{(TE1)} - f_{1,+3\text{dB}}^{(TE1)}}{f_s^{(TE1)}} \right]^{-\frac{1}{2}} \tag{2.56}$$

$$\hat{f}_p^{(TE1)} = f_p^{(TE1)} \left[1 - i \frac{f_{2,\text{-3dB}}^{(TE1)} - f_{2,+3\text{dB}}^{(TE1)}}{f_p^{(TE1)}} \right]^{-\frac{1}{2}} \tag{2.57}$$

$$\tag{2.58}$$

where

$f_s^{(TE1)}$: real frequency at TE1 defined as the maximum for the real part of $Y(\omega)/\omega$
$f_p^{(TE1)}$: real frequency at TE1 defined as the maximum for the real part of $\omega Z(\omega)$

The complex dielectric constant $\hat{\varepsilon}^S_{33}$ can be written as [23]

$$\hat{\varepsilon}^S_{33} = \frac{t}{i\omega\pi a^2 Z(\omega)} \left[1 - \hat{k}_t^2 \frac{\tan\left(\omega/4\hat{f}_p^{(TE1)}\right)}{\omega/4\hat{f}_p^{(TE1)}} \right] \tag{2.59}$$

where $\omega = 2\pi f$ is a arbitrary frequency, however [23] advises choosing a frequency between the first and second thickness extension resonance to avoid errors being magnified near resonances.

[19] however determines $\hat{\varepsilon}^S_{33}$ from the dielectric loss factor $Q_e = B^T/G^T$ calculated at frequencies $f \leq 0.01 \times f_s^{(R1)}$.

$$\hat{\varepsilon}_{33}^{T} = \varepsilon_{33}^{T}\left(1 - i\frac{1}{Q_e}\right) \tag{2.60}$$

which can be inserted into Equation 2.49 for a complex-valued ε_{33}^{S}. This will further be used to give rise to complex material constants $\hat{e}_{33}, \hat{s}_{13}^{E}, \hat{s}_{33}^{E}, \hat{c}_{11}^{E}, \hat{c}_{12}^{E}$ and $\hat{c}_{13}^{E}$ in Equations 2.50 - 2.55.

Chapter 3

Measurement Setup and Methods

This section discusses the measurables mentioned in Table 2.2, and the instruments and methods used for obtaining them. The elements considered are piezoceramics manufactured by Ferroperm of type Pz37 High Density (Pz37HD). This material is described as having very low acoustic impedance and at the same time high coupling coefficient and coupling [8].

A total of 10 elements were measured upon:

- 5 piezoceramics specified to have diameter $D = 20mm$ and thickness $t = 1mm$.
- 5 piezoceramics specified to have diameter $D = 30mm$ and thickness $t = 1.5mm$.

To accurately determine f_s^{R2} from measurements IEEE recommends a diameter-thickness (D/t) ratio > 20 [13]. Both groups of elements were requested to have a D/t ratio close to 20, which were also chosen for comparison purposes with another piezoceramic PZT-5A in work done by Fardal [7]. This is discussed in Section 5.3.

3.1 Dimensional measurements

3.1.1 Equipment

Table 3.1: Table of equipment used to measure parameters used in material constant calculations. All equipment are procured in-house.

Name	Manufacturer	Model	Serial No.	Precision	Range
Digimatic Micrometer	Mitutuyo	MDH-25M	15229628	$\pm 0.5\mu m$	$0 - 25mm$
Electronic Calipers	Sylvac	S_Cal Pro	34264	$\pm 0.02mm$	$0 - 40mm$
Electronic Scale	Ohaus	SC2020 SCOUT		$\pm 0.01g$	$0 - 200g$

3.1.2 Measurement Methods

The average thickness t were estimated by measuring the elements 10 times each at randomly selected areas on the discs, then calculating the mean and standard deviation for each elements results. The micrometer were used for all elements.

The average diameter $D = 2a$ were estimated by measuring the elements 10 times each at randomly selected areas on the discs, then calculating the mean and standard deviation for each elements results. The micrometer were used for elements No. 1 - 5, and the calipers for elements No. 6 - 10.

The average mass m were estimated by weighing the elements 10 times each, then calculating the mean and standard deviation for each elements results. The electronic scale were used for all elements.

The electrodes contributions to the mass and volume have been subtracted when calculating the average density ρ

$$\rho = \frac{m - 2m_e}{V - 2V_e} = \frac{m - 2t_e\rho_e\pi a^2}{\pi a^2(t - 2t_e)} \tag{3.1}$$

where $m_e = \rho_e t_e \pi a^2$ is the electrode mass, $V_e = t_e \pi a^2$ the electrode volume, and $t_e \sim 10\mu m$ the electrode thickness which is considered to be silver with density $\rho_e = 10500 kg/m^3$ [9]. This gave approximately a 1% decrease in the initial density, meaning a better match with Ferroperms listed density. This is also within Ferroperms $\pm 2,5\%$ tolerance interval for the density [9]. The effects this has on the FEMP simulations are discussed in Section **??**, which were also considered before going through with it. Table **??** shows the mean of the measurables, where the electrode thickness t_e have been subtracted from the measured thickness.

Table 3.2: Mean of measurements of thickness t, diameter d, mass m of the piezoelectric elements. Electrode thickness $t_e = 0,01mm$ are subtracted from the total thickness. Exact measurements are given in Appendix reference. The calculated density ρ is also included, as well as uncertainties for each quantity. See Section 3.1 for details.

	Elem. No.	**1**	**2**	**3**	**4**	**5**	**6**	**7**	**8**	**9**	**10**	**U±**
t	**[mm]**	0.879	0.883	0.884	0.883	0.884	1.440	1.437	1.439	1.437	1.444	0.003
d	**[mm]**	19.06	19.06	19.04	19.05	19.06	29.99	29.99	29.97	29.98	29.98	0.01
m	**[g]**	1.68	1.69	1.69	1.69	1.69	6.76	6.78	6.76	6.78	6.79	0.01
ρ	$[\mathbf{kg/m^3}] \cdot 10^3$	6.45	6.49	6.48	6.46	6.47	6.50	6.53	6.51	6.53	6.51	

Uncertainties listed in Table 3.2 are the standard deviation of the measurement sets, except the mass. The instruments listed measurement errors were all found to be lower than the standard deviation, with the exception of the electronic scale.

3.2 Electrical measurements

An impedance analyzer is used to measure the real and imaginary component of the admittance Y for the 10 piezoceramic discs. The measurements are not only used for deriving important measurables like resonance frequencies used in material constants calculations, but also for comparing with simulations in Chapter 5. Procedures for ensuring accurate and consistent measurements are briefly explained in Section 3.2.2.

3.2.1 Equipment

Figure 3.1 shows the impedance analyzer used to measure the piezoceramics, and Table 3.3 contains the specifications of the analyzer.

Table 3.3: Table of equipment for electrical measurements.

Name	Manufacturer	Model	Serial No.	Precision	Range
Impedance Analyzer	Hewlett Packard	4192 A LF	2150J01344		5Hz - 13kHz

Figure 3.1: Impedance analyzer used for measurements on piezoceramic discs in air. The polystyrene foam brick is used

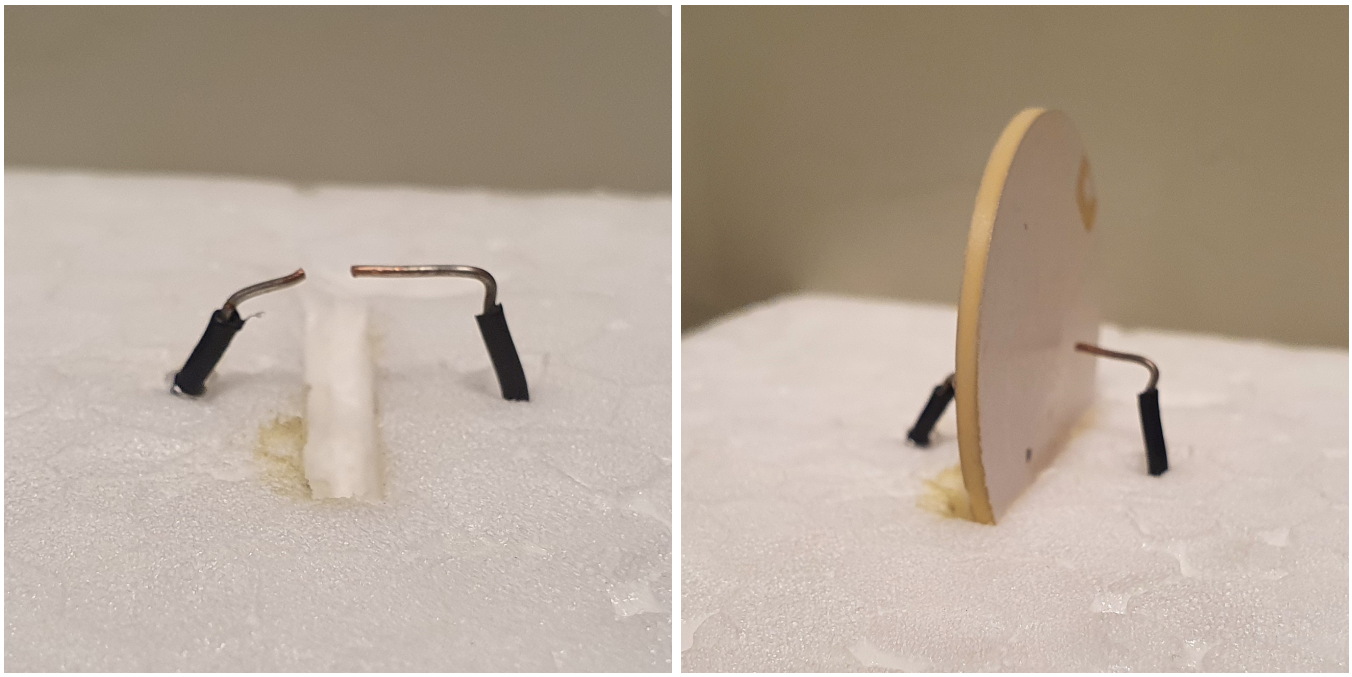

(a) **(b)**

Figure 3.2: a) Setup for the piezoceramic elements when conducting electrical measurements. b) Example of how a piezoceramic disc is placed when conducting electrical measurements. The wires are connected to the electrodes by direct contact alone.

3.2.2 Methods

Before every measurement the analyzer has been calibrated by the built in features which sets the measured admittance at an open circuit to 0, and the measured admittance with a closed circuit to infinity. The calibration is performed while a 1MHz oscillating $0.3V$ voltage is sent through the circuit. A frequency sweep is done by using a MATLAB-script IMPANAL_MATHIAS.M written by co-supervisor Mathias Sæther, and the measured conductance G and susceptance B are stored. These measured values are further used to acquire the admittance $Y = G + iB$, the impedance $Z = 1/Y$, and the resistance R and reactance X which are aquired by taking the real and imaginary part of Z separately.

During measurements the element is connected by two wires in direct contact with the electrodes, standing upright in a track carved out in a polystyrene foam brick as illustrated in Figure 3.2. Uncertainties originating from loss of contact with the electrodes, or improper calibration, have been tested for by performing 10 repeated measurements on the same element and comparing the results. No discrepancies were observed. This was done for all elements before conducting the measurements used for comparisons in Chapter 5.

A frequency resolution $\Delta f = 1$Hz is used when measuring the R1 mode and regions below, while $\Delta f = 50$Hz for the regions above. Similar resolutions were used by Fardal with $\Delta f = 2$Hz below 150kHz, and 50Hz above [7].

Chapter 4

Simulation Setup and Methods

This chapter addresses the simulation software FEMP the Finite Element Method (FEM) formulation used to model a piezoelectric disc in vacuum. Additional information regarding the user-configured files for FEMP are provided in Appendix B.

4.1 Finite Element Modeling

This section addresses the FE formulation for a piezoelectric resonator in vacuum [17, 18], which builds on the set of constitutive equations given in Equations 2.11 and 2.12:

$$\begin{aligned} T_p &= c_{pq}^E S_q - e_{jp} E_j \\ D_i &= e_{iq} S_q + \varepsilon_{ij}^S E_j \end{aligned}$$

The piezoceramics studied in this thesis are composite materials of Lead Zirconite Titantite (PZT) [1]. The same symmetry can be used as for hexagonal crystal systems of class 6mm, meaning the material constant matrices can be written as [13]

$$\begin{bmatrix} c_{11}^E & c_{12}^E & c_{13}^E & 0 & 0 & 0 \\ c_{12}^E & c_{11}^E & c_{13}^E & 0 & 0 & 0 \\ c_{13}^E & c_{13}^E & c_{33}^E & 0 & 0 & 0 \\ 0 & 0 & 0 & c_{44}^E & 0 & 0 \\ 0 & 0 & 0 & 0 & c_{44}^E & 0 \\ 0 & 0 & 0 & 0 & 0 & c_{66}^E \end{bmatrix}$$

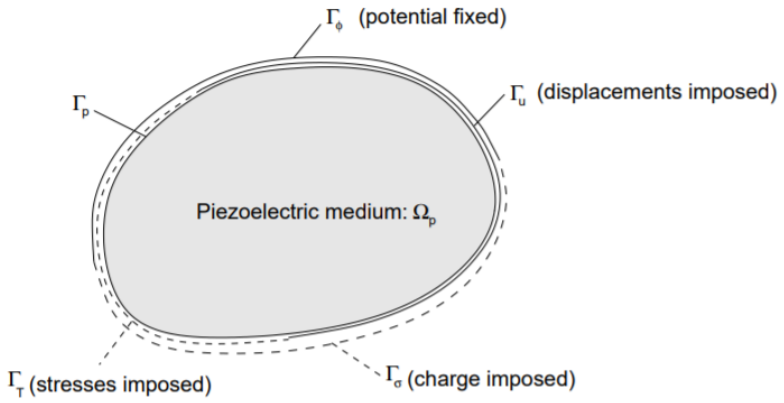

Figure 3.1: A piezoelectric body of volume Ω_p with surface Γ_p vibrating in vacuum. Γ_T is the part of the surface Γ_p on which surface traction $\overline{t}_i$ is applied. Γ_u is the part of the surface Γ_p on which the displacement $\overline{u}_i$ is given. Γ_ϕ is the part of the surface Γ_p on which the electric potential is fixed (set to $\overline{\phi}$). Γ_σ is the part of the surface Γ_p on which the surface charge density $\overline{\sigma}$ is imposed. It is assumed that Γ_u and Γ_T are disjoint with union equal to Γ_p, and that Γ_ϕ and Γ_σ are disjoint with union equal to Γ_p.

Figure 4.1: **Midlertidig figur til jeg skaffer en egen en, hentet fra [17]**

$$\begin{bmatrix} 0 & 0 & 0 & 0 & e_{15} & 0 \\ 0 & 0 & 0 & e_{15} & 0 & 0 \\ e_{31} & e_{31} & e_{33} & 0 & 0 & 0 \end{bmatrix}$$

$$\begin{bmatrix} \varepsilon_{11}^S & 0 & 0 \\ 0 & \varepsilon_{11}^S & 0 \\ 0 & 0 & \varepsilon_{33}^S \end{bmatrix}$$

where $c_{66}^E = 1/2 \cdot \left(c_{11}^E - c_{12}^E\right)$ [13, 20].

The boundary conditions that are imposed on the surfaces of the piezoelectric disc in vacuum are [17]

u_i	$= \bar{u}_i$	at Γ_u	: an imposed displacement $\bar{u}_i$ on the surface Γ_u
$T_{ij}n_j$	$= \bar{t}_i$	at Γ_T	: an imposed traction on the surface Γ_T
$-D_i n_i$	$= \bar{\sigma}$	at Γ_σ	: an imposed surface charge density on the surface Γ_σ
φ	$= \bar{\varphi}$	at Γ_φ	: an imposed electric potential on the surface of the electrodes.

The disc is divided into a finite number of small elements, and each element defined by 8 nodes located around their respective boundaries. At the nodes the physical quantities mechanical displacement, and electric potential are determined.

After imposing weak formulation, cylindrical coordinates, and axis symmetry about the angle, the follow finite element formulations for a piezoelectric disc in vacuum can be derived [17]

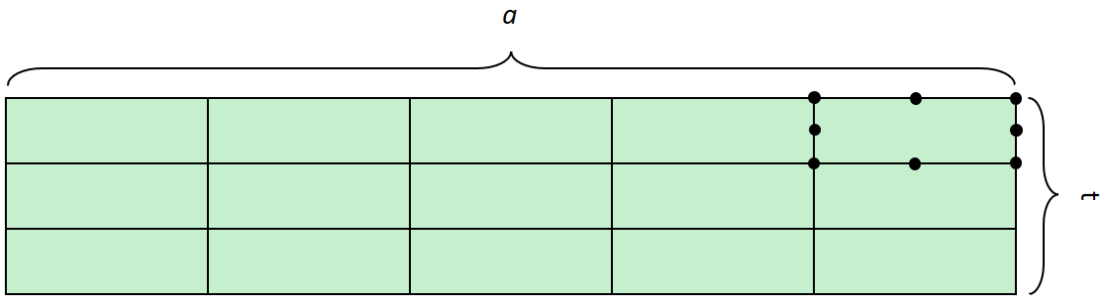

Figure 4.2: Mesh plot generated by FEMP illustrating the node division. t is thickness, a is radius.

$$-\omega^2 \begin{bmatrix} M_{uu} & 0 \\ 0 & 0 \end{bmatrix} \begin{Bmatrix} \hat{u} \\ \varphi \end{Bmatrix} + \begin{bmatrix} H_{uu} & H_{u\varphi} \\ H_{\varphi u}^T & H_{\varphi\varphi} \end{bmatrix} \begin{Bmatrix} \hat{u} \\ \varphi \end{Bmatrix} = \begin{Bmatrix} F \\ -Q_{p\text{total}} \end{Bmatrix} \tag{4.1}$$

When simulating in FEMP Equation 4.1 is solved directly for the admittance Y through matrix manipulation [17]:

$$Y(\omega) = i\omega \left[\{H_{u\phi}\}^T [D]^{-1} \{H_{u\phi}\} - \{H_{\phi\phi}\} \right] \tag{4.2}$$

4.2 Simulation Setup

Appendix B contains the user-specified configurations for recreating this particular setup in FEMP.

4.3 Methods

4.3.1 Sensitivity Analysis

FEMP requires a large amount of input parameters to accurately model the material, and it is of interest to see how a change in one such parameter affects the resulting simulation. To quantify these changes the following 23 input parameters have been considered

- all material constants discussed in Section 4.1: $c_{11}^E, c_{12}^E, c_{13}^E, c_{33}^E, c_{44}^E$, $e_{31}, e_{33}, e_{15}, \varepsilon_{11}^S$ and ε_{33}^S
- all individual Q-factors associated with the material constants above
- the material density ρ

Each input parameter has been increased and decreased by 1% separately, totalling 46 new unique material data sets. Each material data set has been used as input for FEMP producing a simulated admittance $Y(f)$. From the admittance the conductance $G(f)$, susceptance $B(f)$, and resistance $R(f)$ are derived, and compared with the unchanged material data set, meaning the initial material data set before the $\pm 1\%$ change in an input parameter.

When comparing the unchanged and the changed G-,$B-$, and R-plots only a select few observable quantities in these domains are noted. The observed quantities are given in Table 4.2, including the alternative notation used in in Section 5.3 and Fardal [7].

In Section such an sensitivity analysis is performed on the data set in Table 4.1, which are the material constants from Ferroperm supplemented with Q-factors as specified in the table caption. This is done to have a non-null value for the $\pm 1\%$ variation in the Q-factors.

Table 4.1: Material constants acquired from Ferroperm [9] and personal communication with Erling Ringgaard [21], and supplements for the Q-factors as they were not given by Ferroperm. c^E-constants use Ferroperms mechanical Q-factor $Q^E_{m,t}$, e constants uses Q-factor from Aanes' Pz27 [3], and ε^S-constants use the Ferroperms listed $\tan\delta^S_{33}$.

Name	Real Value	Q-factor	Name	Real Value	Q-factor
c^E_{11}	$7.23 \cdot 10^{10}$	130.00	e_{31}	1.11	-166
c^E_{12}	$4.17 \cdot 10^{10}$	130.00	e_{33}	11.00	-324
c^E_{13}	$3.34 \cdot 10^{10}$	130.00	e_{15}	6.89	-200
c^E_{33}	$4.63 \cdot 10^{10}$	130.00	ε^S_{11}	$7.55 \cdot 10^{-9}$	66.67
c^E_{44}	$1.64 \cdot 10^{10}$	130.00	ε^S_{33}	$7.85 \cdot 10^{-9}$	66.67

Table 4.2: Measurables, or interesting quantities, observed under the sensitivity analysis. Alternative notation are used by Fardal in his masters [7], and are also used here. Note that in Section 5 the listed values a given as relative variation from Ferroperms data in percent.

Alternative	**Symbol**	**Description**
1kHz:R		R at f = 1kHz
1kHz:G		G at f = 1kHz
1kHz:B/omega		B/ω at f = 1kHz
R1:R		R at first radial mode
R1:G		G at first radial mode
R1:fs	f_s^{R1}	series resonance frequency at first radial mode
R1:BWs		series resonance bandwidth at first radial mode
R1:fp	f_s^{R1}	parallel resonance frequency at first radial mode
R1:BWp		parallel resonance bandwidth at first radial mode
R2:R		R at second radial mode
R2:G		G at second radial mode
R2:fs	f_s^{R2}	series resonance frequency at second radial mode
R2:BWs		series resonance bandwidth at second radial mode
R2:fp	f_p^{R2}	parallel resonance frequency at second radial mode
R2:BWp		parallel resonance bandwidth at second radial mode
R3:R		R at third radial mode
R3:G		G at third radial mode
R3:fs	f_s^{R3}	series resonance frequency at third radial mode
R3:BWs		series resonance bandwidth at third radial mode
R3:fp	f_p^{R3}	parallel resonance frequency at third radial mode
R3:BWp		parallel resonance bandwidth at third radial mode
TE1:R		R at first thickness extensional mode
TE1:G		G at first thickness extensional mode
TE1:fs	f_s^{TE1}	series resonance frequency at first thickness extensional mode
TE1:BWs		series resonance bandwidth at first thickness extensional mode
TE1:fp	f_p^{TE1}	parallel resonance frequency at first thickness extensional mode
TE1:BWp		parallel resonance bandwidth at first thickness extensional mode

Chapter 5

Results

5.1 Simulations from Manufacturer's Material Data

Meggit Ferroperm have published an extensive data sheet with material properties for their products on their webpage [9]. The material constants c_{44}^E, e_{15} and ε_{11}^S, which are not listed in the sheet, have been procured through personal communications Erling Ringgaard [21]- a researcher with Ferroperm. These three material constants are, as recommended by [13], determined by measurements on a long piezoelectric bar polarized along the longest dimension, and an electric field perpendicular to the polarization direction [13]. The ones used in this thesis are empirically estimated by Ringgaard.

The loss tangent tan $\delta_{33}^{\varepsilon^T}$ and Q-factor $Q_{33}^{c^D}$ are often listed in material data sheets under the abbreviations $tan\delta^e$ and Q_m [24]. This is also the case with Ferroperm [9]. The listed Q-factor Q_m are used for all elastic stiffness Q-factors, and the listed loss tangent tan δ^e are converted to Q-factor form with Equation 2.18, and then used for $Q_{11}^{\varepsilon^S}$. The piezoelectric loss factors are not listed, likely since the piezoelectric loss are often negligible [13]. In Figure all piezoelectric loss factors Q^e are set to infinity, meaning the imaginary terms of the piezoelectric material constants e''_{jp} are set to 0.

Table 5.1: Material constants acquired from Ferroperm [9] and personal communication with Erling Ringgaard [21].

Name	Real Value	Q-factor	Name	Real Value	Q-factor
c_{11}^E	$7.23 \cdot 10^{10}$	130.00	e_{31}	1.11	∞
c_{12}^E	$4.17 \cdot 10^{10}$	130.00	e_{33}	11.00	∞
c_{13}^E	$3.34 \cdot 10^{10}$	130.00	e_{15}	6.89	∞
c_{33}^E	$4.63 \cdot 10^{10}$	130.00	ε_{11}^S	$7.55 \cdot 10^{-9}$	66.67
c_{44}^E	$1.64 \cdot 10^{10}$	130.00	ε_{33}^S	$7.85 \cdot 10^{-9}$	66.67

5.1.1 Comparison to Measurements

Figure 5.1-5.2 compares the measurement and simulation for element #1 using the material constants from Table 5.1. The sporadic modes, especially visible in-between the first radial modes in Figure 5.2a and 5.2c, are consistent throughout

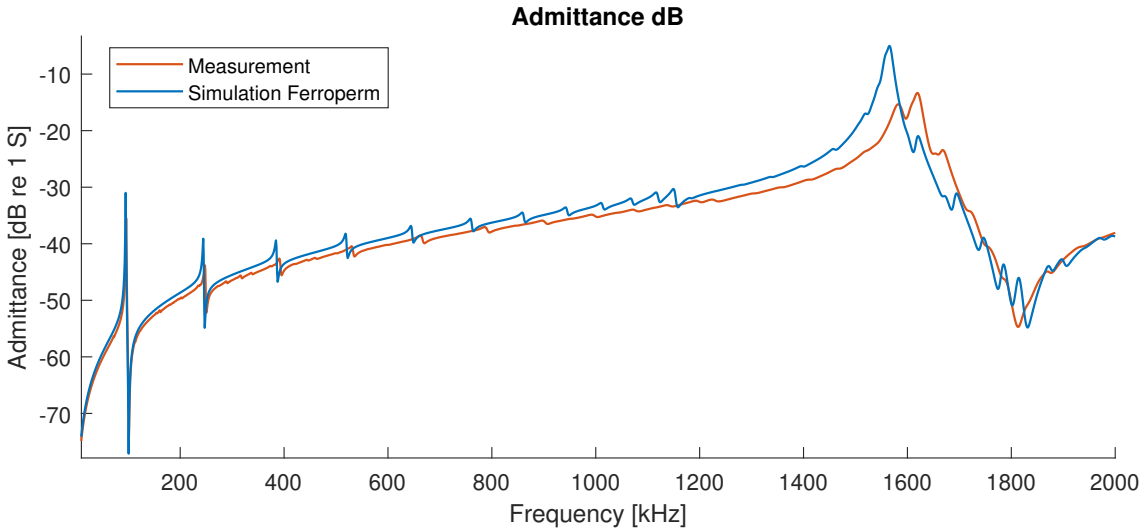

Figure 5.1: Measurement and simulation of Pz37-disc with thickness $t = 0.88mm$ and radius $a = 9.53mm$. Frequency resolution $= 0.05kHz$ for both.

repeated measurements. Thus the possibility of it being noise is excluded. Similar sporadic modes have not been observed in measurements on Pz27 and PZT-5A from previous work conducted at UiB [3, 7].

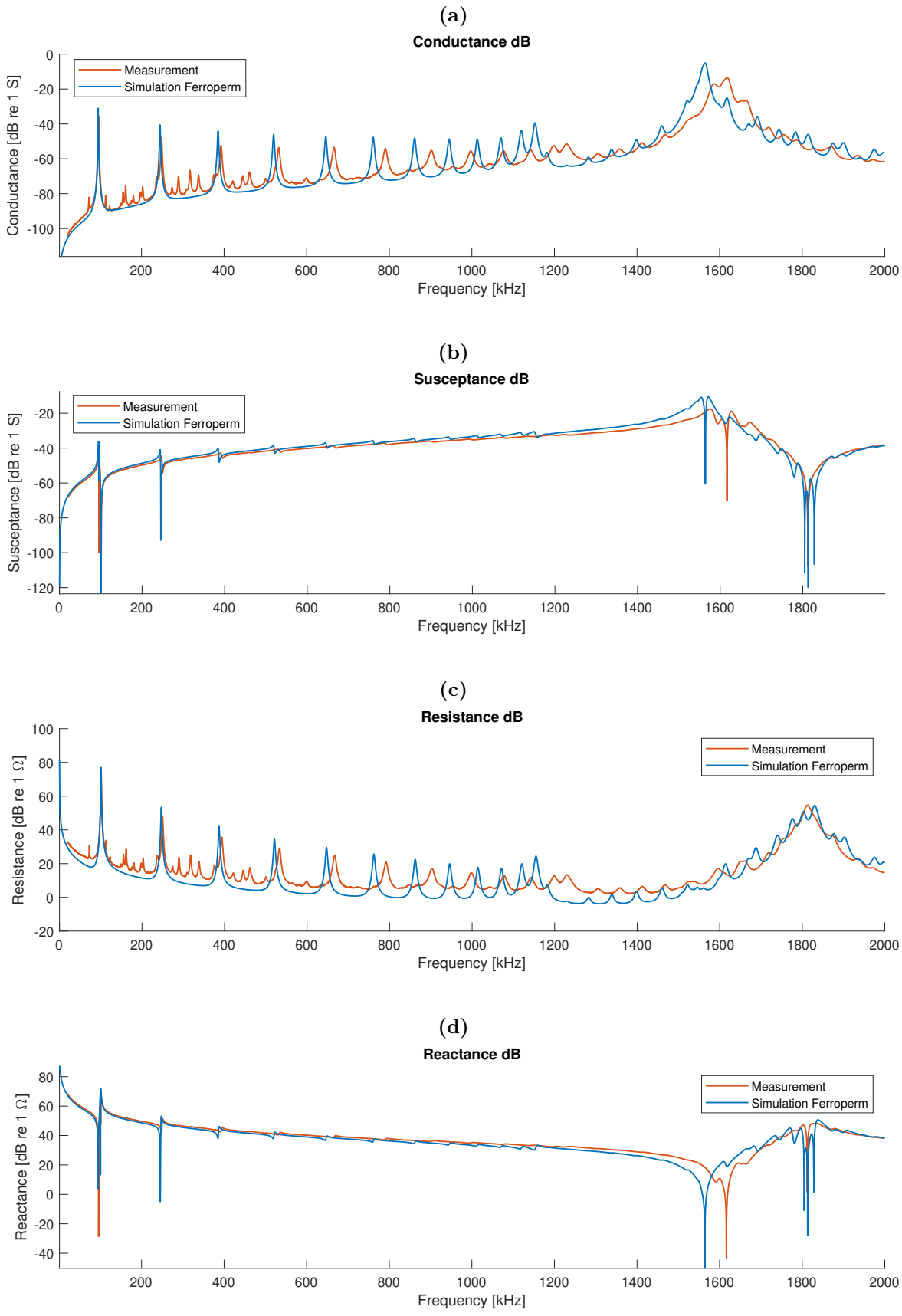

Figure 5.2: a) Conductance G, b) susceptance B, c) resistance R, and d) reactance X of a Pz37 disc with radius $a = 9.53mm$ and thickness $t = 0.88mm$. Frequency resolution $= 0.05kHz$.

5.2 Material Constants from Measurements

This section contains calculated material constants as a result of following the methods described in Sections 2.4 and 2.5. The MATLAB-scripts ReelleMatKonst.m and KompleksematKonst.m borrowed from Lohne's thesis are used to calculate the material constants [19].

5.2.1 Calculated from Measurements on a Disc

The material constants c_{33}^E, e_{33} and ε_{33}^S have been calculated following the methods described in Section 2.4.1-2.4.3. Using the methods described in Section 2.4 [19], 4 more material constants have been calculated and are given in Table 5.2. The Q-factors listed are acquired from Ferroperm.

Name	Real Value	Q-factor	Name	Real Value	Q-factor
c_{11}^E	$7.68 \cdot 10^{10}$	130	e_{31}	1.11	∞
c_{12}^E	$4.63 \cdot 10^{10}$	130	e_{33}	9.90	∞
c_{13}^E	$3.75 \cdot 10^{10}$	130	e_{15}	6.89	∞
c_{33}^E	$4.99 \cdot 10^{10}$	130	ε_{11}^S	$7.55 \cdot 10^{-9}$	66.67
c_{44}^E	$1.64 \cdot 10^{10}$	130	ε_{33}^S	$6.26 \cdot 10^{-9}$	66.67

Table 5.2: Material constants for element no. 1, calculated from methods described in Section 2.4.

Using the methods described in Section 2.5 [19, 22, 23], complex material constants have been calculated and are given in Table 5.3.

Name	Real Value	Q-factor	Name	Real Value	Q-factor
c_{11}^E	$7.68 \cdot 10^{10}$	35.82	e_{31}	1.11	-166.00
c_{12}^E	$4.57 \cdot 10^{10}$	25.57	e_{33}	8.85	-132.26
c_{13}^E	$3.33 \cdot 10^{10}$	19.05	e_{15}	6.89	∞
c_{33}^E	$3.97 \cdot 10^{10}$	21.31	ε_{11}^S	$7.55 \cdot 10^{-9}$	66.67
c_{44}^E	$1.64 \cdot 10^{10}$	130.00	ε_{33}^S	$6.26 \cdot 10^{-9}$	293.10

Table 5.3: Complex material constants for element no. 1, calculated from methods described in Section 2.5.

5.2.2 Comparison to Measurements

Figure 5.3 shows the simulated admittance Y for the calculated real material data set, that is the material constants given in Table 5.2, in comparison with the simulated Ferroperm set and measurements.

Figure 5.4 shows the conductance G, susceptance B, resistance R, and reactance X from the same data set as in Figure 5.3.

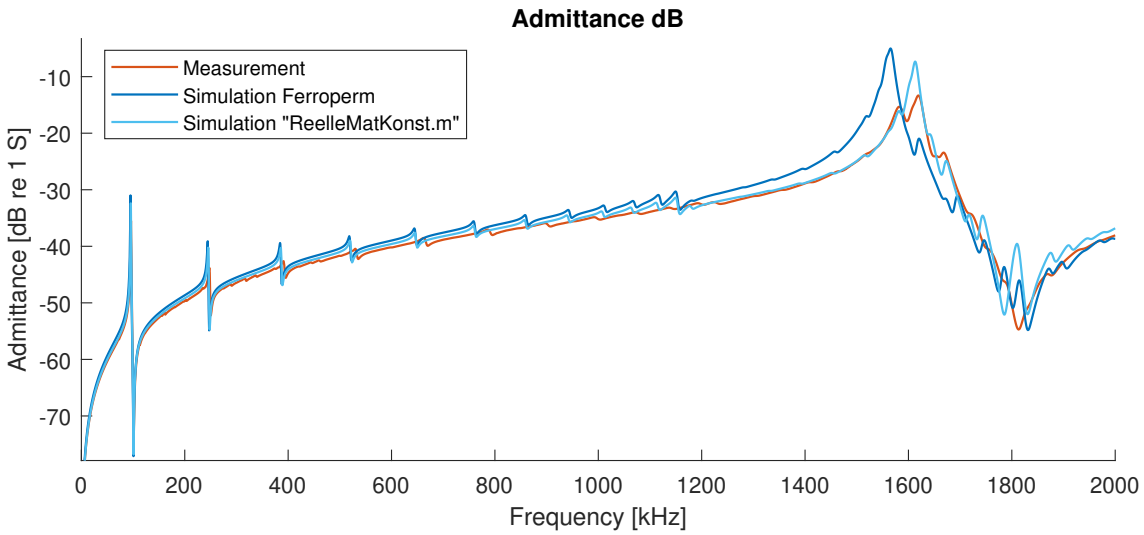

Figure 5.3: Measurement and simulation of a Pz37-disc with radius $a = 9.53mm$ and thickness $t = 0.88mm$. Parameters for the Ferroperm-simulation are given in Table 5.1, and "ReelleMatKonst.m"-simulation in Table 5.2. Frequency resolution $= 0.05kHz$ for all plots.

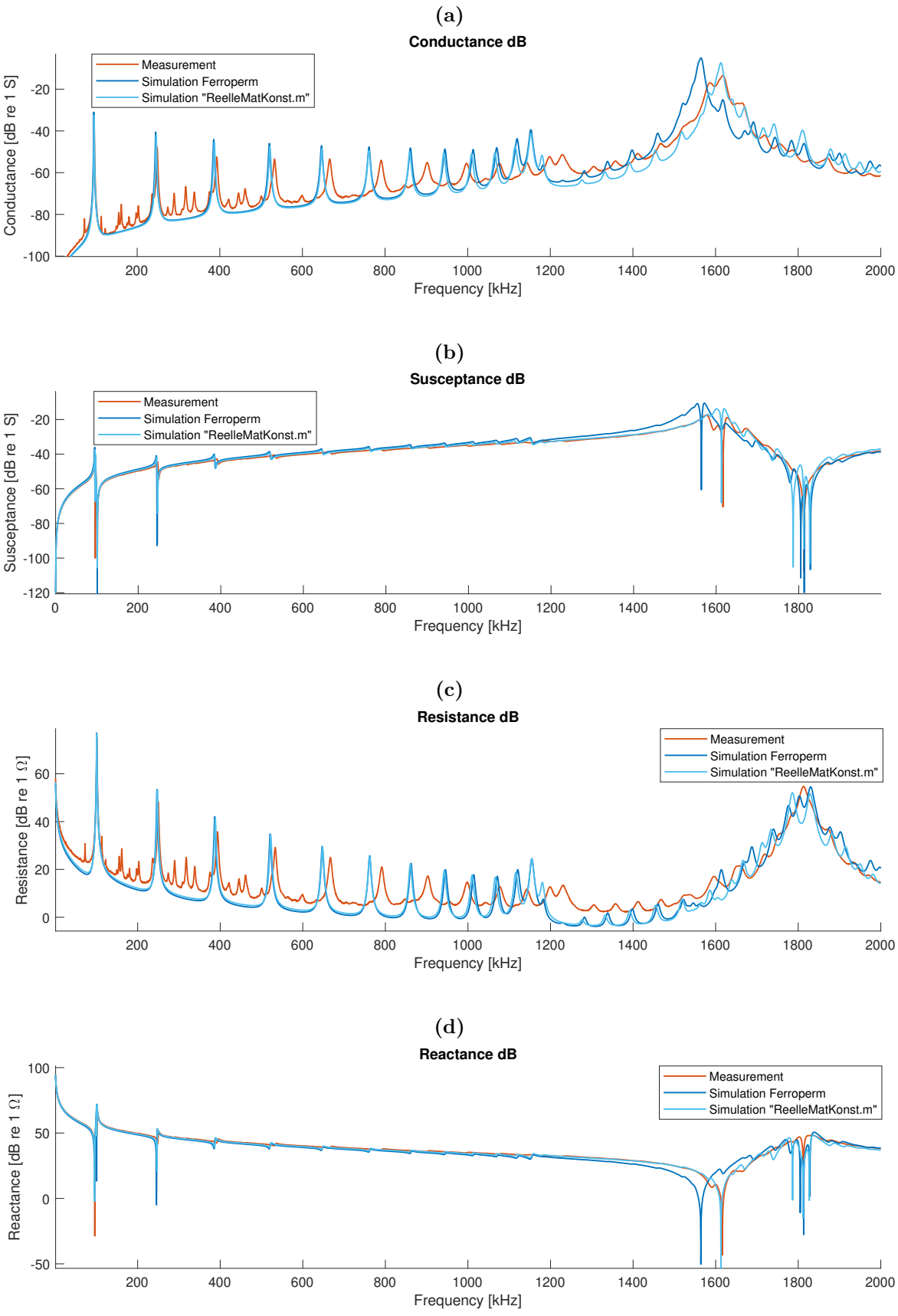

Figure 5.4: a) Conductance G, b) susceptance B, c) resistance R, and d) reactance X of a Pz37 disc with radius $a = 9.53m$ and thickness $t = 0.88m$. Frequency resolution $= 0.05kHz$.

Figure 5.5 shows simulated admittance Y for the calculated complex material data set, that is the material constants given in Table 5.3, in comparison with the real material data set and measurements.

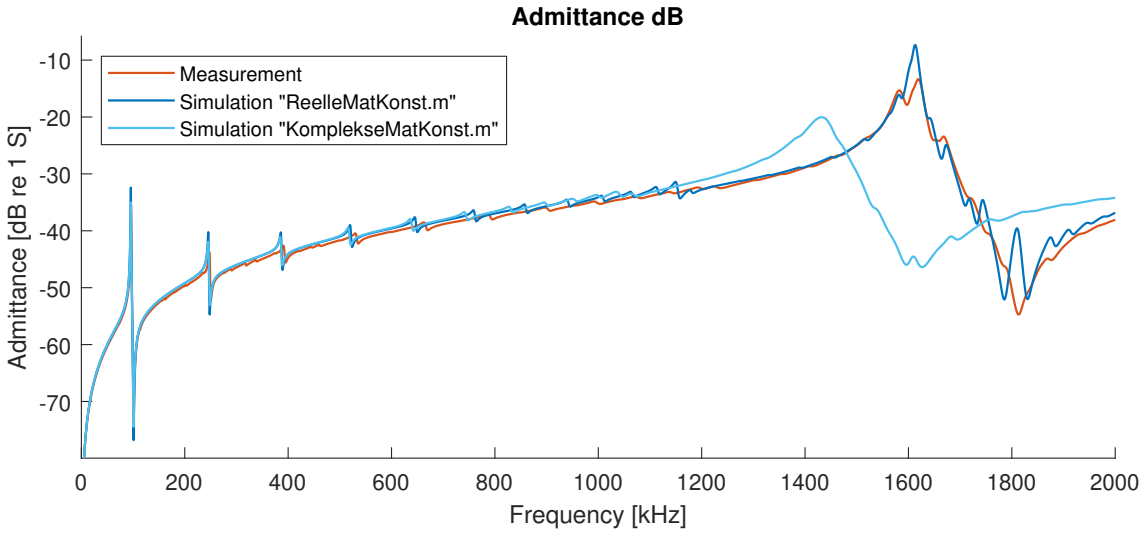

Figure 5.5: Measurement and simulation of a Pz37-disc with radius $a = 9.53m$ and thickness $t = 0.88m$. Parameters for the simulation are given in Table 5.3. Frequency resolution $= 0.05kHz$ for both.

Figure 5.6 shows the conductance G, susceptance B, resistance R, and reactance X from the same data set as in Figure 5.5.

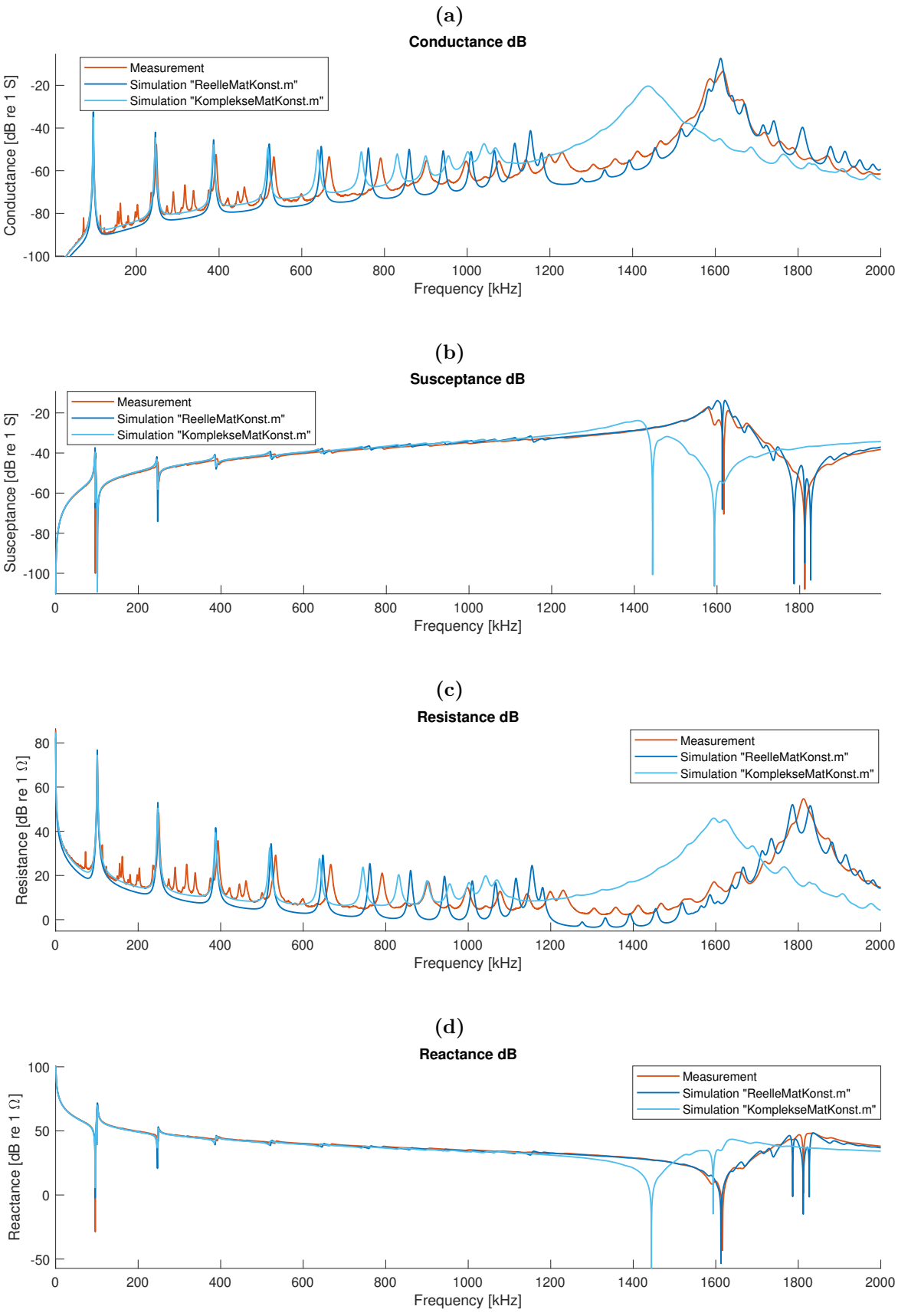

Figure 5.6: a) Conductance G, b) susceptance B, c) resistance R, and d) reactance X of a Pz37 disc with radius $a = 9.53m$ and thickness $t = 0.88m$. Frequency resolution $= 0.05kHz$.

5.3 Sensitivity Analysis

A sensitivity analysis has been performed with the material data set in Table 4.1 as a starting point. Two compact tables containing the results are given in Appendix C. In this section the aforementioned tables are split up for each material constants, with accompanying plots to check the validity and usefulness of the results.

For each material constants the relative variation in G, B and R are plotted, or the variation-responses as Fardal calls it. The term relative change is also used interchangeably. Such plots are useful for identifying areas where the material constants affect the most. This is not to be confused by the statistical quantity variance.

The simulations have been solved with DIRECTHARMONICANALYSIS option in FEMP, with 3 elements per wavelength calculated at $f = 2200$kHz. The frequency resolution were 5Hz for radial modes, and 50Hz for the thickness extensional mode. Note that the number of elements per wavelength are lower than the recommended number [7]. This was picked to prioritize speed since the currently initial material data set were acquired late [21].

Table 5.4: Relative variation in the listed derived quantity (row) as a result of a 1% change in the stated material constant and its Q-factor (column). Color spectrum ranges from blue to red, where the former represents a negative difference,the latter a positive difference. The intensity of the color represents the magnitude of the difference from Ferroperm's simulated data.

	c^E_{11} + 1%	c^E_{11} - 1%	Q^{cE}_{11} + 1%	Q^{cE}_{11} - 1%
R1:R	-1,28%	1,30%	1,06%	-1,06%
R1:G	-0,39%	0,39%	1,19%	-1,18%
R1:fs	0,59%	-0,60%	0,00%	0,00%
R1:BWs	0,68%	0,00%	-1,37%	1,37%
R1:fp	0,54%	-0,55%	0,00%	0,00%
R1:BWp	0,63%	-0,63%	-1,26%	0,63%
R2:R	-2,02%	2,09%	1,43%	-1,42%
R2:G	-0,63%	0,64%	1,46%	-1,44%
R2:fs	0,73%	-0,73%	0,00%	0,00%
R2:BWs	1,06%	-0,53%	-1,33%	1,60%
R2:fp	0,72%	-0,72%	0,00%	0,00%
R2:BWp	0,79%	-0,79%	-1,31%	1,31%
R3:R	-2,00%	2,07%	1,45%	-1,44%
R3:G	-0,52%	0,53%	1,46%	-1,45%
R3:fs	0,74%	-0,74%	0,00%	0,00%
R3:BWs	0,68%	-0,68%	-1,35%	1,52%
R3:fp	0,73%	-0,74%	0,00%	0,00%
R3:BWp	0,67%	-0,84%	-1,34%	1,51%
TE1:R	-0,50%	-1,76%	0,32%	-0,33%
TE1:G	6,04%	16,32%	-0,06%	0,07%
TE1:fs	0,00%	0,38%	0,00%	0,00%
TE1:BWs	12,65%	-11,52%	0,00%	0,03%
TE1:fp	0,19%	-0,19%	0,00%	0,00%
TE1:BWp	0,26%	-0,64%	-0,34%	0,37%

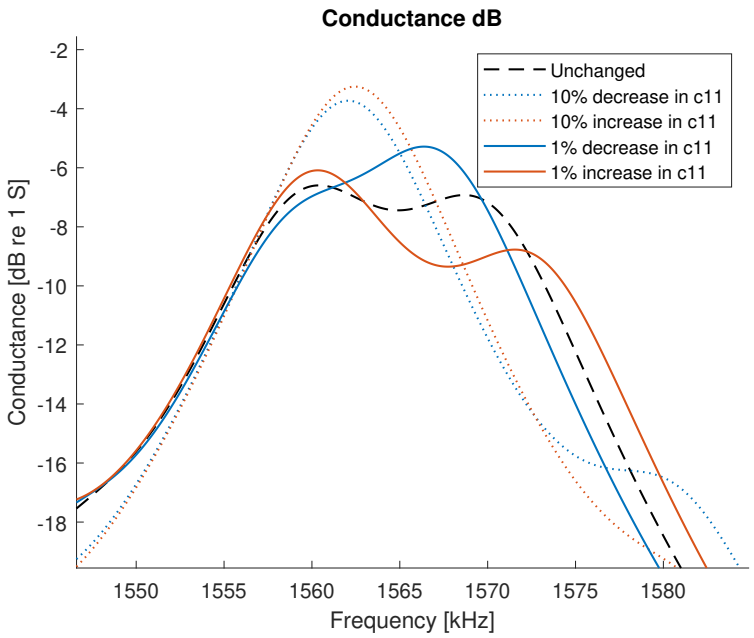

Figure 5.7: Simulated conductance G near the TE1-mode from Ferroperms data set denoted 'Unchanged' in the legend. Additional simulations illustrating the effect $\pm 1\%$ and $\pm 10\%$ variations in c^E_{11} has on Ferroperms data set. Frequency resolution $\Delta f = 5Hz$.

5.3.1 variation in c^E_{11}

The elastic stiffness constant c^E_{11} and its associated Q-factor $Q^{c^E}_{11}$ have been varied by 1% from Ferroperms listed values. The resulting changes in the conductance G-, susceptance B-, and resistance R-domain are given as variation relative to the Ferroperms simulated data in Table 5.4. However the listed values for TE1 must be interpreted with a hint of skepticism. The TE1-mode are the sum of multiple modes' contributions [17], and c^E_{11} seems to affect some modes more than others. This means it can be difficult to derive a reliable parameter for i.e. the change in the displacement of f_s^{TE1}, where a 1% decrease in c^E_{11} is seen to increase the magnitude of the rightmost peak resulting in the apparent relative displacement of TE1:FS $= 0,38\%$ upwards in frequency. This is better illustrated in Figure 5.7 than described here.

c^E_{11} appears in Mason's Radial Model but not Mason's Thickness Model, yet it has a significant impact on the TE1-mode as can be seen in Figure 5.7. This is likely due to the higher order radial modes influencing in the TE1-region, which was also observed for the material PZT-5A [7]. This is further confirmed by

Figure 5.8a and 5.8c which shows relative deviations from Ferroperms simulated data approximately as large as 83% and 88% for G and R respectively in the region between f_s^{TE1} and f_p^{TE1}. Another behaviour that agrees with that of PZT-5A is the strong dampening in the variation of the susceptance B after the parallel resonance f_p^{TE1} [7], shown in Figure 5.8b. The same dampening can be seen for the variation in the reactance X in Figure 5.8d.

The first 3 radial modes R1, R2, R3, pictured in Figure 5.10, are observed to shift up/down in frequency, which agrees well with the data in Table 5.4 and the variation plots in Figure 5.8a. Interestingly PZT-5A shows a similar relationship between the relative variation in the resonance frequency displacement of the first two radial modes R1 and R2, which is compared in Table 5.5, but not for the change in magnitude G at R1. For PZT-5A it it increases as opposed to decreases which it does for G at R2, and for G at R1, R2, and R3 here.

	Pz37HD		**PZT-5A**	
	fs	fp	fs	fp
R1	0.59%	0.54%	0,66%	0,54%
R2	0.73%	0.72%	0,81%	0,77%
R2:f/R1:f	1.24	1.33	1.23	1.43

Table 5.5: Comparison of relative resonance frequency displacement of the first 2 radial modes of 2 different piezoceramics with a D/T-ratio ≈ 20. The last row shows the ratio between row 4 and row 3. Pz37HD values are attained from Table 5.4, while PZT-5A values from Table 5.15 in [7].

In Figure 5.8a and 5.8c c_{11}^E's influence decreases when approaching the series resonance f_s^{TE1}, but not nearly as much when closing in on the parallel resonance f_p^{TE1} which can be clearly seen in Figure 5.9 at the peaks. Similar behaviour is not implied for PZT-5A where the resonance frequencies shows a relative variation lower than 0.02% for a 1% increase in c_{11}^E [7].

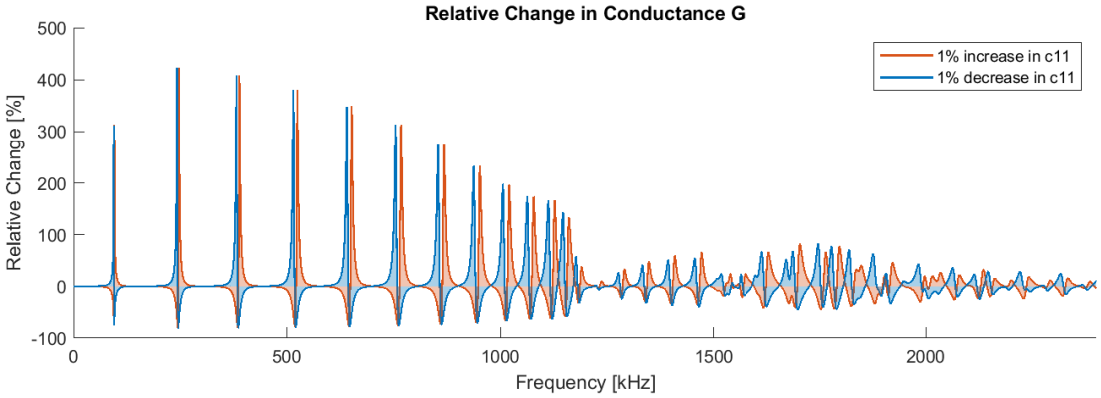

(a)

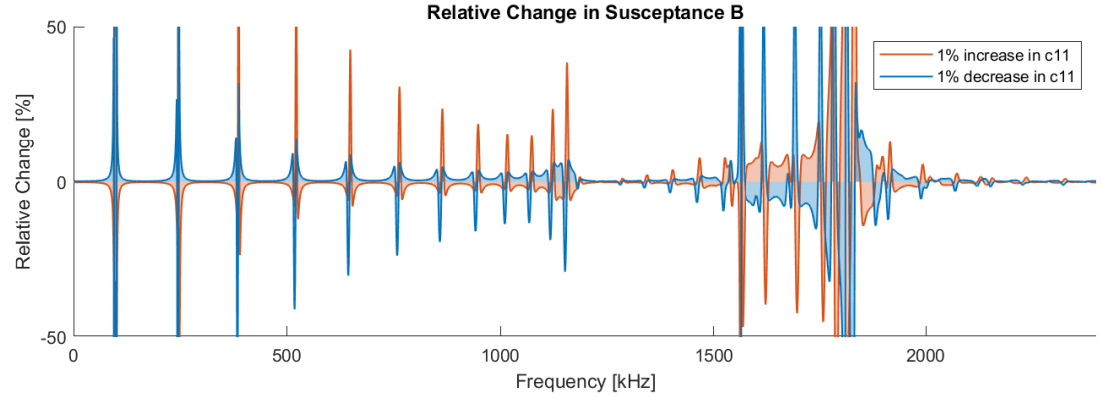

(b)

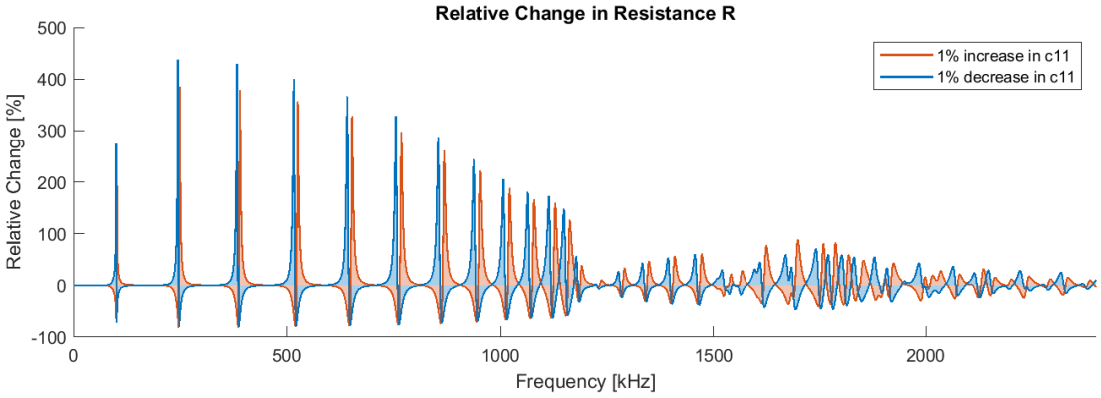

(c)

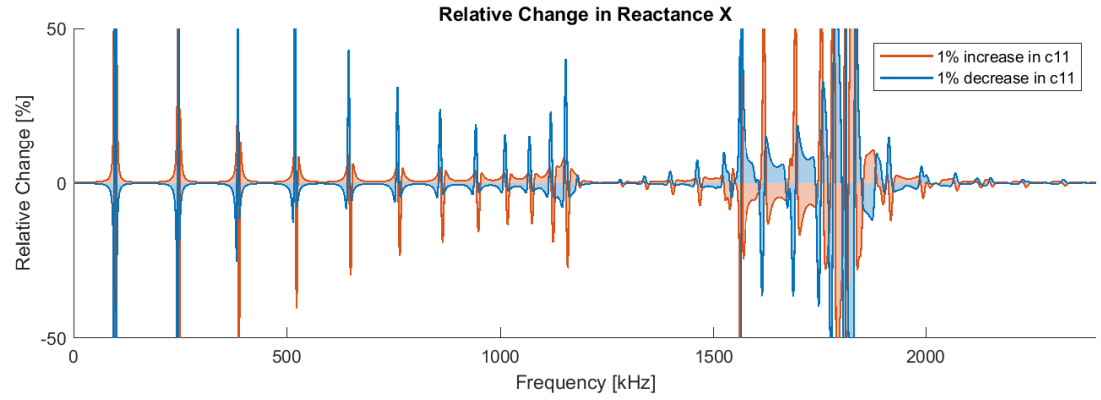

(d)

Figure 5.8: Relative variation in a) conductance G, b) susceptance B, c) resistance R, and d) reactance X from Ferroperms data set for a 1% decrease/increase in material constant c_{11}^{E}.

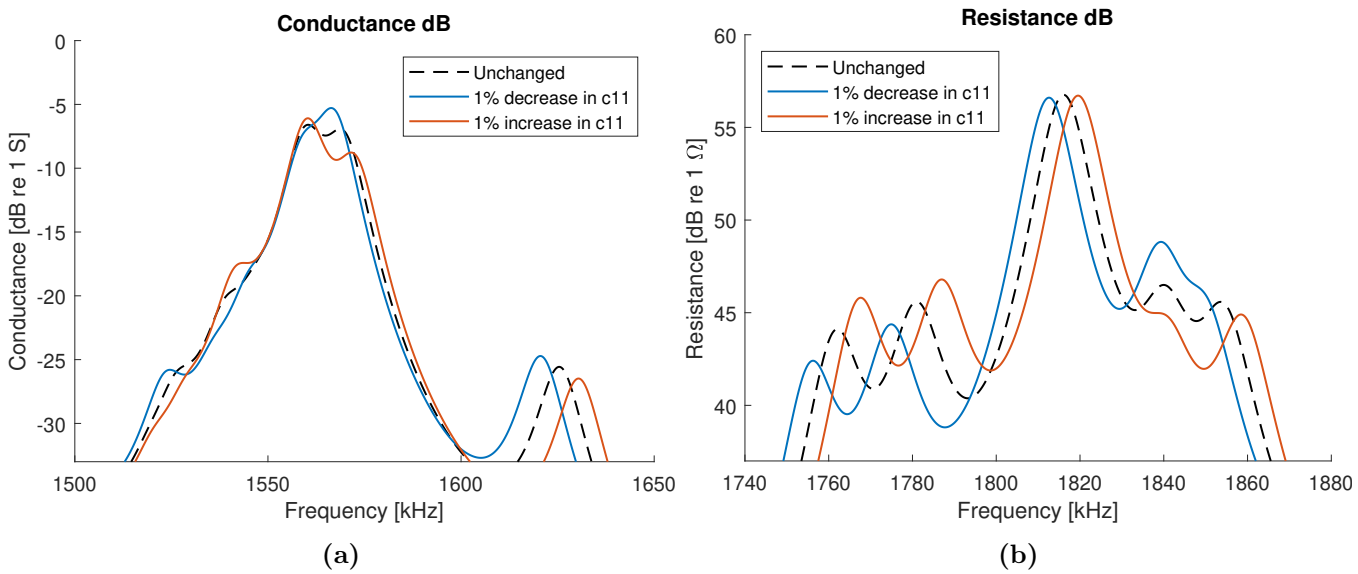

Figure 5.9: a) Simulated conductance G, and b) resistance R from Ferroperms data set, as well as the result a 1% increase/decrease in c_{11}^E has on the simulation. Frequency resolution $\Delta f = 5Hz$.

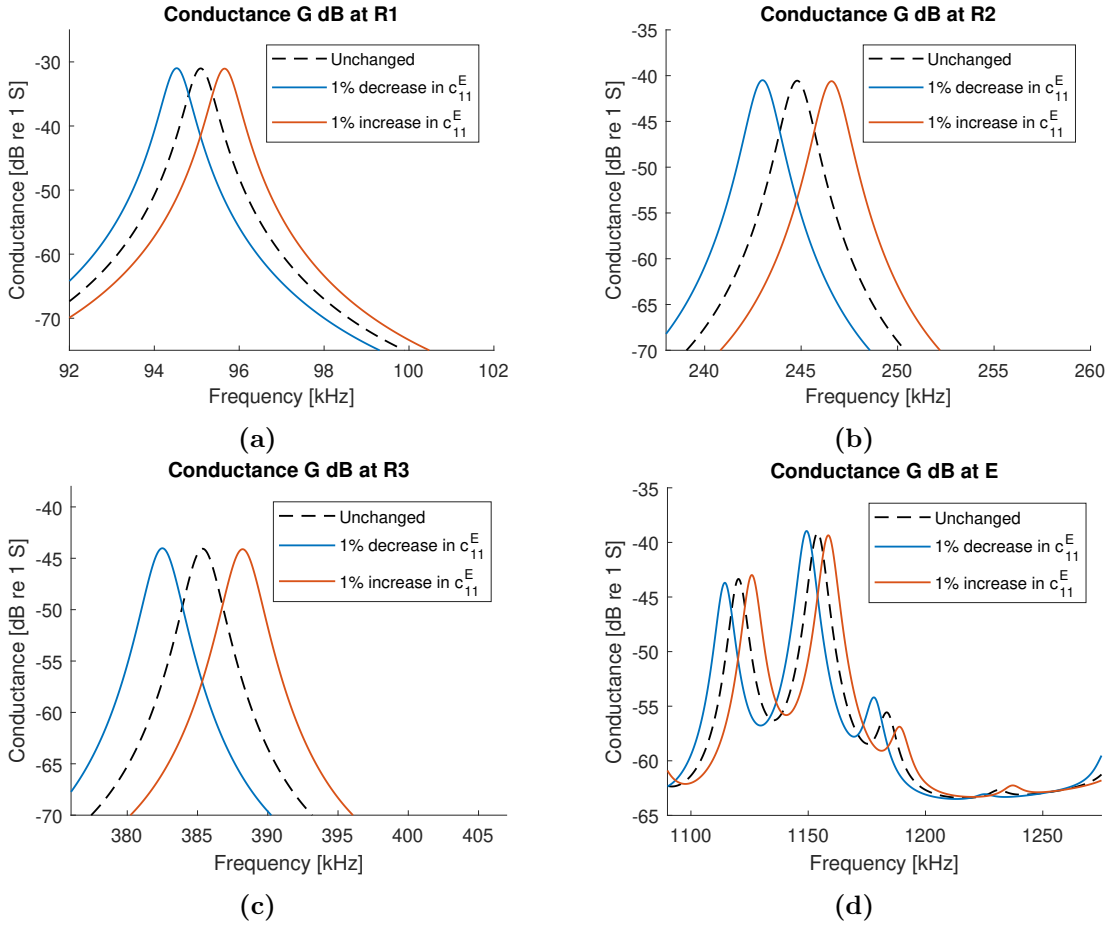

Figure 5.10: a) Simulated conductance G, for a 1% change in c_{11}^E from Ferroperms listed value, at the first three series resonance peaks - a) R1, b) R2 c) R3, and at the E-mode region d). Frequency resolution $\Delta f = 5Hz$ for a) - c), and $50Hz$ for d).

Table 5.6: Relative variation in the listed derived quantity (row) as a result of a 1% change in the stated material constant and its Q-factor (column). Color spectrum ranges from blue to red, where the former represents a negative difference,the latter a positive difference. The intensity of the color represents the magnitude of the difference from Ferroperm's simulated data.

	c^E_{12}+ 1%	c^E_{12} - 1%	Q^{cE}_{12} + 1%	Q^{cE}_{12} - 1%
R1:R	-0,89%	0,90%	0,40%	-0,40%
R1:G	-0,54%	0,55%	0,49%	-0,50%
R1:fs	0,24%	-0,25%	0,00%	0,00%
R1:BWs	0,00%	0,00%	0,00%	0,68%
R1:fp	0,20%	-0,20%	0,00%	0,00%
R1:BWp	0,00%	0,00%	-0,63%	0,63%
R2:R	-0,12%	0,12%	0,06%	-0,06%
R2:G	-0,05%	0,05%	0,06%	-0,06%
R2:fs	0,03%	-0,03%	0,00%	0,00%
R2:BWs	0,27%	0,00%	0,00%	0,27%
R2:fp	0,03%	-0,03%	0,00%	0,00%
R2:BWp	0,00%	0,00%	-0,26%	0,00%
R3:R	-0,05%	0,05%	0,02%	-0,02%
R3:G	-0,02%	0,02%	0,02%	-0,02%
R3:fs	0,01%	-0,01%	0,00%	0,00%
R3:BWs	0,00%	0,00%	0,00%	0,00%
R3:fp	0,01%	-0,01%	0,00%	0,00%
R3:BWp	0,17%	0,00%	0,00%	0,17%
TE1:R	0,01%	-0,01%	0,00%	0,00%
TE1:G	0,00%	0,00%	0,00%	0,00%
TE1:fs	0,00%	0,00%	0,00%	0,00%
TE1:BWs	0,00%	0,00%	0,00%	0,00%
TE1:fp	0,00%	0,00%	0,00%	0,00%
TE1:BWp	0,00%	0,04%	0,00%	0,00%

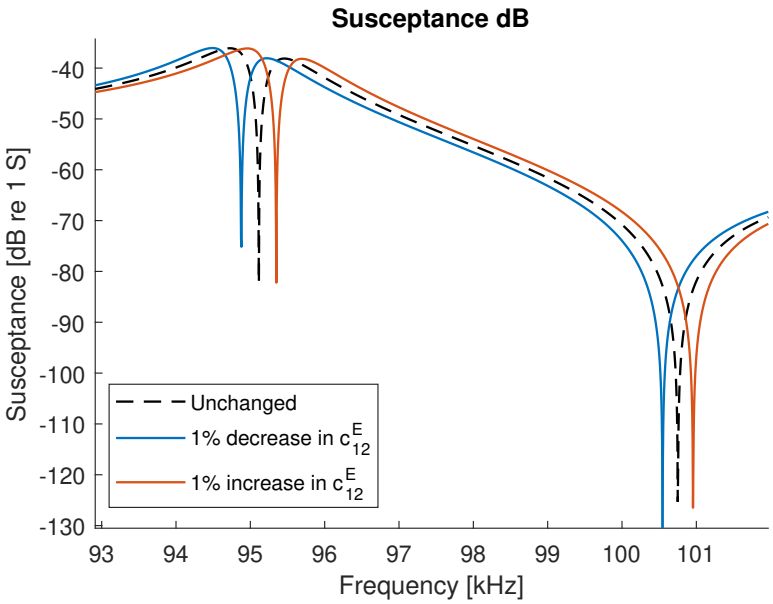

Figure 5.11: Simulated susceptance B for Ferroperms data set denoted 'Unchanged', showing how a 1% variation in c^E_{12} affects the R1-region. Frequency resolution $\Delta f = 5Hz$.

5.3.2 variation in c^E_{12}

The elastic stiffness constant c^E_{12} and its associated Q-factor $Q^{c^E}_{12}$ have been varied by 1% from Ferroperms listed values. The resulting changes in the conductance G-, susceptance B-, and resistance R-domain are given as variation relative to the Ferroperms simulated data in Table 5.6.

In Figure 5.12 it can be observed for G and R that the variation in c^E_{11} mainly affects the first radial mode R1, following a rapidly decreasing influence on the subsequent radial modes until a slight rise again at $f \approx 1200$kHz where the E-mode is thought to reside. This is also observed for PZT-5A [7]. The relative change in resistance R at R1 and R2 when c^E_{12} is increased by 1%, meaning the values listed as R1:R and R2:R in Table 5.6, differ by less than $0,01\%$ from PZT-5A [7]. The same case is not observed for the conductance G at R1 and R2.

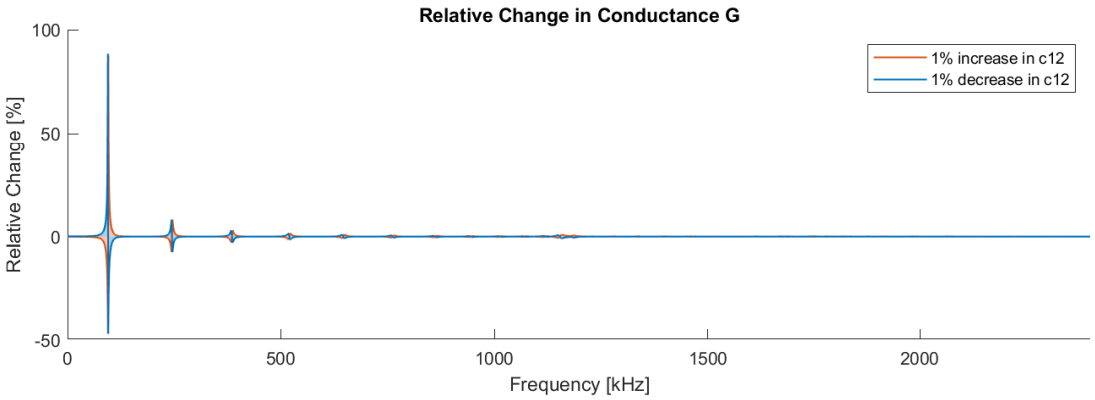

(a)

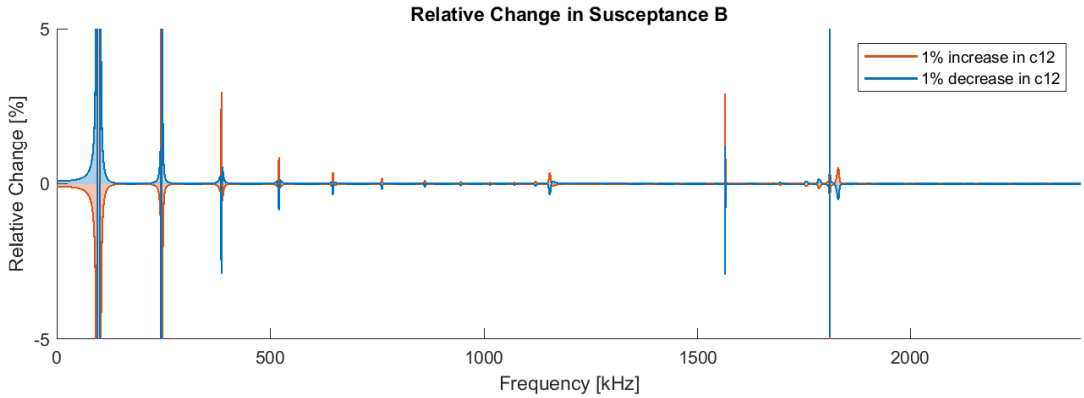

(b)

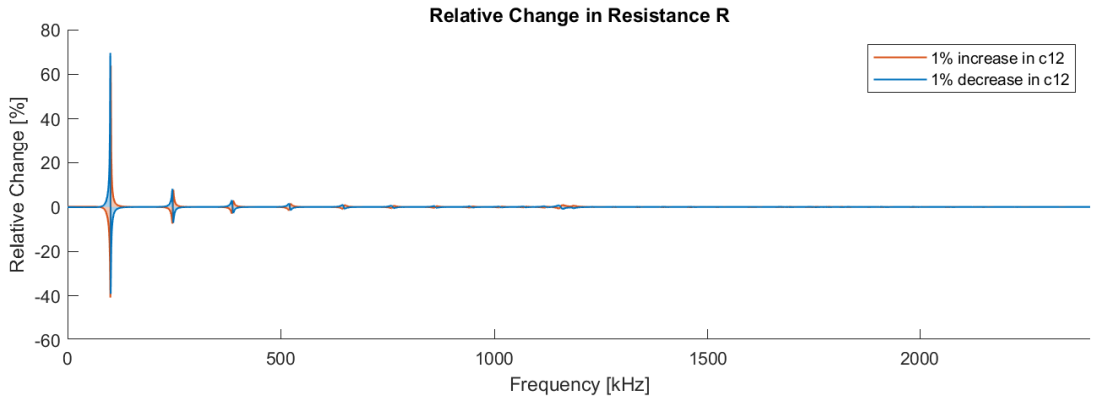

(c)

Figure 5.12: Relative variation in a) conductance G, b) susceptance B, c) resistance R from Ferroperms data set for a 1% decrease/increase in material constant c_{12}^{E}.

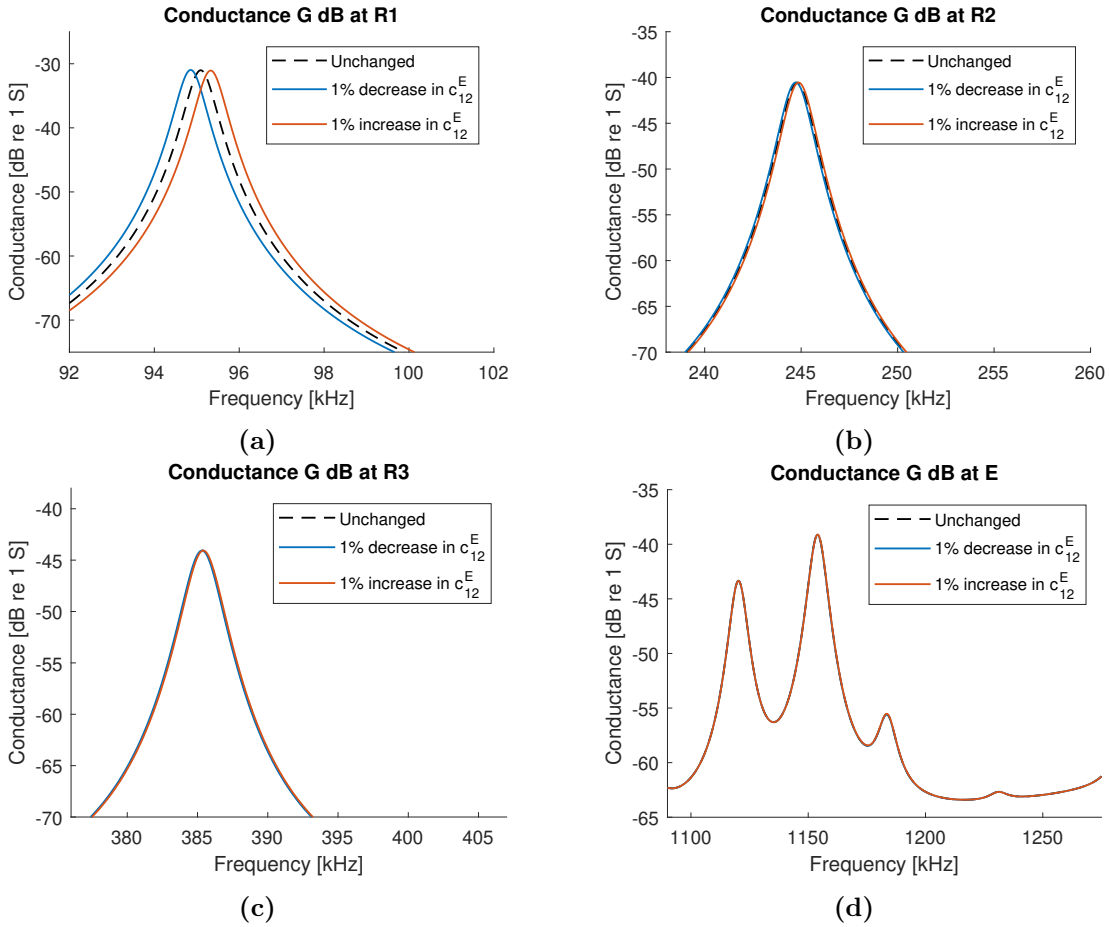

Figure 5.13: a) Simulated conductance G, for a 1% change in c_{12}^{E} from Ferroperms listed value, at the first three series resonance peaks - a) R1, b) R2 c) R3, and at the E-mode region d). Frequency resolution $\Delta f = 5Hz$ for a) - c), and $50Hz$ for d).

Table 5.7: Relative variation in the listed derived quantity (row) as a result of a 1% change in the stated material constant and its Q-factor (column). Color spectrum ranges from blue to red, where the former represents a negative difference,the latter a positive difference. The intensity of the color represents the magnitude of the difference from Ferroperm's simulated data.

	c^E_{13} + 1%	c^E_{13} - 1%	Q^{cE}_{13} + 1%	Q^{cE}_{13} - 1%
R1:R	3,71%	-3,58%	-0,91%	0,95%
R1:G	3,26%	-3,16%	-1,33%	1,40%
R1:fs	-0,69%	0,67%	0,00%	0,00%
R1:BWs	0,00%	1,37%	1,37%	-1,37%
R1:fp	-0,48%	0,47%	0,00%	0,00%
R1:BWp	-0,63%	0,00%	0,63%	-0,63%
R2:R	3,81%	-3,67%	-0,98%	1,02%
R2:G	2,80%	-2,74%	-1,04%	1,08%
R2:fs	-0,54%	0,53%	0,00%	0,00%
R2:BWs	-0,27%	0,53%	1,06%	-1,06%
R2:fp	-0,51%	0,50%	0,00%	0,00%
R2:BWp	-0,52%	0,52%	1,05%	-1,05%
R3:R	3,74%	-3,60%	-1,01%	1,05%
R3:G	2,62%	-2,57%	-1,03%	1,08%
R3:fs	-0,54%	0,53%	0,00%	0,00%
R3:BWs	-0,51%	0,51%	1,01%	-1,01%
R3:fp	-0,53%	0,52%	0,00%	0,00%
R3:BWp	-0,50%	0,67%	1,18%	-1,01%
TE1:R	-5,80%	4,61%	-0,22%	0,23%
TE1:G	7,37%	1,92%	0,04%	-0,04%
TE1:fs	0,42%	-0,01%	0,00%	0,00%
TE1:BWs	-8,09%	8,62%	0,03%	-0,03%
TE1:fp	-0,14%	0,13%	0,00%	0,00%
TE1:BWp	-1,61%	1,35%	0,26%	-0,22%

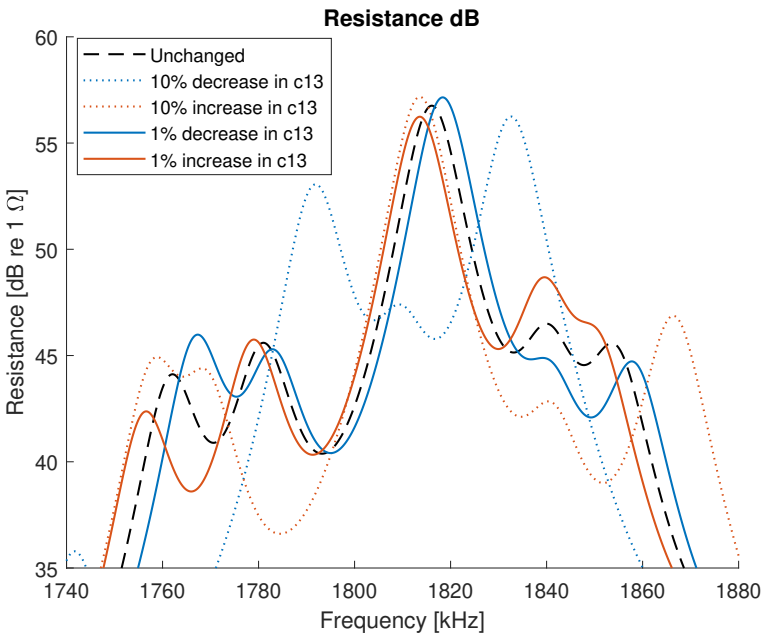

Figure 5.14: Simulated resistance R at the TE1 mode showing how a variation of $\pm 1\%$ in c^E_{13} affects the simulated data from Ferroperm. Frequency resolution $\Delta f = 50Hz$.

5.3.3 variation in c^E_{13}

The elastic stiffness constant c^E_{13} and its associated Q-factor $Q^{c^E}_{13}$ have been varied by 1% from Ferroperms listed values. The resulting changes in the conductance G-, susceptance B-, and resistance R-domain are given as variation relative to the Ferroperms simulated data in Table 5.7.

Figure 5.15 resembles the equivalent variation plots for c^E_{11} given in Figure 5.8, except the graphs are inverted. This becomes apparent when comparing the displacement of the series resonance frequency in the first radial modes in Figure 5.16 with the equivalent plots for c^E_{11} in Figure 5.10. Similar observations were made for PZT-5A [7]. Further comparisons of higher order radial modes after R1 shows that the effect c^E_{13} has on the relative variation in the resonance frequency displacement gradually increases up to the E-mode region, while the opposite is observed for c^E_{11}. This is illustrated in Table 5.8.

Comparing the variation at the TE1-mode for c^E_{11} and c^E_{13} in Figure 5.9 and 5.17, notable differences are observed in the region leading up to the parallel resonance peak f_p^{TE1}.

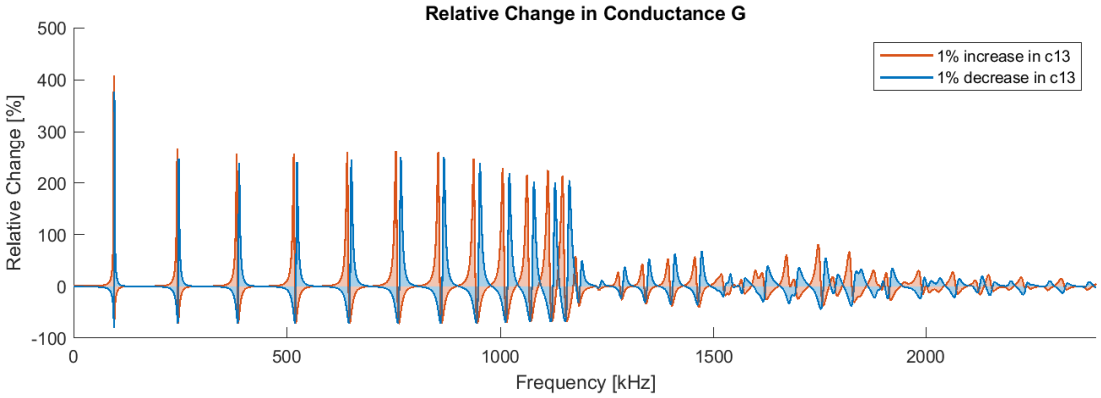

(a)

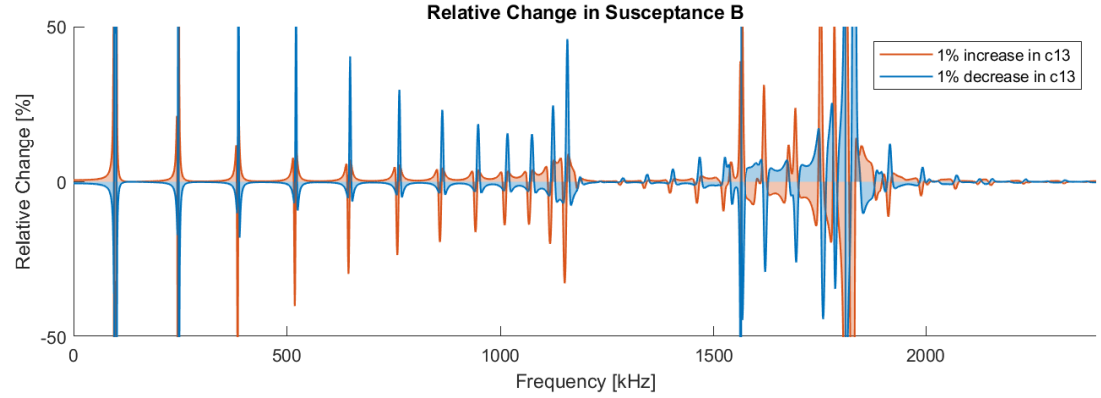

(b)

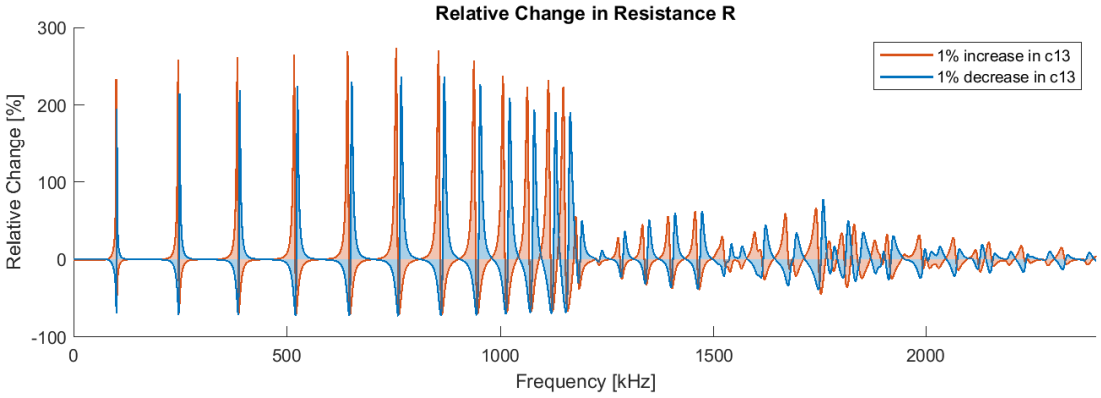

(c)

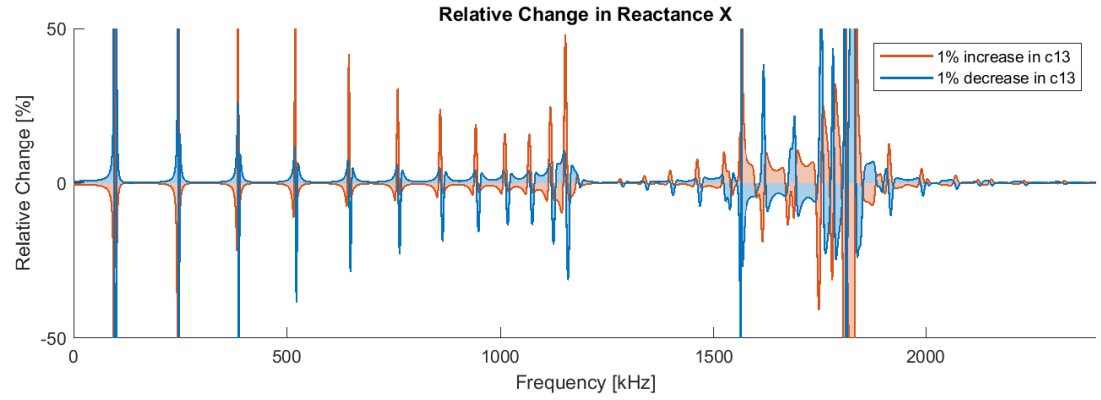

(d)

Figure 5.15: Relative variation in a) conductance G, b) susceptance B, c) resistance R, and d) reactance X from Ferroperms data set for a 1% decrease/increase in material constant c_{13}^{E}.

	c^E_{11} + 1%	c^E_{13} - 1%	c^E_{11} - 1%	c^E_{13} + 1%
R1:fs	0,59%	0,67 %	-0,60 %	-0,69 %
R2:fs	0,73 %	0,53 %	-0,73 %	-0,54 %
R3:fs	0,74 %	0,53 %	-0,74 %	-0,54 %
R4:fs	0,74 %	0,56 %	-0,74 %	-0,56 %
R5:fs	0,74 %	0,59 %	-0,74 %	-0,59 %
R6:fs	0,72 %	0,62 %	-0,72 %	-0,62 %
R7:fs	0,68 %	0,64 %	-0,69 %	-0,66 %
R8:fs	0,64 %	0,66 %	-0,65 %	-0,67 %
R9:fs	0,60 %	0,67 %	-0,60 %	-0,66 %
R10:fs	0,56 %	0,65 %	-0,56 %	-0,65 %
R11:fs	0,51 %	0,62 %	-0,52 %	-0,62 %
R12:fs	0,39 %	0,54 %	-0,41 %	-0,55 %

Table 5.8: Relative displacement in series resonance frequencies from Ferroperms data set, at specified radial modes for an 1% increase/decrease in the material constants c^E_{11} and c^E_{13}. A red cell color indicates a shift upwards in frequency, while a blue color indicates a shift downwards. The intensity of the color represents the magnitude of the displacement. R11 and R12 corresponds to the two pronounced peaks at the E-mode, visible in Figure 5.16 d). Data for R1 - R3 attained from simulations with frequency resolution $\Delta f = 5Hz$, while the remaining at $\Delta f = 50Hz$.

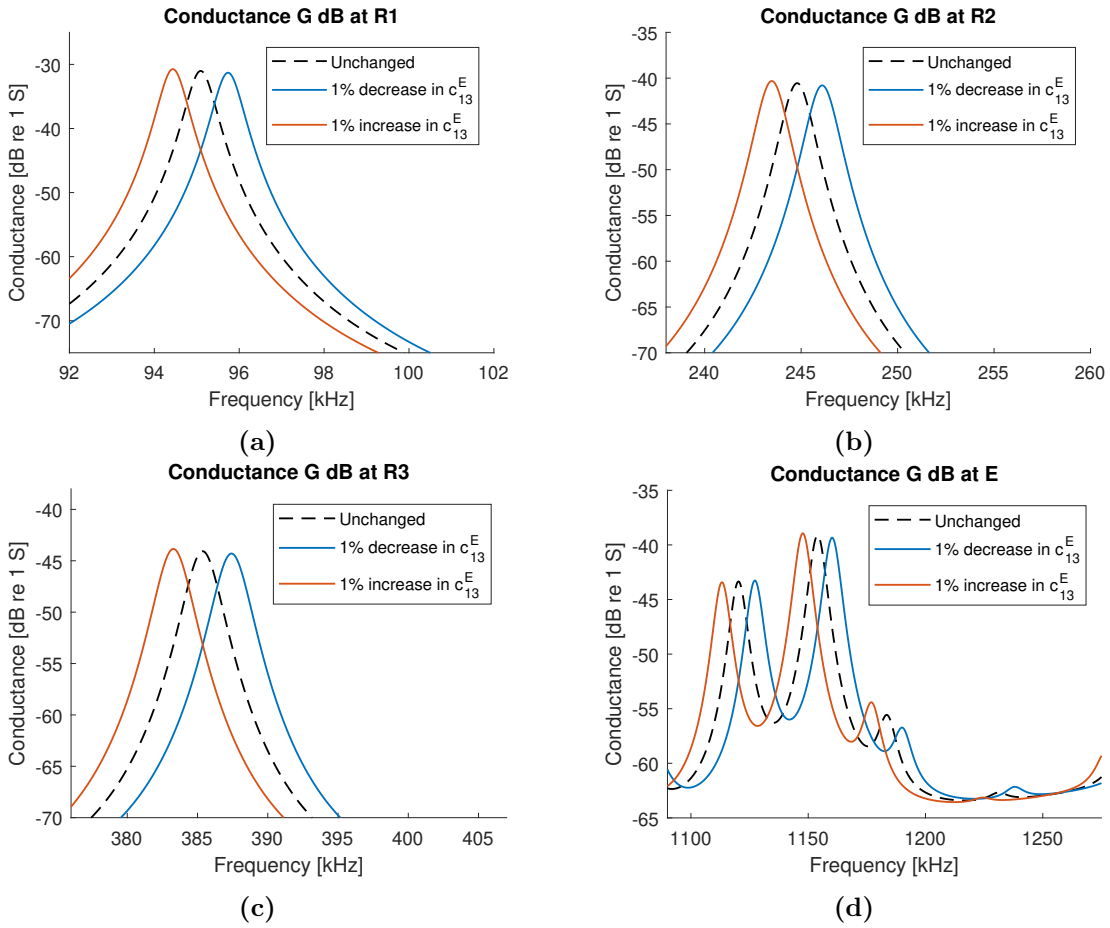

Figure 5.16: a) Simulated conductance G, for a 1% change in c^E_{13} from Ferroperms listed value, at the first three series resonance peaks - a) R1, b) R2 c) R3, and at the E-mode region d). Frequency resolution $\Delta f = 5Hz$ for a) - c), and $50Hz$ for d).

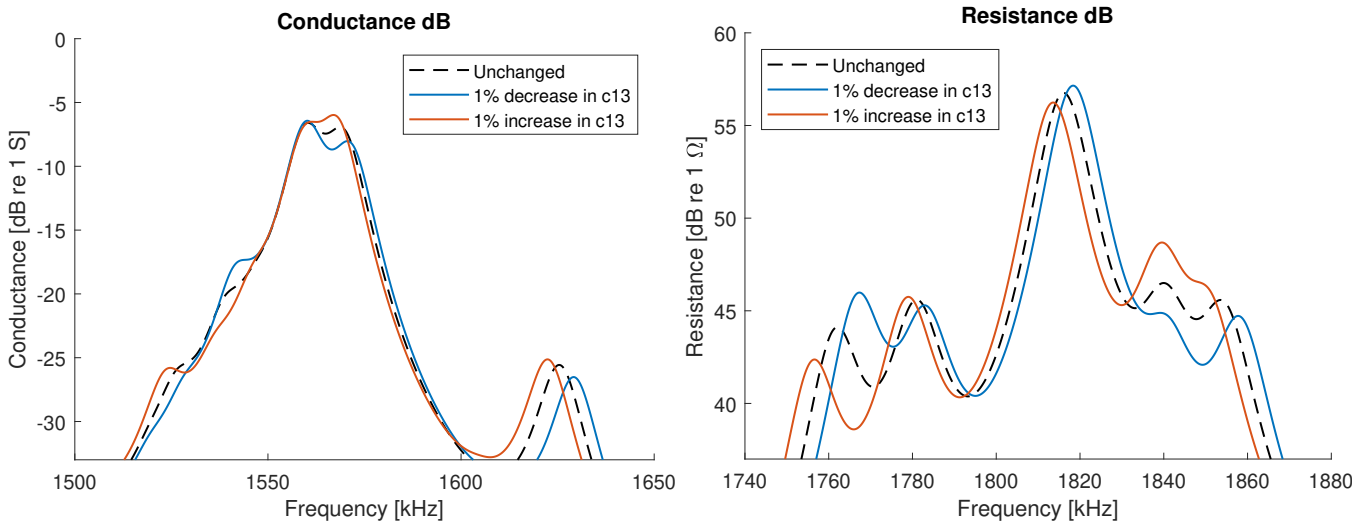

Figure 5.17: Simulated conductance G, and b) resistance R from Ferroperms data set, as well as the result a 1% increase/decrease in c_{13}^{E} has on the simulation. Frequency resolution $\Delta f = 5Hz$.

Table 5.9: Relative variation in the listed derived quantity (row) as a result of a 1% change in the stated material constant and its Q-factor (column). Color spectrum ranges from blue to red, where the former represents a negative difference,the latter a positive difference. The intensity of the color represents the magnitude of the difference from Ferroperm's simulated data.

	c^E_{33}+ 1%	c^E_{33} - 1%	Q^{cE}_{33} + 1%	Q^{cE}_{33} - 1%
R1:R	-2,15%	2,21%	0,38%	-0,38%
R1:G	-2,72%	2,83%	0,68%	-0,69%
R1:fs	0,34%	-0,35%	0,00%	0,00%
R1:BWs	0,68%	0,00%	0,00%	1,37%
R1:fp	0,19%	-0,19%	0,00%	0,00%
R1:BWp	0,00%	0,00%	-0,63%	0,63%
R2:R	-2,38%	2,47%	0,50%	-0,50%
R2:G	-2,53%	2,63%	0,54%	-0,54%
R2:fs	0,27%	-0,28%	0,00%	0,00%
R2:BWs	0,53%	0,00%	-0,53%	0,53%
R2:fp	0,25%	-0,26%	0,00%	0,00%
R2:BWp	0,26%	-0,26%	-0,52%	0,52%
R3:R	-2,40%	2,48%	0,53%	-0,54%
R3:G	-2,50%	2,59%	0,55%	-0,56%
R3:fs	0,28%	-0,29%	0,00%	0,00%
R3:BWs	0,34%	-0,34%	-0,51%	0,68%
R3:fp	0,27%	-0,28%	0,00%	0,00%
R3:BWp	0,34%	-0,17%	-0,50%	0,50%
TE1:R	-0,10%	-0,99%	0,55%	-0,55%
TE1:G	9,92%	9,33%	0,63%	-0,63%
TE1:fs	0,92%	-0,46%	0,00%	0,00%
TE1:BWs	-5,36%	6,39%	-0,43%	0,40%
TE1:fp	0,29%	-0,29%	0,00%	0,00%
TE1:BWp	-0,04%	-0,30%	-0,49%	0,52%

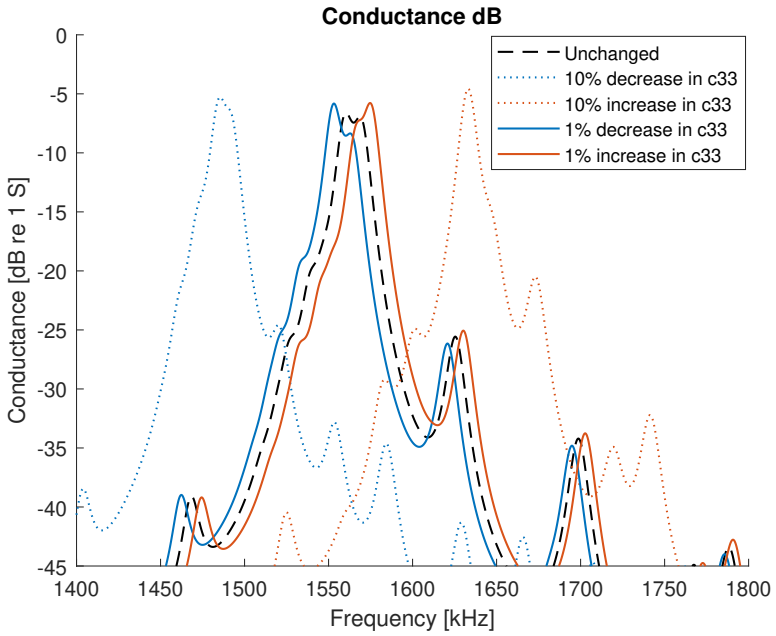

Figure 5.18: Simulated conductance G at the TE1 mode showing how a variation of $\pm 1\%$ and $\pm 10\%$ in c^E_{33} affects the simulated data from Ferroperm. Frequency resolution $\Delta f = 50Hz$.

5.3.4 variation in c^E_{33}

The elastic stiffness constant c^E_{33} and its associated Q-factor Q^{cE}_{33} have been varied by 1% from Ferroperms listed values. The resulting changes in the conductance G-, susceptance B-, and resistance R-domain are given as variation relative to the Ferroperms simulated data in Table 5.9.

In Figure 5.21 similar, but smaller, relative displacement of resonance frequencies for the R and E modes to that of c^E_{11} in Figure 5.10 can be seen. However larger relative differences can be observed for the conductance G and resistance R at the first three radial modes when c^E_{33} is varied by $\pm 1\%$.

Among the elastic stiffness constants c^E_{33} is the only one observed to shift the whole cluster of modes at the series resonance peak f_s^{TE1} in the G-domain, pictured in Figure **??**. This also means the results for the relative series resonance frequency displacement at TE1, TE1:FS, given in Table 5.9 are usable outside the boundaries for which it was attained, e.g. a 2% increase in c^E_{33} can be expected to yield approximately double the listed value. Similar results are observed for f_p^{TE1} in the R-domain.

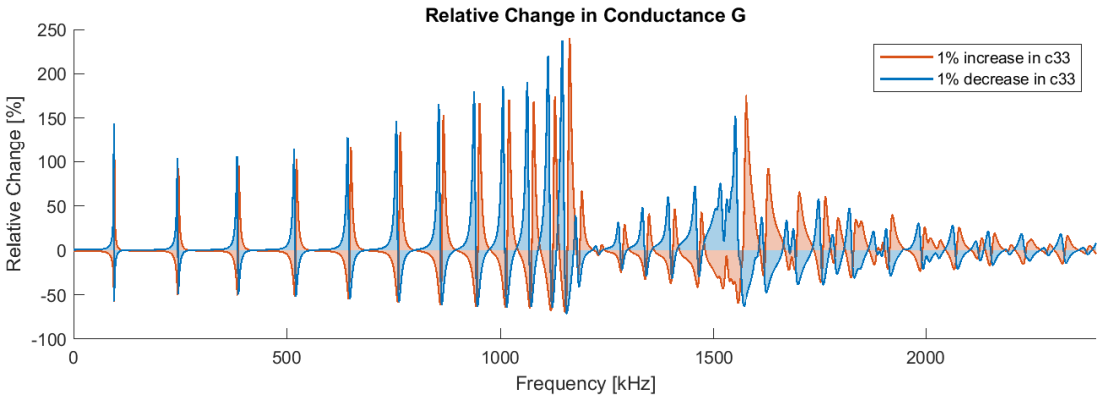

(a)

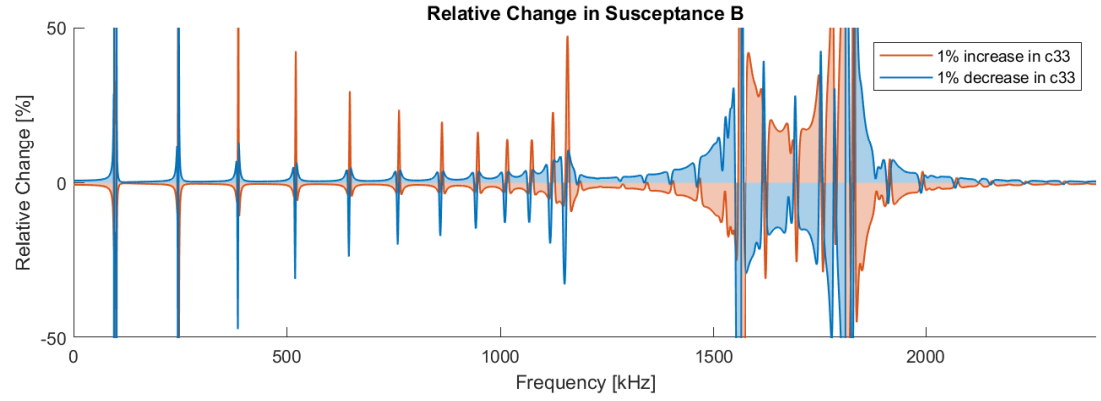

(b)

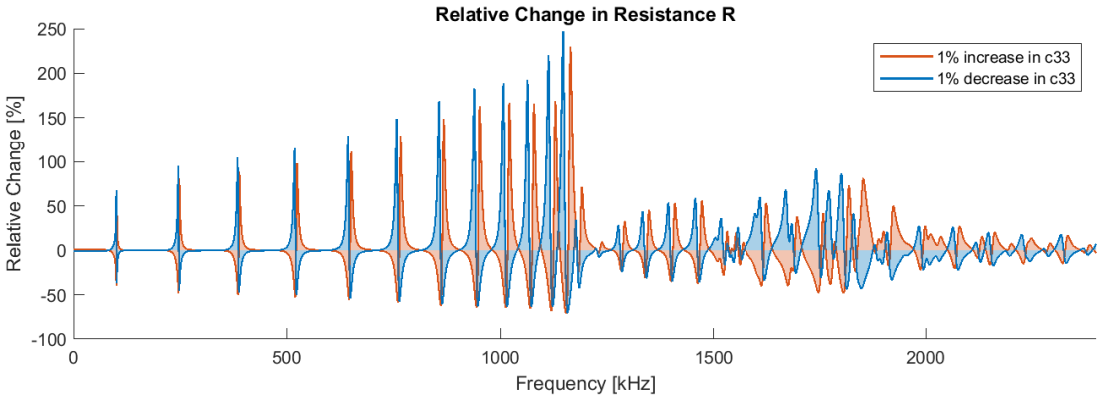

(c)

Figure 5.19: Relative variation in a) conductance G, b) susceptance B, c) resistance R from Ferroperms data set for a 1% decrease/increase in material constant c_{33}^{E}.

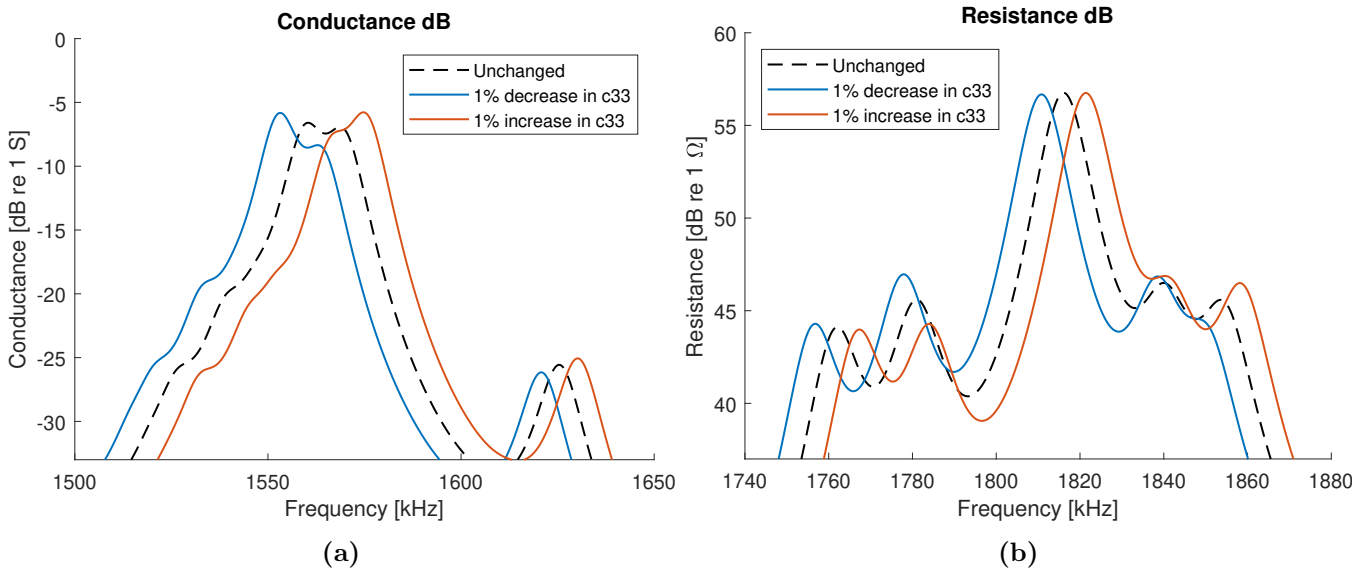

(a) (b)

Figure 5.20: Simulated conductance G, and b) resistance R from Ferroperms data set, as well as the result a 1% increase/decrease in c_{33}^{E} has on the simulation. Frequency resolution $\Delta f = 50Hz$.

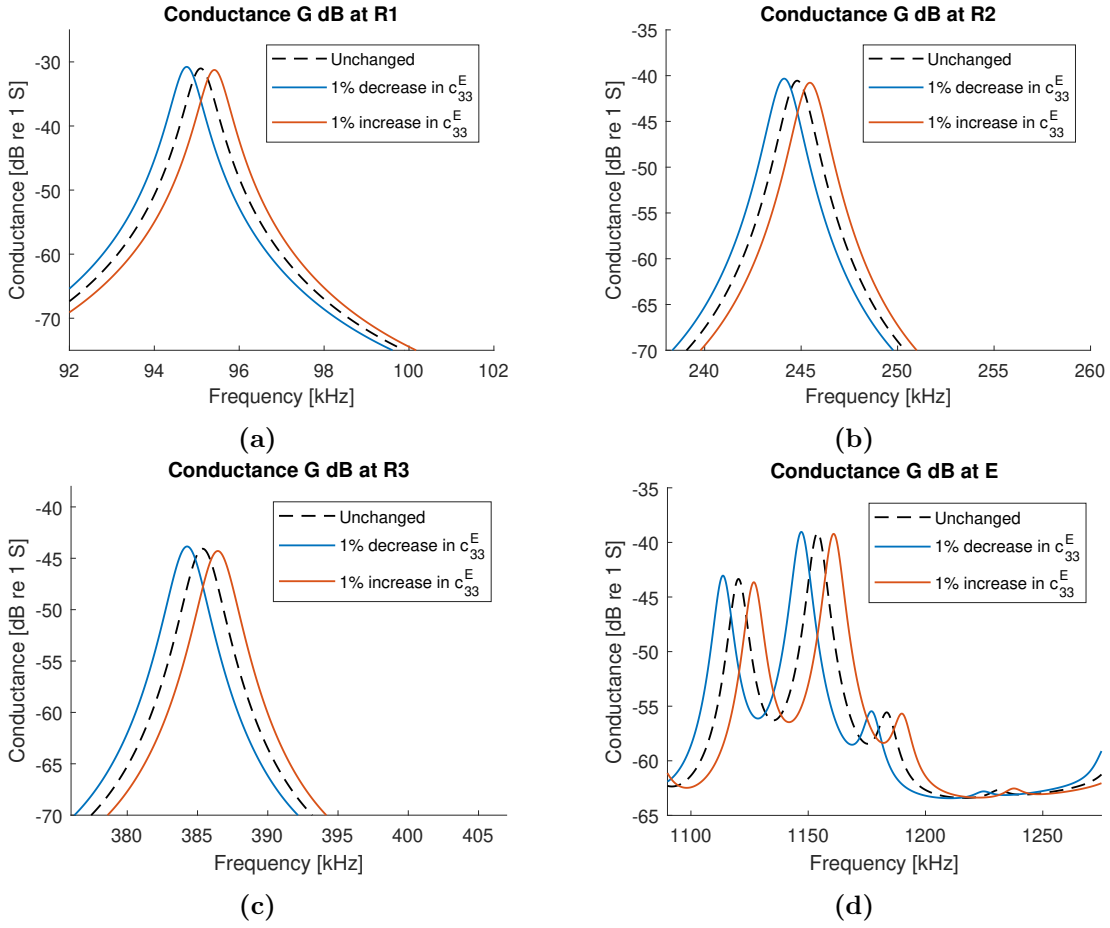

(a) (b)

(c) (d)

Figure 5.21: a) Simulated conductance G, for a 1% change in c_{33}^{E} from Ferroperms listed value, at the first three series resonance peaks - a) R1, b) R2 c) R3, and at the E-mode region d). Frequency resolution $\Delta f = 5Hz$ for a) - c), and $50Hz$ for d).

Table 5.10: Relative variation in the listed derived quantity (row) as a result of a 1% change in the stated material constant and its Q-factor (column). Color spectrum ranges from blue to red, where the former represents a negative difference,the latter a positive difference. The intensity of the color represents the magnitude of the difference from Ferroperm's simulated data.

	c^E_{44}+ 1%	c^E_{44} - 1%	Q^{cE}_{44} + 1%	Q^{cE}_{44} - 1%
R1:R	0,00%	0,00%	0,00%	0,00%
R1:G	0,00%	0,00%	0,00%	0,00%
R1:fs	0,00%	0,00%	0,00%	0,00%
R1:BWs	0,00%	0,00%	0,00%	0,00%
R1:fp	0,00%	0,00%	0,00%	0,00%
R1:BWp	0,00%	0,00%	0,00%	0,00%
R2:R	0,00%	0,00%	0,00%	0,00%
R2:G	0,00%	0,00%	0,00%	0,00%
R2:fs	0,00%	0,00%	0,00%	0,00%
R2:BWs	0,00%	0,00%	0,00%	0,00%
R2:fp	0,00%	0,00%	0,00%	0,00%
R2:BWp	0,00%	0,00%	0,00%	0,00%
R3:R	0,00%	0,00%	0,00%	0,00%
R3:G	0,00%	0,00%	0,00%	0,00%
R3:fs	0,00%	0,00%	0,00%	0,00%
R3:BWs	0,00%	0,00%	0,00%	0,00%
R3:fp	0,00%	0,00%	0,00%	0,00%
R3:BWp	0,00%	0,00%	0,00%	0,00%
TE1:R	2,52%	-6,87%	0,08%	-0,08%
TE1:G	3,76%	3,70%	0,00%	0,00%
TE1:fs	0,01%	0,47%	0,00%	0,00%
TE1:BWs	2,03%	-3,18%	-0,03%	0,00%
TE1:fp	0,05%	-0,10%	0,00%	0,00%
TE1:BWp	1,20%	254,37%	-0,11%	0,11%

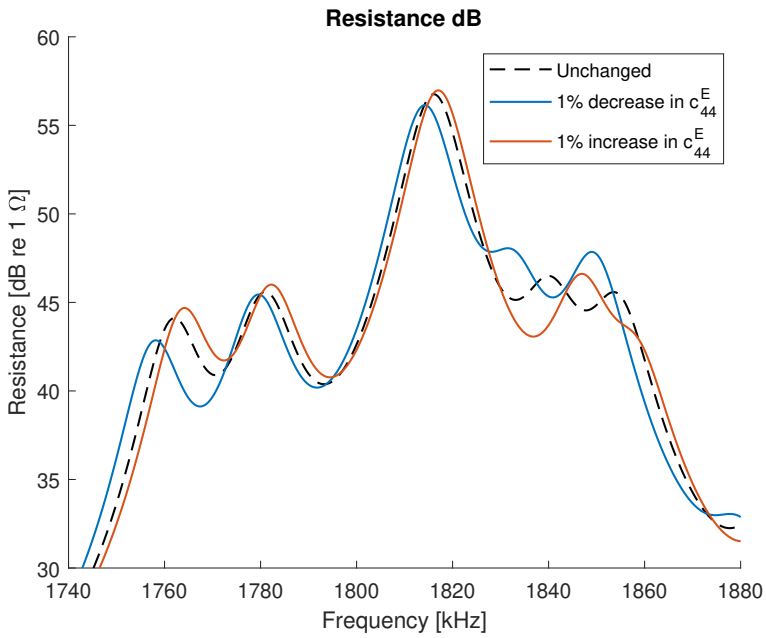

Figure 5.22: Simulated resistance R at the parallel resonance peak f_p^{TE1} showing how an increase/decrease of 1% affects the TE1-mode from Ferroperms data set. Frequency resolution $\Delta f = 50$Hz.

5.3.5 variation in c^E_{44}

The elastic stiffness constant c^E_{44} and its associated Q-factor $Q^{c^E}_{44}$ have been varied by 1% from Ferroperms listed values. The resulting changes in the conductance G-, susceptance B-, and resistance R-domain are given as variation relative to the Ferroperms simulated data in Table 5.10. Again due to the multitude of modes composing the TE1 mode, and c^E_{44} only affecting some of them significantly, it is difficult to draw any reliable quantities describing how c^E_{44} affects the TE1 mode as a whole. Meaning the results of Table 5.10 bear little analytical value. Relate to coupling factor k15

The first observed influence of c^E_{44} is at $f \approx 370$kHz for no larger than $\pm 0.003\%$ relative change in conductance G, barely visible in Figure 5.23a. A gradually fluctuating increase in the variation is observed until reaching the E-mode where it dampens again. Again an increase in the variation is seen until reaching the series resonance peak f_s^{TE1} at 1567.15kHz where it dampens, then to rapidly increase until reaching the parallel resonance peak f_p^{TE1} at 1811.40kHz. After f_p^{TE1} the variation slowly deteriorates for conductance G and resistance R, contrary to the

susceptance B and reactance X where it deteriorates rapidly. This agree well with the comparing analysis for PZT-5A, with the exception of the TS-mode [7].

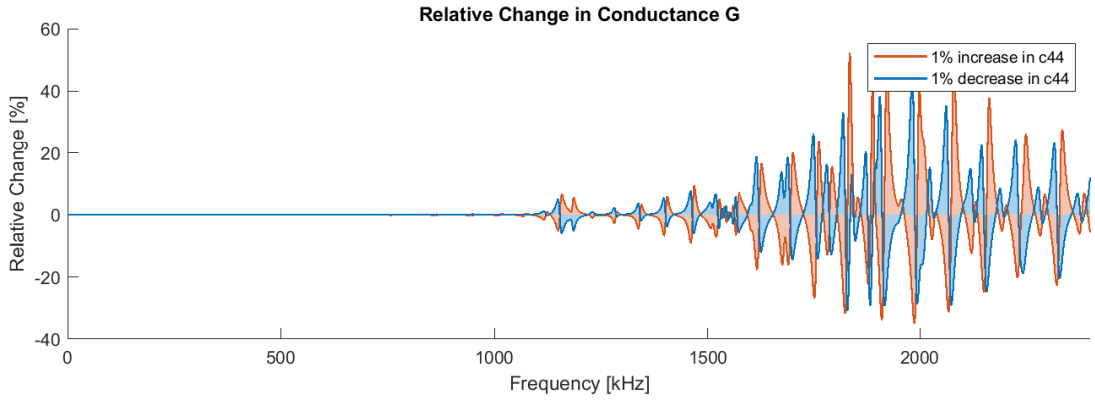

(a)

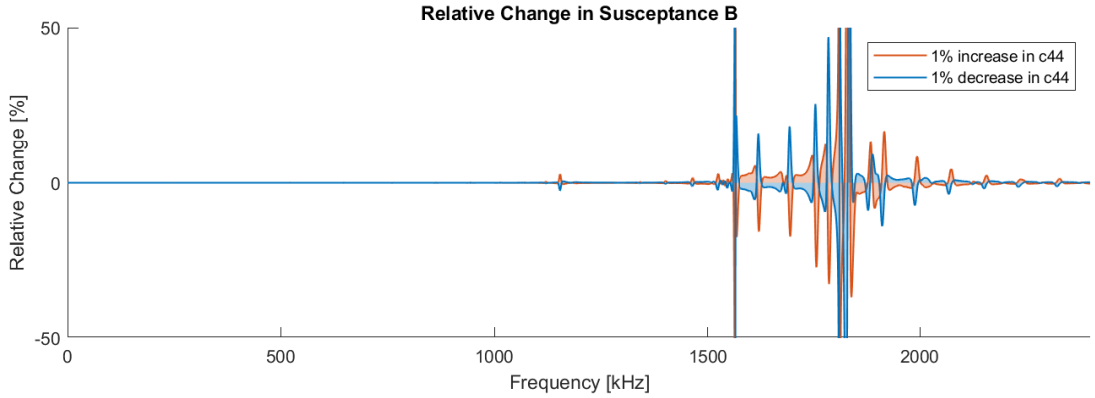

(b)

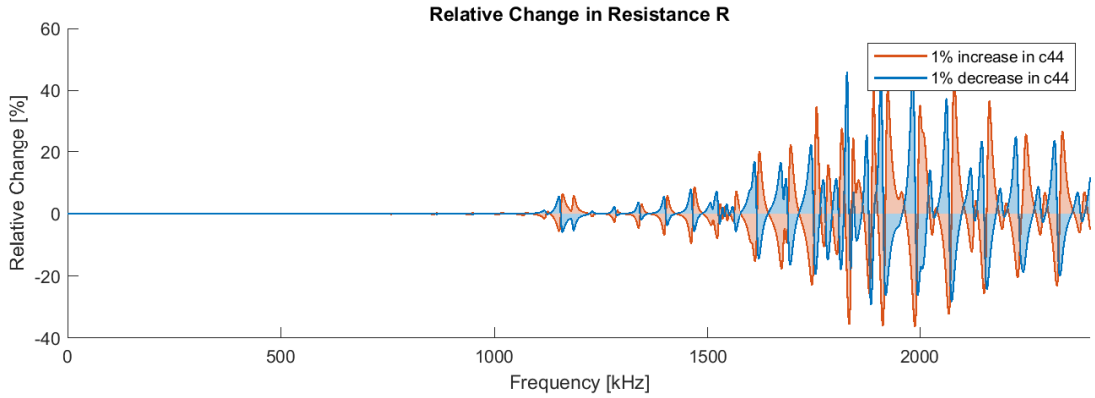

(c)

Figure 5.23: Relative variation in a) conductance G, b) susceptance B, c) resistance R, and d) reactance X from Ferroperms data set for a 1% decrease/increase in material constant c_{44}^{E}.

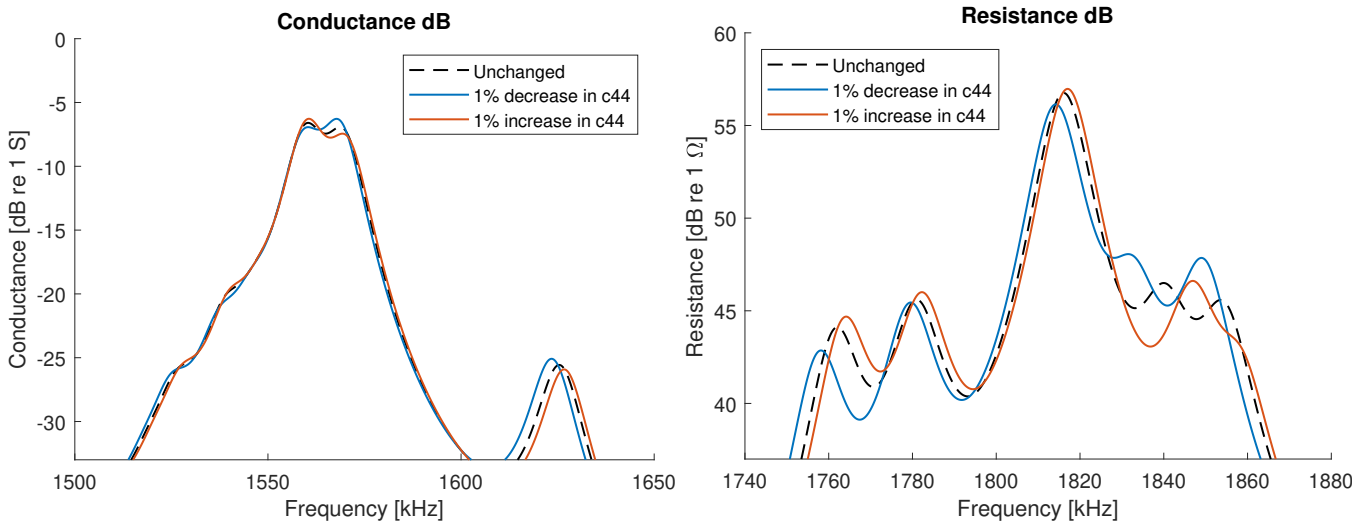

Figure 5.24: Simulated conductance G, and b) resistance R from Ferroperms data set, as well as the result a 1% increase/decrease in c_{44}^{E} has on the simulation. Frequency resolution $\Delta f = 5Hz$.

Table 5.11: Relative variation in the listed derived quantity (row) as a result of a 1% change in the stated material constant and its Q-factor (column). Color spectrum ranges from blue to red, where the former represents a negative difference,the latter a positive difference. The intensity of the color represents the magnitude of the difference from Ferroperm's simulated data.

	ρ + 1%	ρ - 1%
R1:R	0,50%	-0,50%
R1:G	-0,49%	0,51%
R1:fs	-0,50%	0,50%
R1:BWs	-0,68%	0,68%
R1:fp	-0,50%	0,50%
R1:BWp	-0,63%	0,00%
R2:R	0,50%	-0,50%
R2:G	-0,50%	0,50%
R2:fs	-0,50%	0,50%
R2:BWs	-0,53%	0,80%
R2:fp	-0,50%	0,50%
R2:BWp	-0,52%	0,52%
R3:R	0,50%	-0,50%
R3:G	-0,50%	0,50%
R3:fs	-0,50%	0,50%
R3:BWs	-0,51%	0,51%
R3:fp	-0,50%	0,50%
R3:BWp	-0,50%	0,67%
TE1:R	-2,25%	-0,50%
TE1:G	-0,54%	0,50%
TE1:fs	-0,49%	0,50%
TE1:BWs	-1,88%	0,50%
TE1:fp	-0,54%	0,50%
TE1:BWp	-1,31%	0,52%

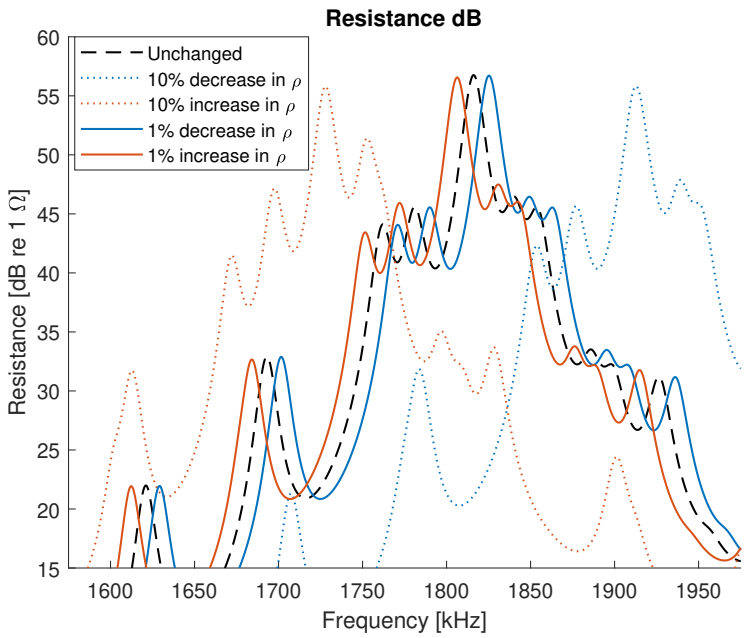

Figure 5.25: Simulated resistance R at the TE1 mode showing how a variation of $\pm 1\%$ and $\pm 10\%$ in ρ affects the simulated data from Ferroperm. Frequency resolution $\Delta f = 50Hz$.

5.3.6 variation in ρ

The material density of the piezoceramic ρ have been varied by 1% from Ferroperms listed values. The resulting changes in the conductance G-, susceptance B-, and resistance R-domain are given as variation relative to the Ferroperms simulated data in Table 5.11. The relative deviation for G, B and R from Ferroperms data in the range $0 - 2400kHz$ are shown in Figure **??**. The plots resembles that of an inverted c_{33}^E, which is to be expected as both are critically linked to f_p^{TE1}:

$$\nu^D = \sqrt{\frac{c_{33}^D}{\rho}} = 2tf_p^{\text{TE1}}$$

where c_{33}^D are associated with c_{33}^E by the thickness coupling factor k_t.

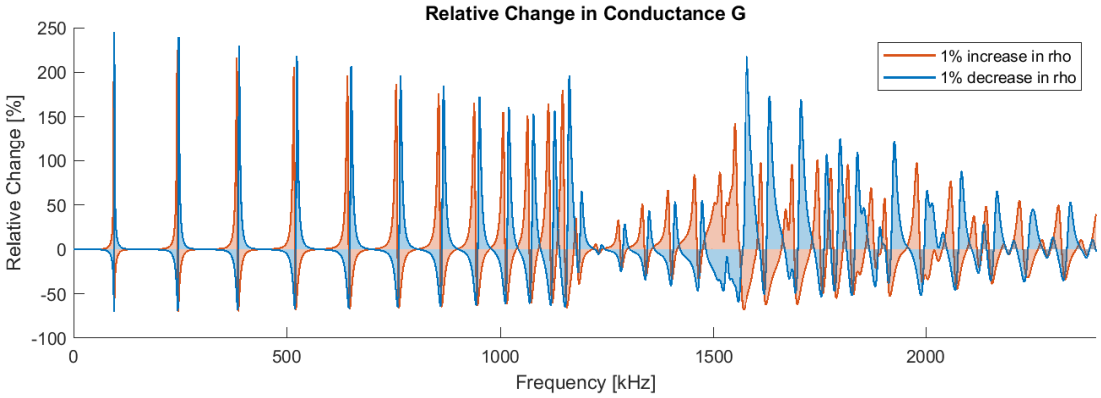

(a)

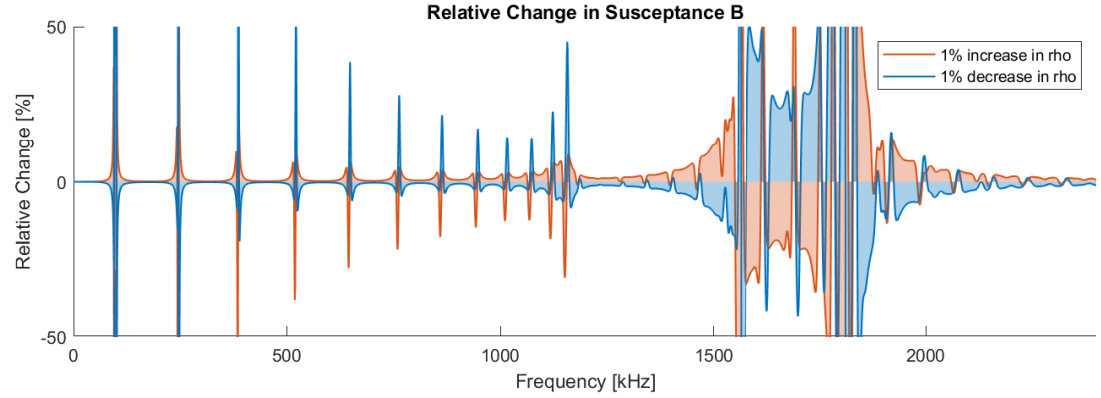

(b)

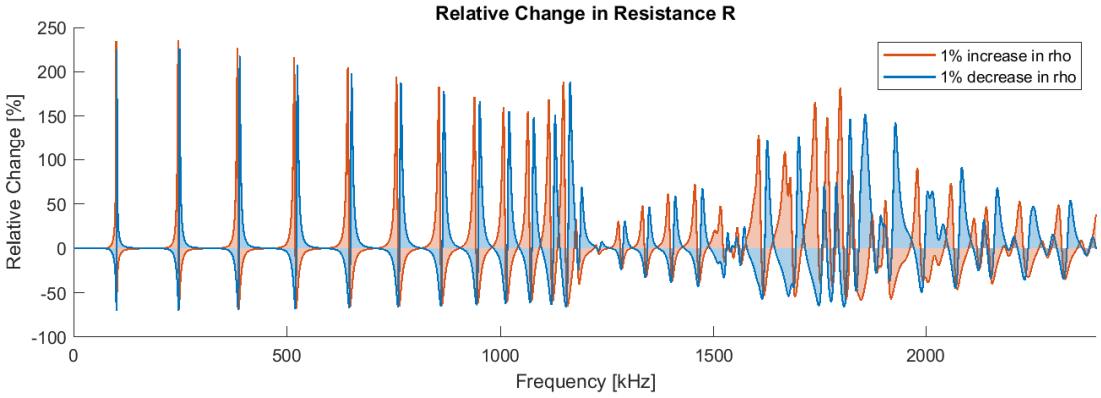

(c)

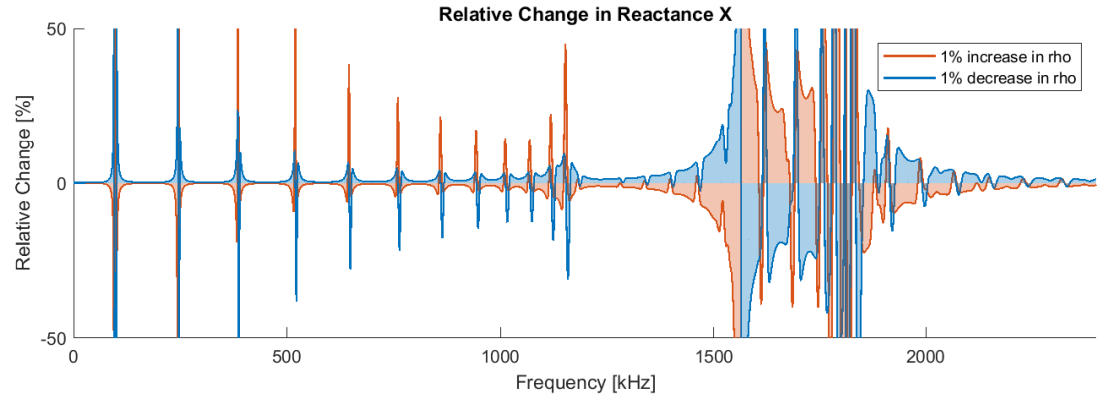

(d)

Figure 5.26: Relative variation in a) conductance G, b) susceptance B, c) resistance R, and d) reactance X from Ferroperms data set for a 1% decrease/increase in materialdensity ρ.

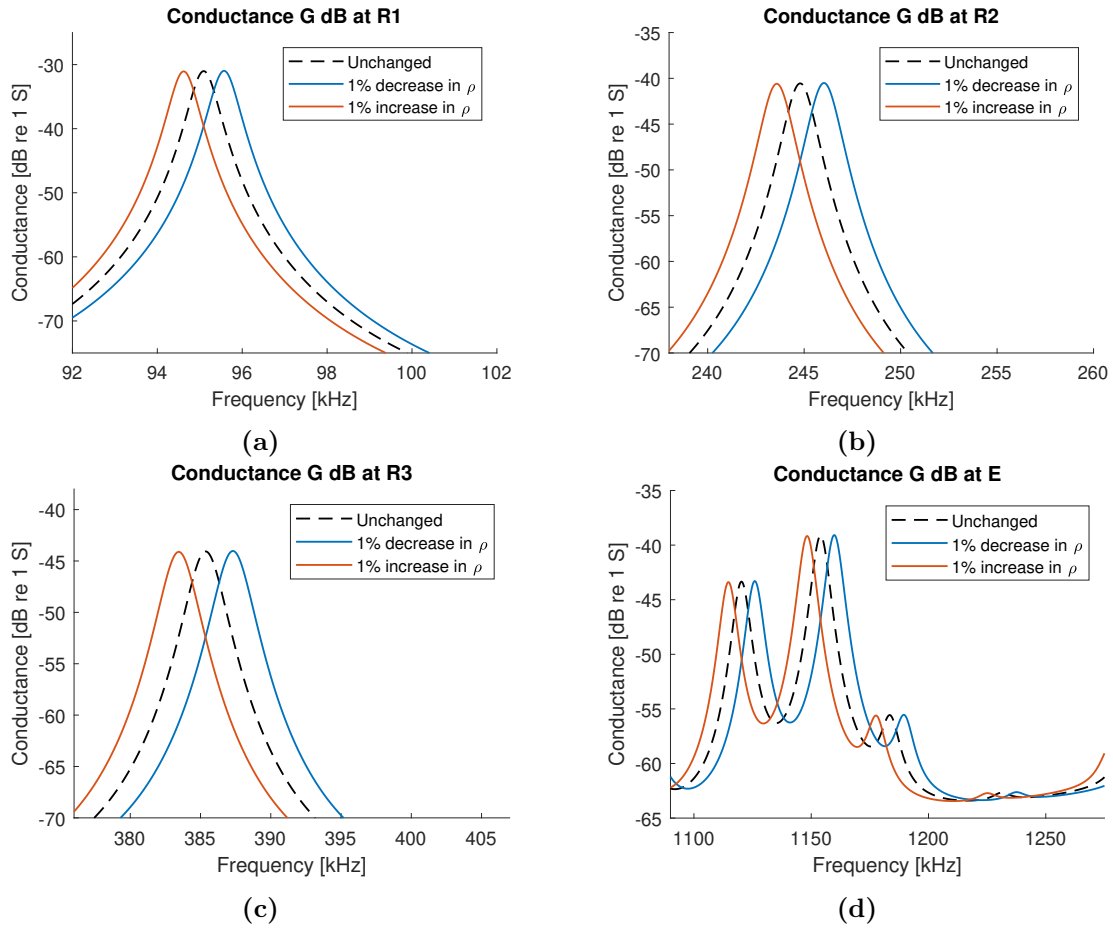

Figure 5.27: a) Simulated conductance G, for a 1% change in ρ from Ferroperms listed value, at the first three series resonance peaks - a) R1, b) R2 c) R3, and at the E-mode region d). Frequency resolution $\Delta f = 5Hz$ for a) - c), and $50Hz$ for d).

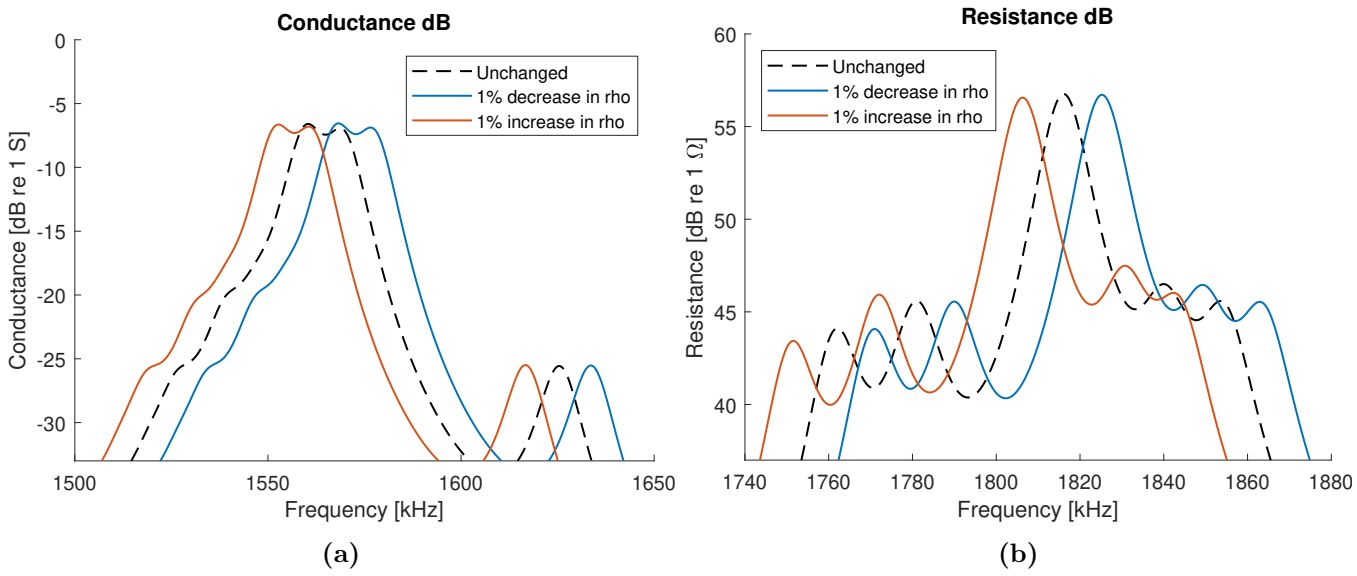

Figure 5.28: Simulated conductance G, and b) resistance R from Ferroperms data set, as well as the result a 1% increase/decrease in ρ has on the simulation. Frequency resolution $\Delta f = 50Hz$.

Table 5.12: Relative variation in the listed derived quantity (row) as a result of a 1% change in the stated material constant and its Q-factor (column). Color spectrum ranges from blue to red, where the former represents a negative difference,the latter a positive difference. The intensity of the color represents the magnitude of the difference from Ferroperm's simulated data.

	e_{31} + 1%	e_{31} - 1%	Q^e_{31} + 1%	Q^e_{31} - 1%
R1:R	-0,26%	0,25%	0,03%	-0,03%
R1:G	-0,32%	0,32%	0,00%	0,00%
R1:fs	0,00%	0,00%	0,00%	0,00%
R1:BWs	0,00%	0,00%	0,00%	0,00%
R1:fp	-0,02%	0,01%	0,00%	0,00%
R1:BWp	0,00%	0,00%	-0,63%	0,00%
R2:R	-0,31%	0,31%	0,00%	0,00%
R2:G	-0,31%	0,32%	0,00%	0,00%
R2:fs	0,00%	0,00%	0,00%	0,00%
R2:BWs	0,00%	0,00%	0,00%	0,00%
R2:fp	0,00%	0,00%	0,00%	0,00%
R2:BWp	0,00%	0,00%	0,00%	0,00%
R3:R	-0,30%	0,30%	0,00%	0,00%
R3:G	-0,30%	0,30%	0,00%	0,00%
R3:fs	0,00%	0,00%	0,00%	0,00%
R3:BWs	0,00%	0,00%	0,00%	0,00%
R3:fp	0,00%	0,00%	0,00%	0,00%
R3:BWp	0,17%	0,00%	0,00%	0,00%
TE1:R	-0,14%	0,14%	0,00%	0,00%
TE1:G	-0,14%	0,14%	0,00%	0,00%
TE1:fs	0,00%	0,00%	0,00%	0,00%
TE1:BWs	-0,25%	0,23%	0,00%	0,00%
TE1:fp	0,00%	0,00%	0,00%	0,00%
TE1:BWp	0,00%	0,04%	0,00%	0,00%

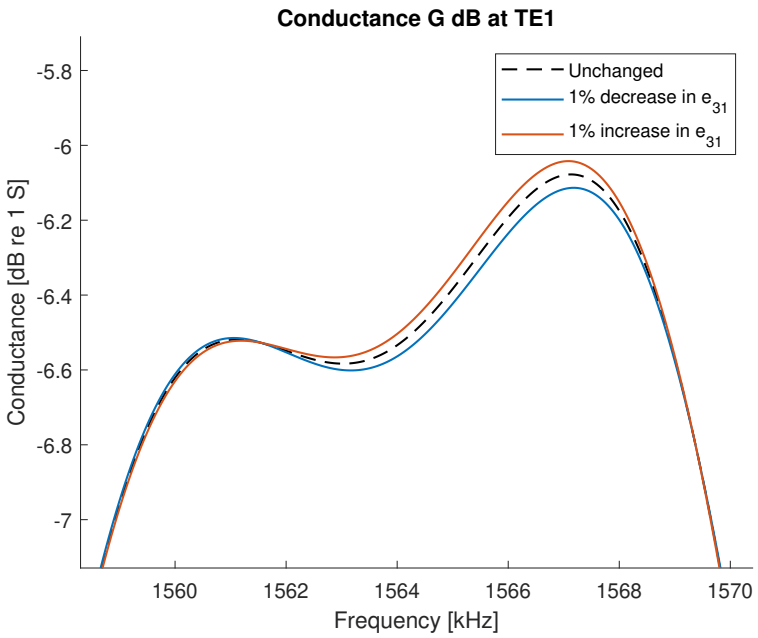

Figure 5.29: Simulated conductance G from Ferroperms data set showing how a 1% increase/decrease in e_{31} affects the series resonance peak f_s^{TE1}. Frequency resolution $\Delta f =$ 50Hz.

5.3.7 variation in e_{31}

The piezoelectric constant e_{31} and its associated Q-factor Q^e_{31} have been varied by 1% from Ferroperms listed values. The resulting changes in the conductance G-, susceptance B-, and resistance R-domain are given as variation relative to the Ferroperms simulated data in Table 5.12.

In Figure **??** e_{31} are seen to affect most of the observed spectrum, however not by more than $\pm 2\%$. For the conductance G at the first radial modes a rounded and even shape of the variation is observed. This can be interpreted as an increase/decrease in only the conductance G without affecting the series resonance frequencies, whilst the tall spikes seen in Figure 5.30c in the R-domain for R1 and R2 are due to the modes being shifted in parallel resonance frequency.

From Table 5.12 the relative change in the conductance G at R1, R2, and R3, and the relative change in the resistance R at R2 and R3 are all of similar absolute values. The relative change in the resistance R at R1 is smaller in magnitude. This behaviour agrees well with PZT-5A [7], except the results are of the opposite sign. This is likely due to PZT-5A having a negative e_{31} value, while Pz37HD a

positive.

Table 5.12 shows only that the parallel resonance frequency of R1 are affected by varying e_{31} 1%. Consulting the extended sensitivity analysis tables in Appendix Table C.1 and C.2 the relative displacement in the parallel resonance frequencies for R2 and R3 are listed as $\pm 0,002\%$ and $\pm 0,001\%$ for a $\mp 1\%$ change respectively. Such a rapid decrease in the relative displacement of the parallel resonance frequencies for the first two radial modes is also seen for PZT-5A [7], with the exception of the displacement going the opposite way than for Pz37HD. This again is likely due to the PZT-5A having a negative e_{31} value, while Pz37HD a positive. Figure 5.31 a) and b) are plotted with the same resolution and aspect ratio to illustrate how much the influence e_{31} has on the resonance frequencies decreases between the first and second radial mode.

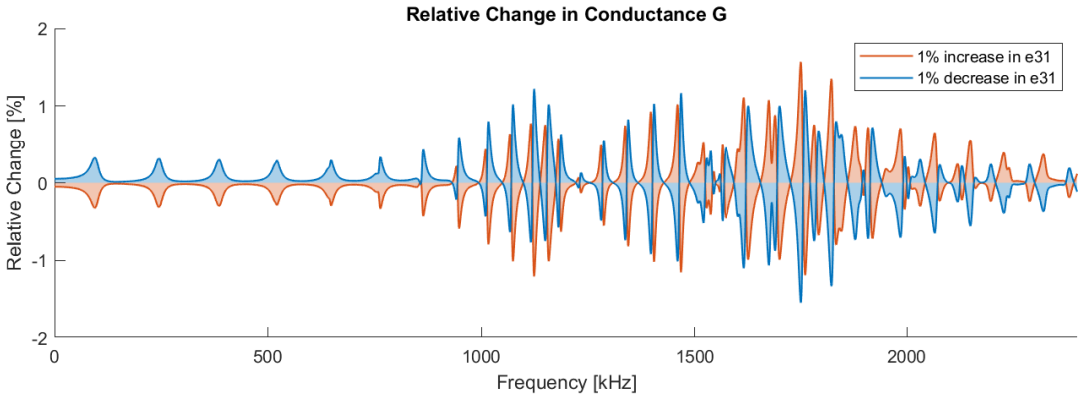

(a)

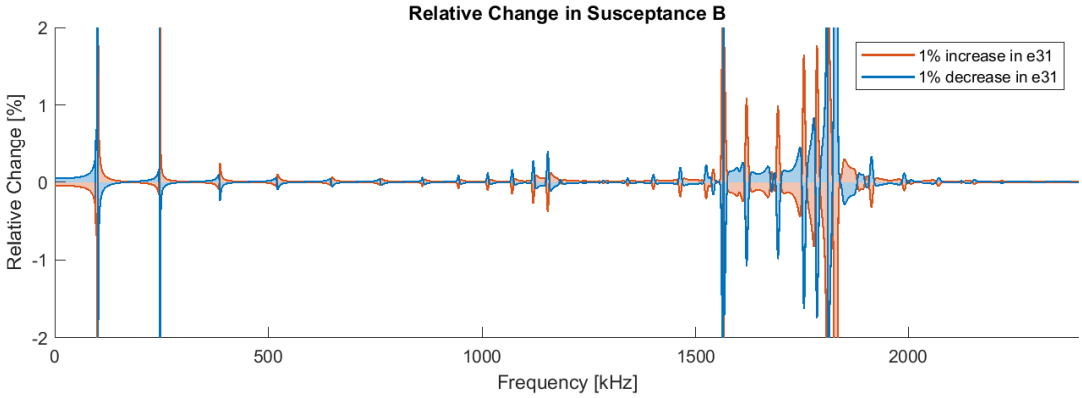

(b)

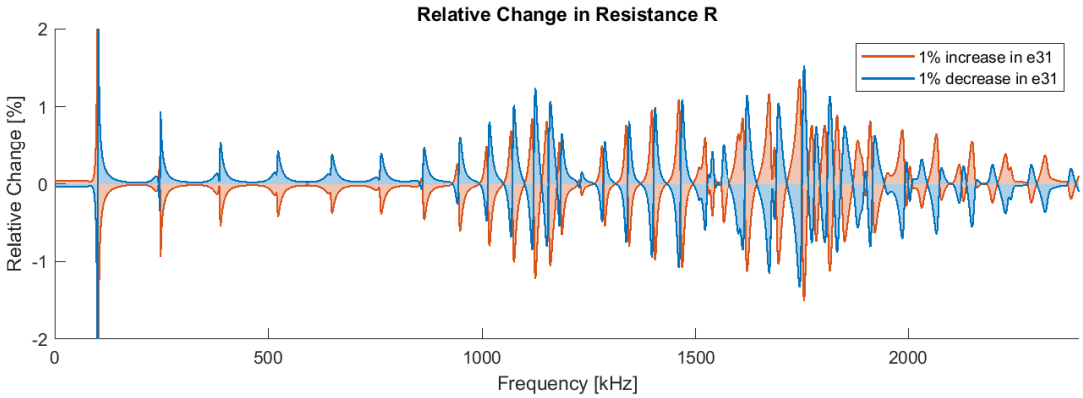

(c)

Figure 5.30: Relative variation from Ferroperms data for a 1% change in e_{31} in a) conductance G, b) susceptance B, and c) resistance R. Frequency resolution $\Delta f = 50$Hz.

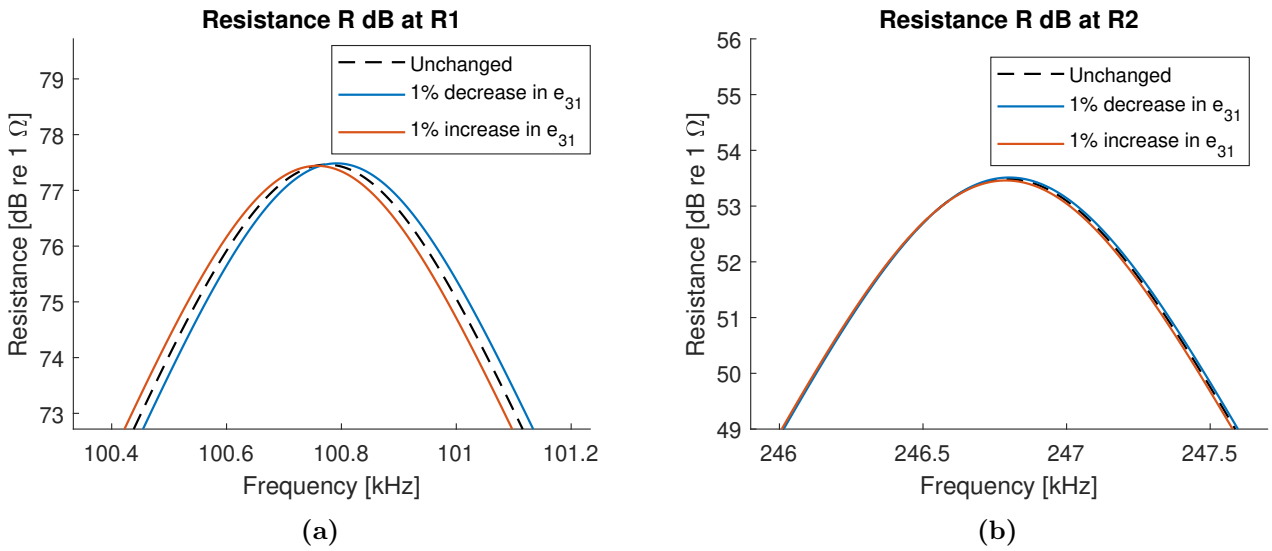

Figure 5.31: a) Simulated resistance R, for a 1% change in e_{31} from Ferroperms data, at a) R1, and b) R2. Frequency resolution $\Delta f = 5Hz$.

Table 5.13: Relative variation in the listed derived quantity (row) as a result of a 1% change in the stated material constant and its Q-factor (column). Color spectrum ranges from blue to red, where the former represents a negative difference,the latter a positive difference. The intensity of the color represents the magnitude of the difference from Ferroperm's simulated data.

	e_{33} + 1%	e_{33} - 1%	Q^e_{33} + 1%	Q^e_{33} - 1%
R1:R	0,69%	-0,72%	-0,07%	0,07%
R1:G	2,34%	-2,31%	0,00%	0,00%
R1:fs	0,00%	0,00%	0,00%	0,00%
R1:BWs	0,00%	0,00%	0,00%	0,00%
R1:fp	0,09%	-0,09%	0,00%	0,00%
R1:BWp	0,00%	0,00%	0,00%	-0,63%
R2:R	1,02%	-1,04%	-0,01%	0,01%
R2:G	2,32%	-2,29%	0,00%	0,00%
R2:fs	0,00%	0,00%	0,00%	0,00%
R2:BWs	0,00%	0,00%	0,00%	0,00%
R2:fp	0,01%	-0,01%	0,00%	0,00%
R2:BWp	0,00%	0,00%	0,00%	0,00%
R3:R	1,00%	-1,02%	-0,01%	0,01%
R3:G	2,29%	-2,26%	0,00%	0,00%
R3:fs	0,00%	0,00%	0,00%	0,00%
R3:BWs	0,00%	0,00%	0,00%	0,00%
R3:fp	0,01%	-0,01%	0,00%	0,00%
R3:BWp	0,00%	0,00%	0,00%	0,00%
TE1:R	-1,37%	-0,58%	-0,14%	0,14%
TE1:G	2,79%	-2,72%	-0,02%	0,02%
TE1:fs	0,04%	-0,04%	0,00%	0,00%
TE1:BWs	0,88%	-0,88%	0,00%	-0,03%
TE1:fp	0,17%	-0,17%	0,00%	0,00%
TE1:BWp	-0,97%	0,45%	0,15%	-0,07%

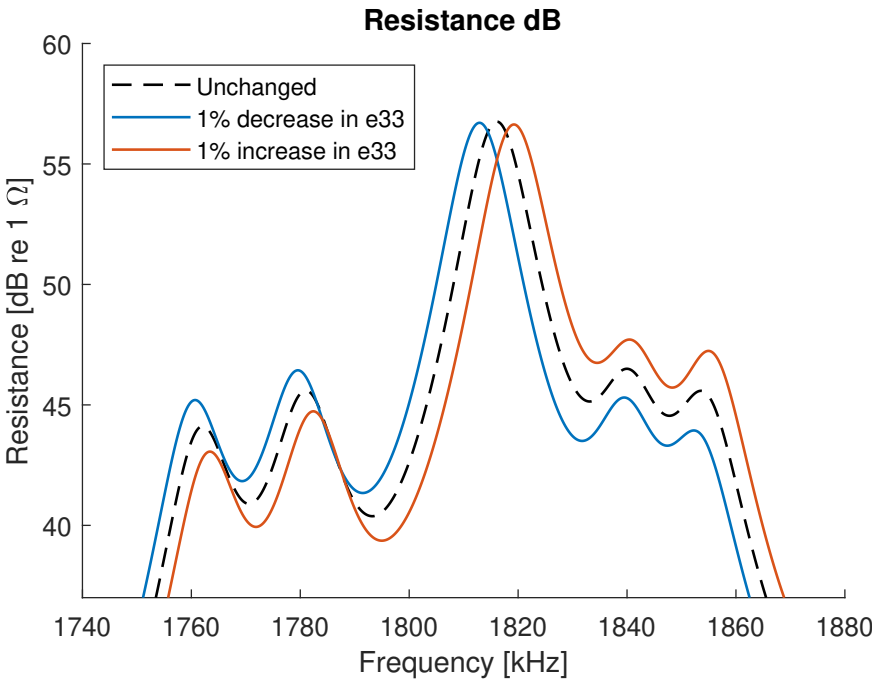

Figure 5.32: Simulated resistance R at the TE1 mode showing how a variation of $\pm 1\%$ in e^E_{33} affects the simulated data from Ferroperm. Frequency resolution $\Delta f = 50Hz$.

5.3.8 variation in e_{33}

The piezoelectric constant e_{33} and its associated Q-factor Q^e_{33} have been varied by 1% from Ferroperms listed values. The resulting changes in the conductance G-, susceptance B-, and resistance R-domain are given as variation relative to the Ferroperms simulated data in Table 5.13.

In Figure 5.33a a 1% increase/decrease in e_{33} is seen to raise/lower the overall curve of the conductance G for the first 6 radial modes. The same is observed for PZT-5A, where Fardal comments that this is likely the radial modes working seemingly undisturbed by other modes [7]. No displacement of the series resonance frequencies are observed for the radial modes.

In Figure 5.33b a 1% increase in e_{33} show relative change in susceptance B starting out at approximately $0,85$ for $f < f_s^{\mathrm{R1}}$, decreasing slightly after R1, then steadily increasing while approaching the E-mode region at $f \approx 1150$kHz. After this it rapidly decreases, then increases to a steady level of approximately 1% until reaching f_s^{TE1}, only to be dampened for a moment when at the series resonance frequency. After this it keeps a high relative variation until exponentially decreas-

ing again after the parallel resonance frequency f_p^{TE1}. For a 1% decrease the same is observed, but with a negative relative change. The same behaviour is seen for PZT-5A [7].

In Figure 5.33c a 1% increase/decrease in e_{33} shows similar behaviour to that of the relative variation in conductance G in a), but shows a larger variation near the parallel resonance region for the TE1 mode. The parallel resonance frequencies for the radial modes are also observed to be displaced, with R1 being shifted the most. This is further illustrated in Figure 5.35 and **??**, and agrees well with the results for PZT-5A [7].

In Figure 5.34 a 1% increase appears to shift the whole cluster of modes at TE1, for both the series and parallel resonance peaks, upwards in frequency, while a 1% decrease shifting it downwards. The relatively larger frequency shift for the parallel resonance are both observable in the variation for the resistance R in Figure 5.33c, and the derived value for the relative parallel resonance frequency displacement in Table 5.13. The latter being TE1:FP $= 0,17\%$, which is close to PZT-5A's value - $0,15\%$ [7]. The relative series resonance frequency displacement TE1:FS $= 0,04\%$ is also similar to that of PZT-5A coming in at approximately $0,03\%$ [7].

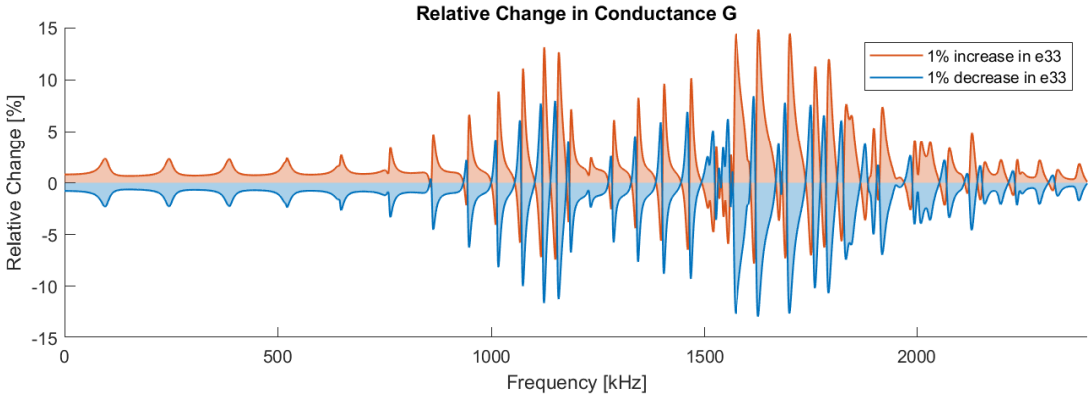

(a)

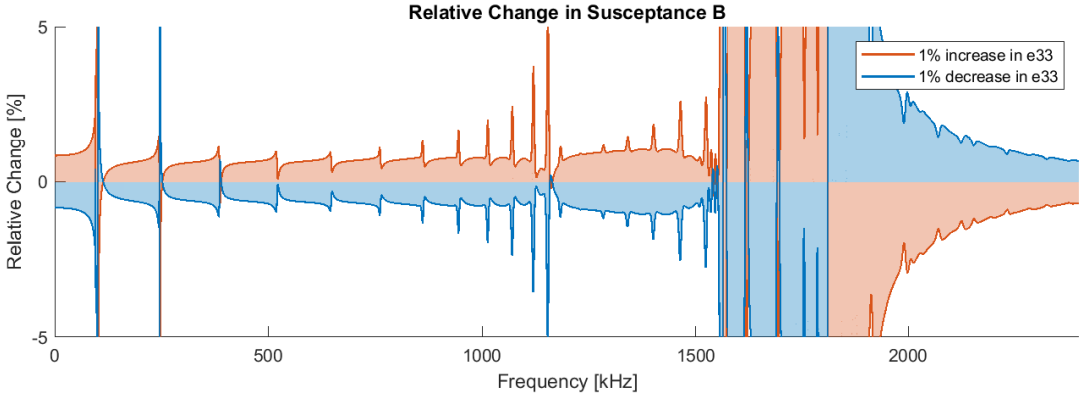

(b)

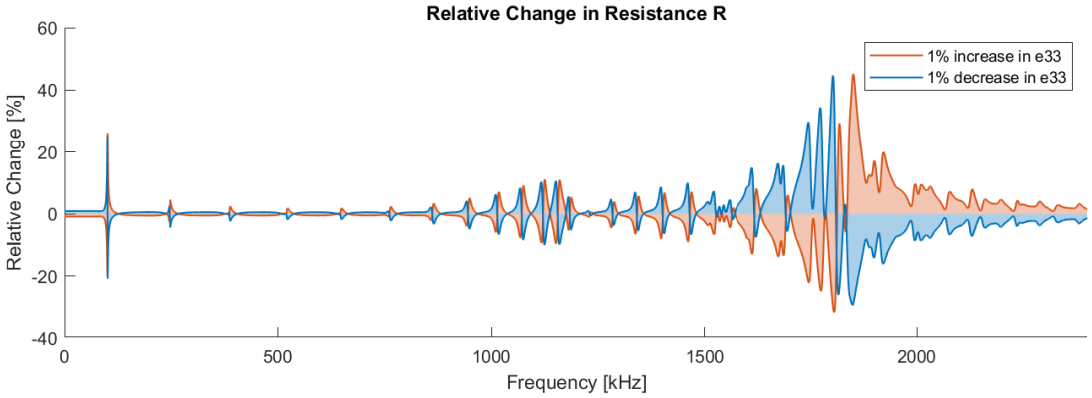

(c)

Figure 5.33: Relative change or variation from Ferroperms data set for the simulated a) conductance G, b) susceptance B, and c) resistance R when subject to a $\pm 1\%$ change in e_{33}. Frequency resolution $\Delta f = 50$Hz.

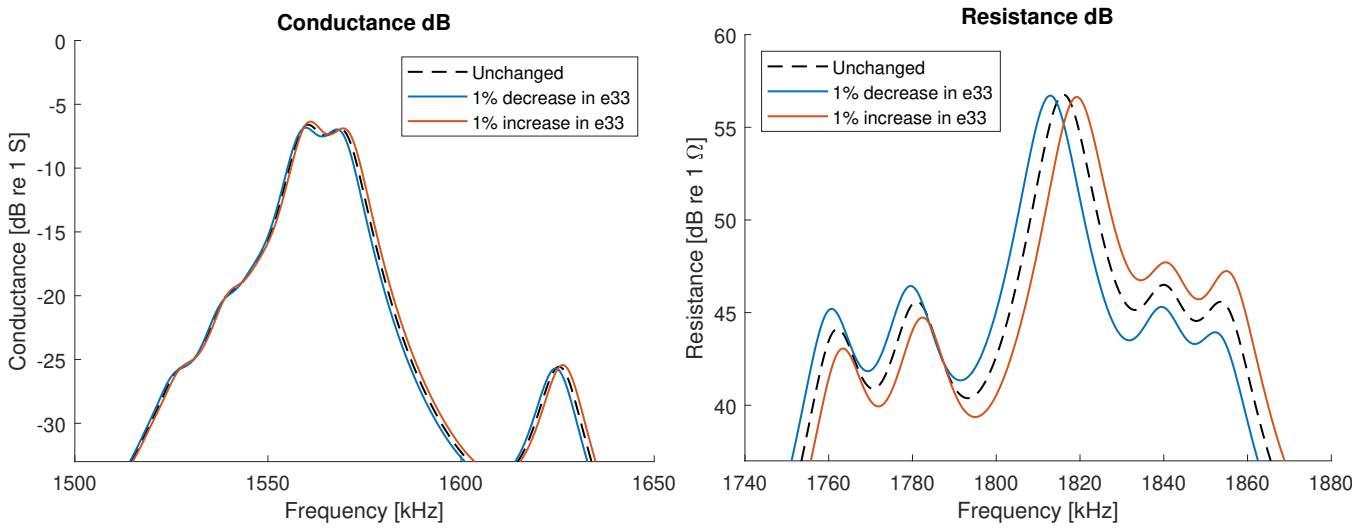

(a) (b)

Figure 5.34: a), b) description.

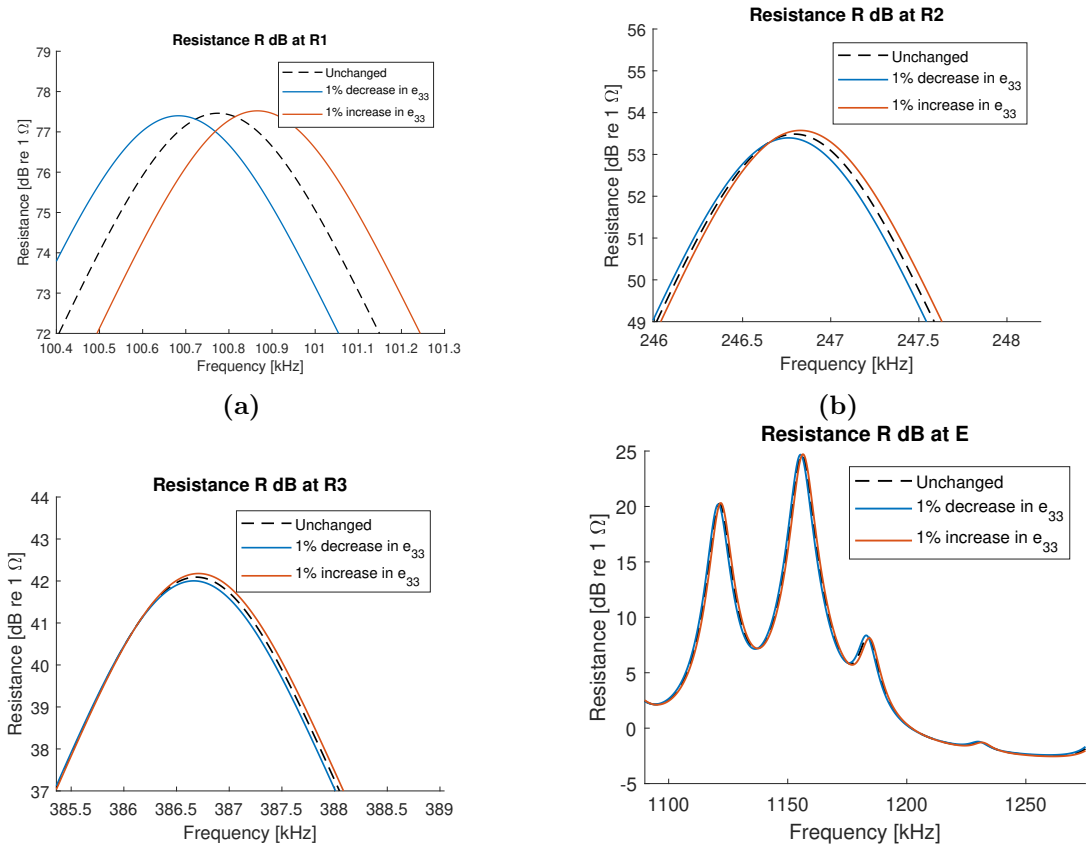

(a) (b) (c) (d)

Figure 5.35: a) Simulated resistance R, for a 1% change in e_{33} from Ferroperms listed value, at the first three parallel resonance peaks - a) R1, b) R2 c) R3, and at the E-mode region d). Frequency resolution $\Delta f = 5Hz$ for a) - c), and $50Hz$ for d).

Table 5.14: Relative variation in the listed derived quantity (row) as a result of a 1% change in the stated material constant and its Q-factor (column). Color spectrum ranges from blue to red, where the former represents a negative difference,the latter a positive difference. The intensity of the color represents the magnitude of the difference from Ferroperm's simulated data.

	e_{15} + 1%	e_{15} - 1%	Q^e_{15} + 1%	Q^e_{15} - 1%
R1:R	0,00%	0,00%	0,00%	0,00%
R1:G	0,00%	0,00%	0,00%	0,00%
R1:fs	0,00%	0,00%	0,00%	0,00%
R1:BWs	0,00%	0,00%	0,00%	0,00%
R1:fp	0,00%	0,00%	0,00%	0,00%
R1:BWp	0,00%	0,00%	0,00%	0,00%
R2:R	0,00%	0,00%	0,00%	0,00%
R2:G	0,00%	0,00%	0,00%	0,00%
R2:fs	0,00%	0,00%	0,00%	0,00%
R2:BWs	0,00%	0,00%	0,00%	0,00%
R2:fp	0,00%	0,00%	0,00%	0,00%
R2:BWp	0,00%	0,00%	0,00%	0,00%
R3:R	0,00%	0,00%	0,00%	0,00%
R3:G	0,00%	0,00%	0,00%	0,00%
R3:fs	0,00%	0,00%	0,00%	0,00%
R3:BWs	0,00%	0,00%	0,00%	0,00%
R3:fp	0,00%	0,00%	0,00%	0,00%
R3:BWp	0,00%	0,00%	0,00%	0,00%
TE1:R	1,66%	-1,76%	-0,02%	0,02%
TE1:G	-0,47%	0,52%	0,00%	0,00%
TE1:fs	0,00%	0,00%	0,00%	0,00%
TE1:BWs	0,63%	-0,63%	0,00%	0,00%
TE1:fp	0,02%	-0,02%	0,00%	0,00%
TE1:BWp	0,49%	-0,49%	0,04%	0,00%

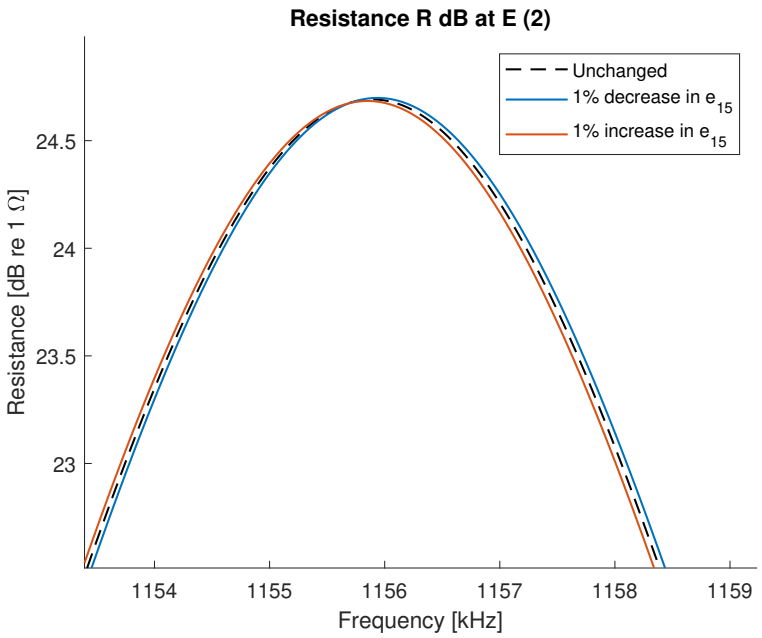

Figure 5.36: Simulated resistance R, showing how a 1% variation in e_{15} from Ferroperms data set affects the rightmost peak in the E-mode region. Frequency resolution $\Delta f = 50$Hz.

5.3.9 variation in e_{15}

The piezoelectric constant e_{15} and its associated Q-factor Q^e_{15}, not to be confused with the dielectric loss factor on Q-form $\tan\delta_e = 1/Q_e$, have been varied by 1% from Ferroperms listed values. The resulting changes in the conductance G-, susceptance B-, and resistance R-domain are given as variation relative to the Ferroperms simulated data in Table 5.14.

In Figure 5.37a a 1% change in e_{15} appears to first show a relative variation in the conductance G at $f \approx 380$kHz. Similarly as for c^E_{44}, a gradually fluctuating increase in the variation is observed until reaching the E-mode where it dampens again, then increasing steadily until reaching the series resonance frequency f_s^{TE1} where it is decreased again. After this the relative variation in G rapidly increases until approaching the parallel resonance frequency f_p^{TE1} where it slowly decreases. The same behaviour is observed for the relative change in resistance R in Figure 5.37c. For PZT-5A a broader frequency span is observed showing that the relative variation in both G and R increases again at around $1.5 \times f_s^{\text{TE1}}$, but with the exception of this the observations here agrees well with that of PZT-5A [7].

In Figure 5.37b a 1% change in e_{15} is observed to affect the relative variation in the susceptance B first at $f \approx 245$kHz, and then afterwards at $f \approx 380$kHz which is the same as for G and R. A steady increase in the relative variation is seen until reaching the series resonance frequency f_s^{TE1} where a narrow spike appears. The relative variation in B are further increased while creeping up on the parallel resonance frequency f_p^{TE1} where it increases rapidly, only to deteriorate quickly after. Similar behaviour is observed for PZT-5A [7].

Notable variations near the E-mode can be seen in the variation plots for conductance G and resistance R in Figure 5.37a and 5.37c. This variation originates from the rightmost pronounced peak, i.e. for the resistance R, in Figure 5.39, which is zoomed in at in Figure **??**. Similar plots can be shown for the conductance G.

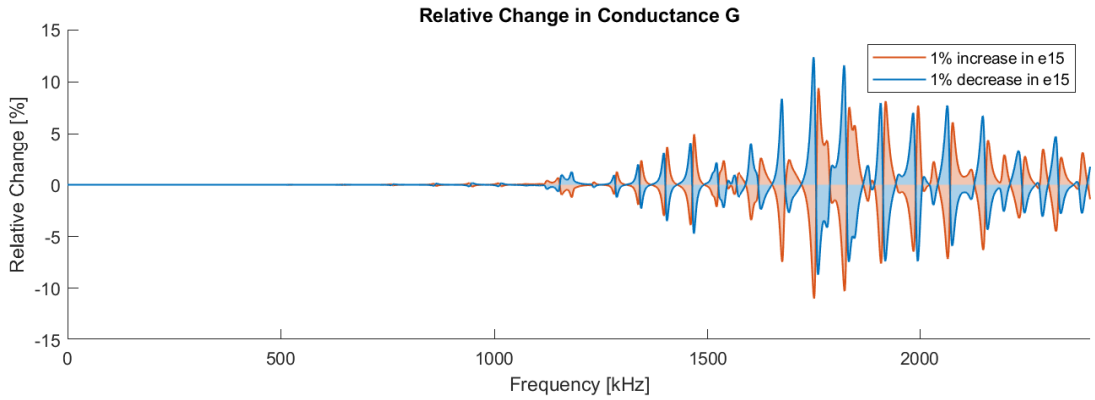

(a)

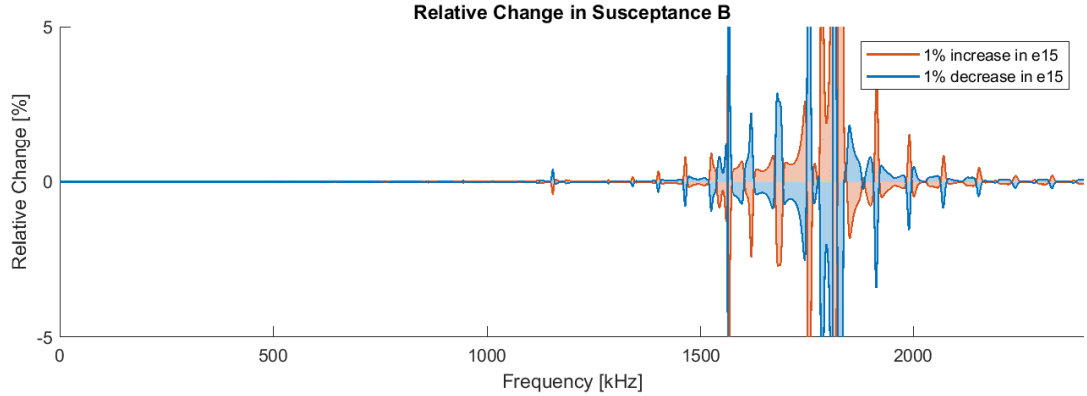

(b)

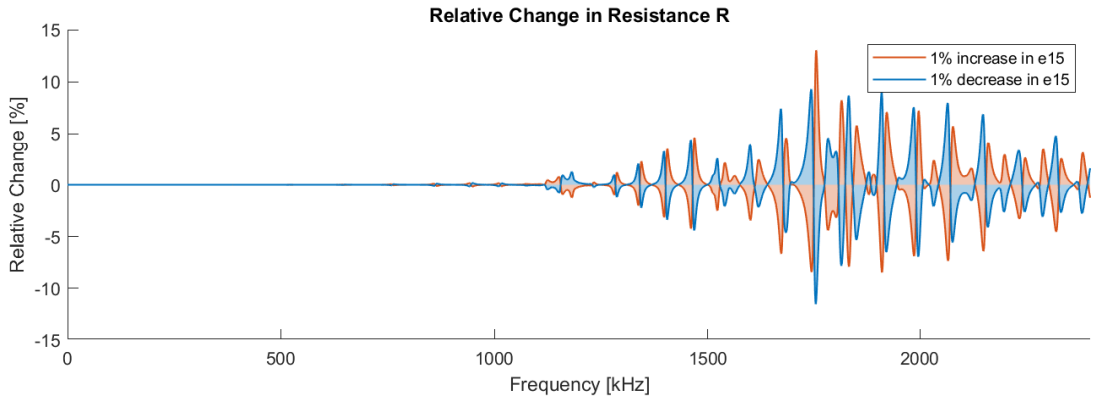

(c)

Figure 5.37: Relative variation from Ferroperms data for a 1% change in e_{15} in a) conductance G, b) susceptance B, and c) resistance R. Frequency resolution $\Delta f = 50$Hz.

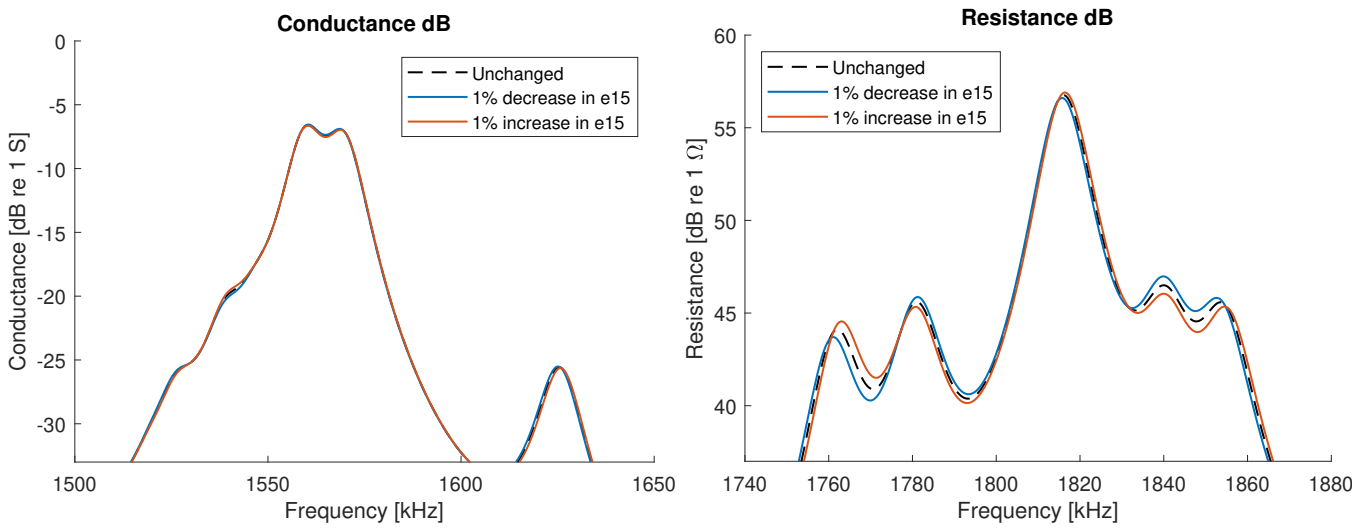

(a) **(b)**

Figure 5.38: Simulated conductance G, and b) resistance R from Ferroperms data set, as well as the result a 1% increase/decrease in e_{15} has on the simulation. Frequency resolution $\Delta f = 5Hz$.

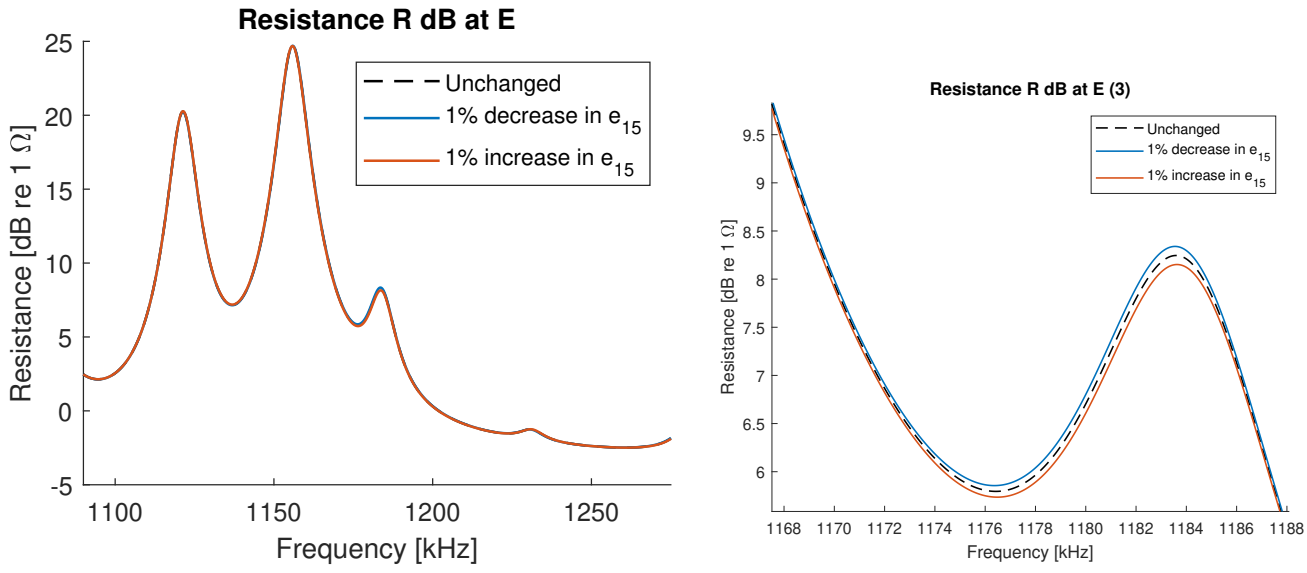

(a) **(b)**

Figure 5.39: a) Simulated resistance R and b) resistance R from Ferroperms data set showing how a 1% change in e_{15} affects the E-mode region. Frequency resolution $\Delta f = 50$Hz.

5.3.10 variation in ε_{11}^S

The dielectric constant ε_{11}^S and its associated Q-factor $Q_{11}^{\varepsilon^S}$ have been varied by 1% from Ferroperms listed values. The resulting changes in the conductance G-, susceptance B-, and resistance R-domain are given as variation relative to the Ferroperms simulated data in Table 5.15.

In accordance with the other 2 shear material constants, c_{44}^E and e_{15}, when the dielectric material constant ε_{11}^S is varied by 1% it is first observed in Figure 5.41a to affect the conductance G around $f = 380$kHz by a relative variation in G less than $0,0004\%$. Afterwards the variation steadily increases until passing the E-mode region where it decreases, and then increasing again till the frequency has reached the series resonance TE1 mode. At the peak the relative variation in G is slightly decreased, only to rapidly increase afterwards. After reaching the parallel resonance frequency f_p^{TE1} the variation decreases slowly to a seemingly stable level of 2% for both relative variation in conductance G and resistance R.

In Figure 5.41b a 1% increase/decrease in ε_{11}^S first starts showing changes in the relative variation of the susceptance B at approximately $f = 240$kHz, same as for c_{44}^E and e_{15}. After this the relative variation in B follows the same patters as described for the conductance G, with the exception that the variation increases at the series resonance frequency f_s^{TE1}, and that the variation decreases rapidly after the parallel resonance frequency f_p^{TE1}.

The variation plot for the resistance R in Figure 5.41c bears great resemblance to that for the conductance G in Figure 5.41a.

Table 5.15: Relative variation in the listed derived quantity (row) as a result of a 1% change in the stated material constant and its Q-factor (column). Color spectrum ranges from blue to red, where the former represents a negative difference,the latter a positive difference. The intensity of the color represents the magnitude of the difference from Ferroperm's simulated data.

	ε^{S}_{11} + 1%	ε^{S}_{11} - 1%	Q^{ES}_{11} + 1%	Q^{ES}_{11} - 1%
R1:R	0,00%	0,00%	0,00%	0,00%
R1:G	0,00%	0,00%	0,00%	0,00%
R1:fs	0,00%	0,00%	0,00%	0,00%
R1:BWs	0,00%	0,00%	0,00%	0,00%
R1:fp	0,00%	0,00%	0,00%	0,00%
R1:BWp	0,00%	0,00%	0,00%	0,00%
R2:R	0,00%	0,00%	0,00%	0,00%
R2:G	0,00%	0,00%	0,00%	0,00%
R2:fs	0,00%	0,00%	0,00%	0,00%
R2:BWs	0,00%	0,00%	0,00%	0,00%
R2:fp	0,00%	0,00%	0,00%	0,00%
R2:BWp	0,00%	0,00%	0,00%	0,00%
R3:R	0,00%	0,00%	0,00%	0,00%
R3:G	0,00%	0,00%	0,00%	0,00%
R3:fs	0,00%	0,00%	0,00%	0,00%
R3:BWs	0,00%	0,00%	0,00%	0,00%
R3:fp	0,00%	0,00%	0,00%	0,00%
R3:BWp	0,00%	0,00%	0,00%	0,00%
TE1:R	-0,53%	0,52%	0,03%	-0,03%
TE1:G	-0,09%	0,09%	-0,01%	0,01%
TE1:fs	0,00%	0,00%	0,00%	0,00%
TE1:BWs	-0,50%	0,50%	0,00%	0,00%
TE1:fp	-0,01%	0,01%	0,00%	0,00%
TE1:BWp	-0,15%	0,19%	-0,04%	0,07%

Figure 5.40:

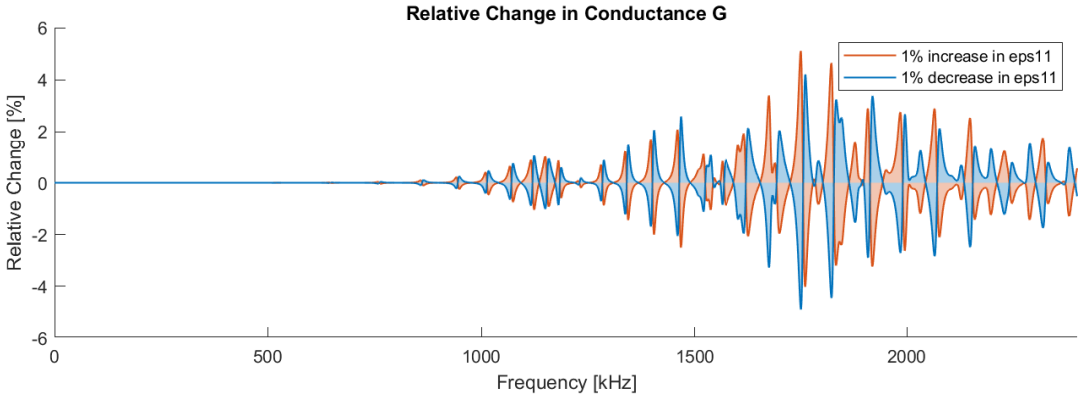

(a)

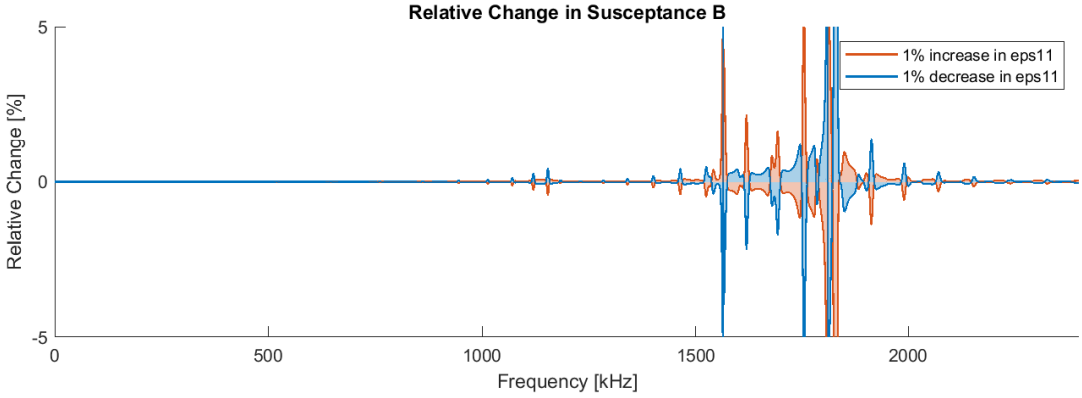

(b)

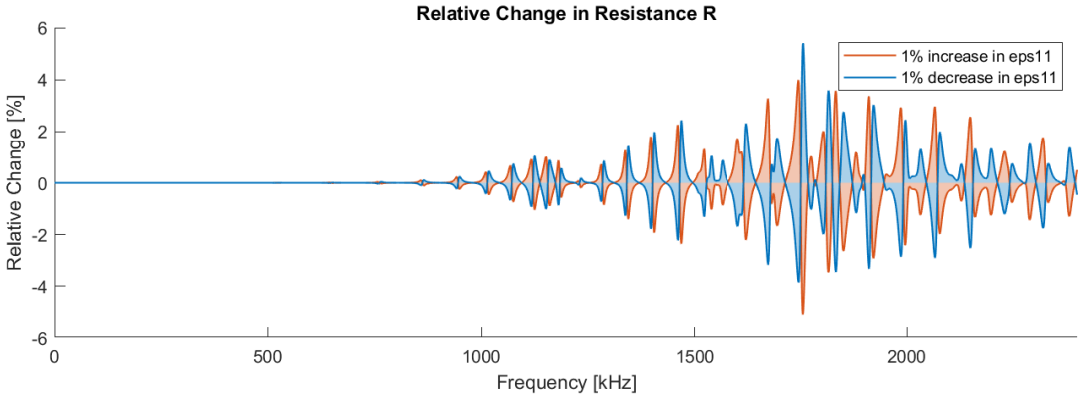

(c)

Figure 5.41: Relative change or variation from Ferroperms data set for the simulated a) conductance G, b) susceptance B, and c) resistance R when subject to a $\pm 1\%$ change in ε_{11}^{S}. Frequency resolution $\Delta f = 50$Hz.

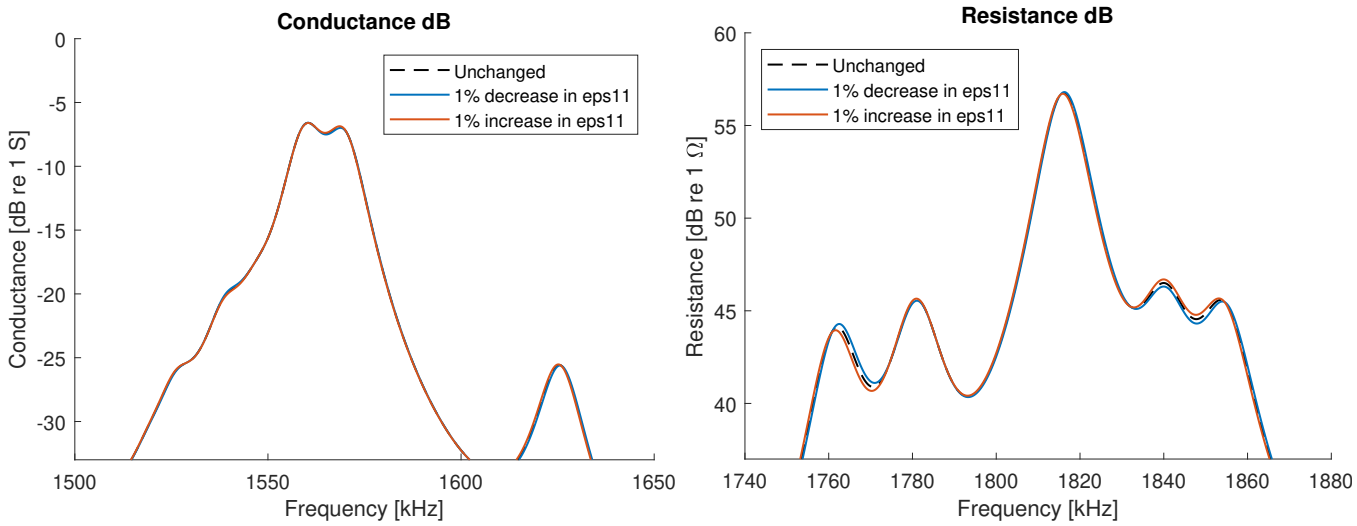

Figure 5.42: Simulated conductance G, and b) resistance R from Ferroperms data set, as well as the result a 1% increase/decrease in ε_{11}^{S} has on the simulation. Frequency resolution $\Delta f = 50Hz$.

Table 5.16: Relative variation in the listed derived quantity (row) as a result of a 1% change in the stated material constant and its Q-factor (column). Color spectrum ranges from blue to red, where the former represents a negative difference,the latter a positive difference. The intensity of the color represents the magnitude of the difference from Ferroperm's simulated data.

	ε^S_{33} + 1%	ε^S_{33} - 1%	$Q^{\varepsilon S}_{33}$ + 1%	$Q^{\varepsilon S}_{33}$ - 1%
R1:R	-1,22%	1,23%	0,14%	-0,14%
R1:G	0,00%	0,00%	0,00%	0,00%
R1:fs	0,00%	0,00%	0,00%	0,00%
R1:BWs	0,00%	0,00%	0,00%	0,00%
R1:fp	-0,03%	0,03%	0,00%	0,00%
R1:BWp	0,00%	0,00%	-0,63%	0,00%
R2:R	-1,35%	1,38%	0,02%	-0,02%
R2:G	0,00%	0,00%	0,00%	0,00%
R2:fs	0,00%	0,00%	0,00%	0,00%
R2:BWs	0,00%	0,00%	0,00%	0,00%
R2:fp	-0,01%	0,01%	0,00%	0,00%
R2:BWp	0,00%	0,00%	0,00%	0,00%
R3:R	-1,34%	1,37%	0,00%	0,00%
R3:G	0,01%	-0,01%	-0,01%	0,01%
R3:fs	0,00%	0,00%	0,00%	0,00%
R3:BWs	0,00%	0,00%	0,00%	0,00%
R3:fp	0,00%	0,00%	0,00%	0,00%
R3:BWp	0,17%	0,00%	0,00%	0,17%
TE1:R	-1,31%	0,82%	0,32%	-0,33%
TE1:G	0,03%	-0,03%	0,05%	-0,05%
TE1:fs	-0,02%	0,02%	0,00%	0,00%
TE1:BWs	-0,15%	0,13%	-0,05%	0,03%
TE1:fp	-0,08%	0,09%	0,00%	0,00%
TE1:BWp	0,22%	-0,34%	-0,26%	0,30%

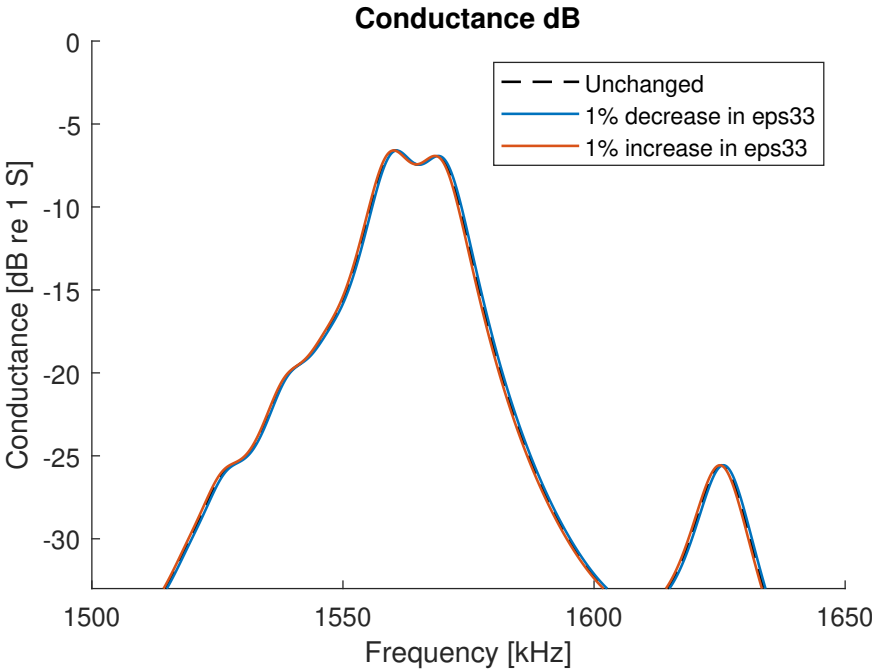

Figure 5.43: s

5.3.11 variation in ε^S_{33}

The dielectric constant ε^S_{33} and its associated Q-factor $Q^{\varepsilon^S}_{33}$ have been varied by 1% from Ferroperms listed values. The resulting changes in the conductance G-, susceptance B-, and resistance R-domain are given as variation relative to the Ferroperms simulated data in Table 5.16.

The listed values in Table 5.16 for the relative variation in both conductance G and resistance R at the radial modes agrees well with that of PZT-5A [7]. The relative parallel resonance frequency displacement however are all some magnitudes smaller than that for PZT-5A [7], For PZT-5A an increasing magnitude of the relative variation in conductance G for succeeding radial modes are observed [7]. This pattern is not visible with the 2 decimals resolution in Table 5.16, however a higher resolution table where it can be seen is available in Appendix . From the aforementioned table the relative displacement in the resonance frequencies at TE1, $TE1 : fs = -0,020\%$ and $TE : fp = -0,084$, are seen to only be slightly larger in magnitude than what is observed for PZT-5A, $-0,018\%$ and $-0,076\%$ respectively [7]. The rest of the listed TE1 quantities in Table 5.16 do not match well.

In Figure 5.44a for the relative variation in conductance G a 1% increase/decrease

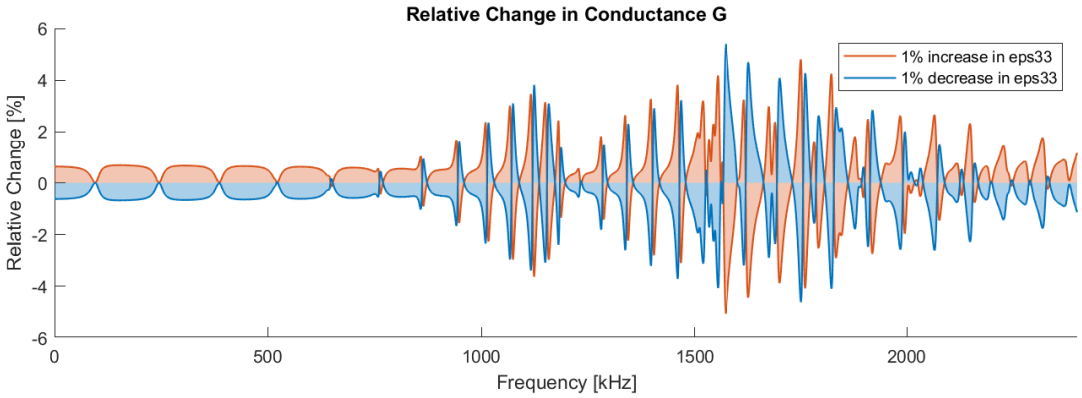

(a)

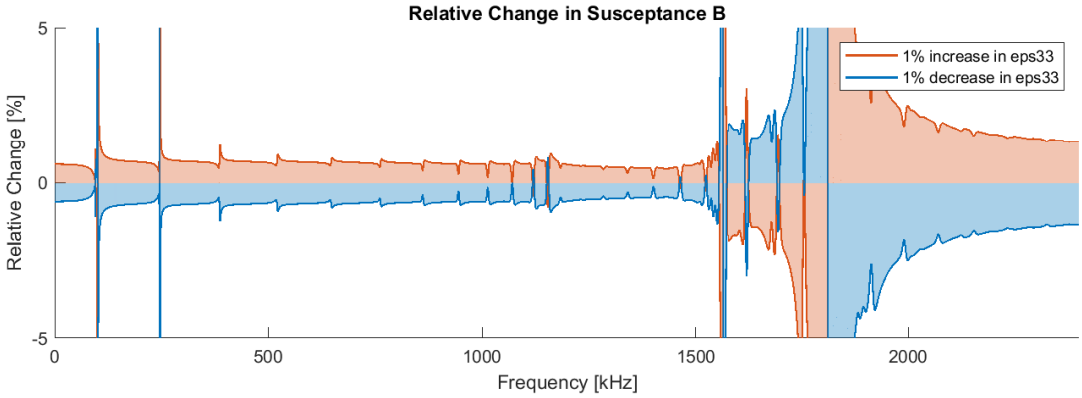

(b)

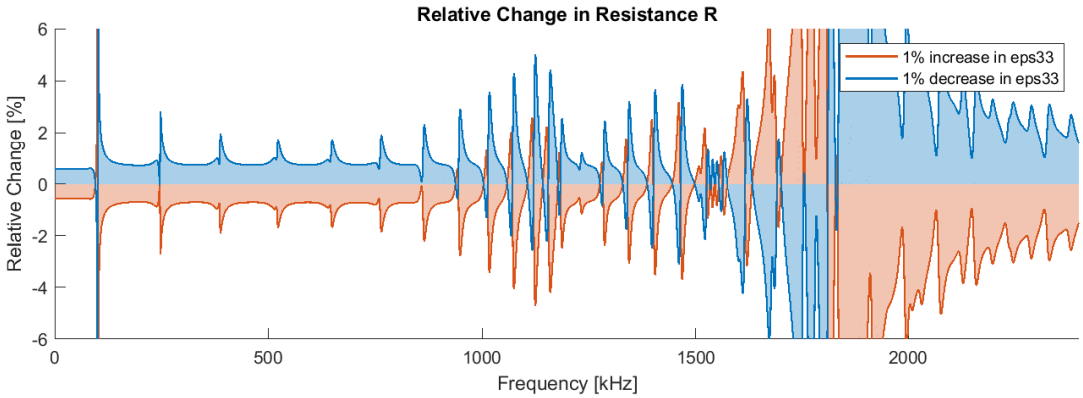

(c)

Figure 5.44: a), b), c)

in ε_{33}^S is seen to raise/lower the conductance in the regions between the radial modes without affecting the radial peaks notably. It is not before the 7th radial mode R7 the resonance frequency of the peak is observed to shift, by a relative frequency displacement of $R7 : fs = -0,006\%$. Note however that the plots in Figure 5.44 are from simulations with frequency resolution of $\Delta f = 0,05$kHz, meaning ε_{33}^S may very well affect radial peaks lower than R7. The relative variation in G increases when approaching the E-mode region, decreasing quickly right after, then increasing again till it reaches the series resonance frequency f_s^{TE1}. From this point out the variation in G keeps the same level, then decreasing again after the parallel resonance frequency f_p^{TE1}, reaching a seemingly steady oscillating level of around $f = 2200$kHz.

In Figure 5.44b a 1% change in ε_{33}^S shows a steady relative variation in the susceptance B starting at approximately $0,7\%$ between the R1 and R2 mode, then slowly decreasing to approximately $0,5\%$ until closing in on the series resonance frequency f_s^{TE1}. The relative variation then increases rapidly until reaching the parallel resonance frequency f_p^{TE1}, where it thereafter decreases exponentially until reaching a seemingly steady level of $1,4\%$ variation.

In Figure 5.44c a 1% increase/decrease in ε_{33}^S shows an $0,7\%$ absolute relative variation in the resistance R between the first 7 radial modes. Contrary to the relative variation in conductance G in Figure 5.44a, the relative variation in R increases at the radial peaks as a result of the parallel resonance frequencies being shifted. The variation increases when approaching the E-mode region, decreasing again right after only to slightly increase again when closing in on the series resonance frequency f_s^{TE1} where the relative variation is dampened. After this a rapid increase in the variation can be seen, and an equally rapid decrease afterwards upon reaching the parallel resonance frequency f_p^{TE1}.

The overall shape of the variation responses in Figure **??** agrees well with that of PZT-5A [7].

More descriptive about the places with high variations and zoom in plot.

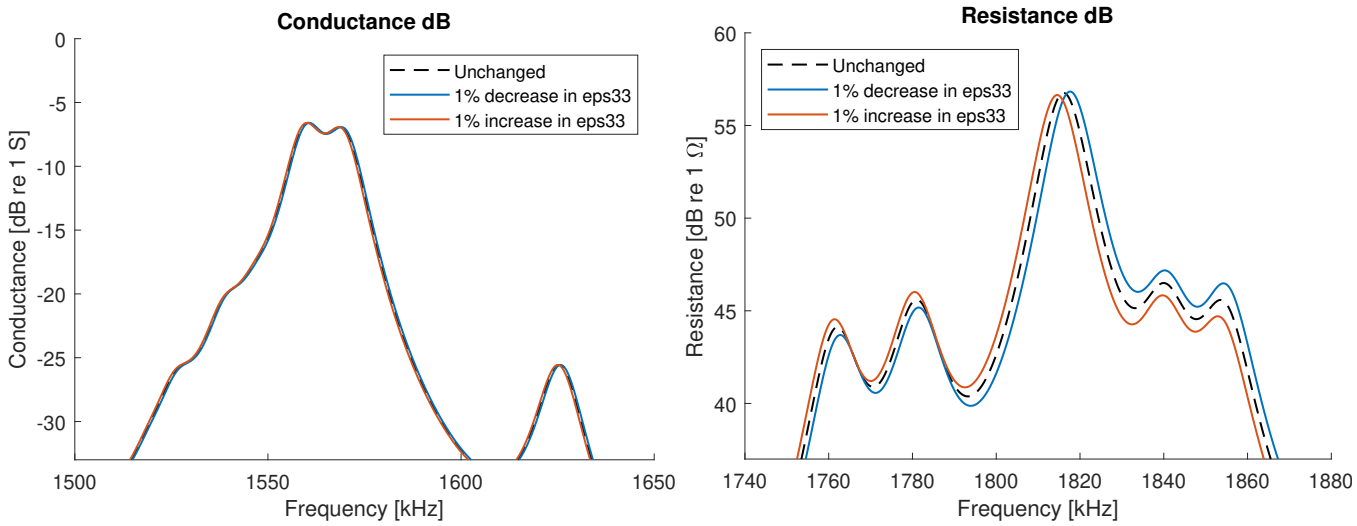

(a) **(b)**

Figure 5.45: Simulated conductance G, and b) resistance R from Ferroperms data set, as well as the result a 1% increase/decrease in ε_{33}^{S} has on the simulation. Frequency resolution $\Delta f = 50Hz$.

5.4 Iterative Curvefitting

This section describes the work done to approximate a material data set through FEM modeling. Similar work has been done in a previous M. Sc. for the material PZT-5A with great success [7]. When curve-fitting Fardal conducted 10 simulations using FEMP's solution method modal analysis with a frequency resolution of $1kHz$, 4 elements per wavelength calculated at $2MHz$, and an $f_max = 2.2MHz$. The following material properties were changed during the curve-fitting process to achieve a satisfactory result [7]:

- c_{11}^E increased to shift the R-modes up in frequency.
- c_{12}^E decreased to shift the R1-mode down in frequency.
- ε_{11}^S increased for higher resonance peaks at the TE1-mode.
- ε_{33}^S increased for higher G and lower R between the R-modes and over the TE1-mode.
- $Q_{33}^{\varepsilon^S}$ decreased for higher G and lower R between the R-modes and over the TE1-mode.
- e_{33} increased for a higher G and R at both the R- and TE1-modes.
- Q_{33}^e decreased for a higher G and R at both the R- and TE1-modes.

Note that material constants attained from such a procedure are not necessarily physically correct, even if the G- and R-plots corresponds well with measurements [7].

A similar curve-fitting have been conducted with Ferroperms material constants from Table 5.1 as a starting point. This has yielded no satisfactory results due to the large deviation in measurements and simulations as seen in Figure 5.1, especially around the TE1 mode.

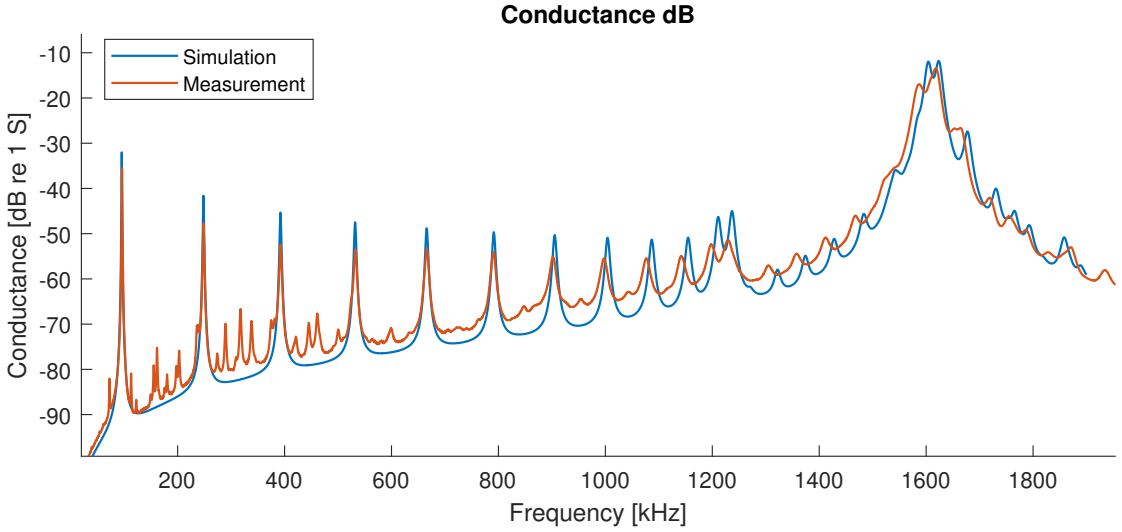

Figure 5.46: Measurement and curve-fitted simulation of a Pz37-disc with thickness $t = 0.88mm$ and radius $a = 9.53mm$. Frequency resolution $= 0.05kHz$ for both.

The following procedure for curve-fitting the resonance peaks were used:

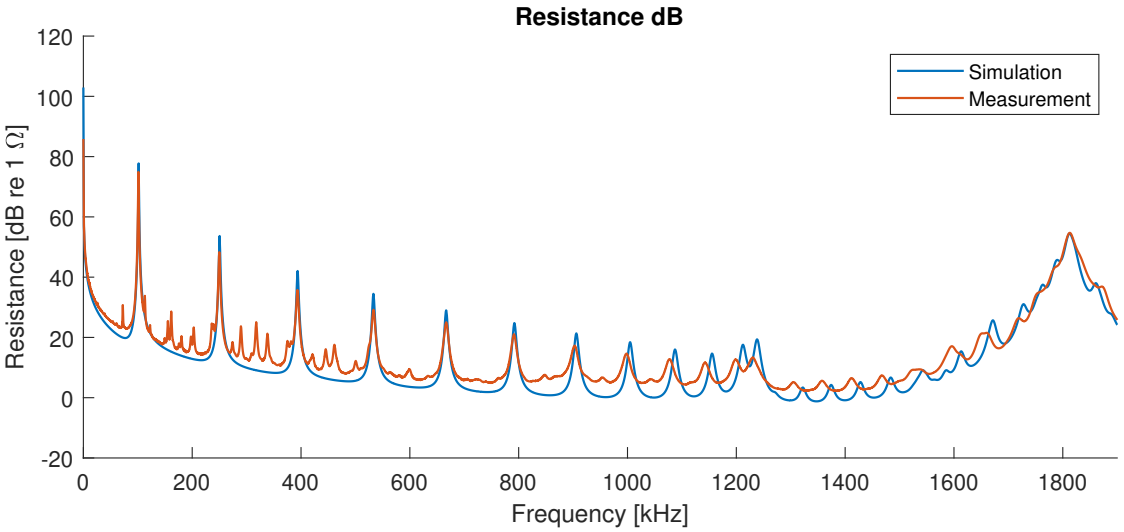

Figure 5.47: Measurement and curve-fitted simulation of Pz37-disc with thickness $t = 0.88mm$ and radius $a = 9.53mm$. Frequency resolution $= 0.05kHz$ for both.

1. vary c_{33}^E, e_{33} and ε_{33}^S to align f_s^{TE1} and f_p^{TE1} with measurements in the B/ω-domain.
2. vary c_{11}^E and c_{13}^E to align f_s^{R2} and f_s^{R3} with measurements in the G-domain. Increase both to increase the gap in frequency between f_s^{R2} and f_s^{R3}, decrease both to decrease the gap.
3. vary c_{12}^E to align f_s^{R1} with measurements in the B/ω-domain.
4. if f_p^{R2} and f_p^{R3} does not agree well with measurements in the R-domain - repeat steps 1 - 3.
5. vary e_{31} to align f_p^{R1} with measurements in the B/ω-domain.

This only aligns the resonance frequencies, whereas the overall shape and magnitude of each electric quantity are not guaranteed to agree well with the measurements. The untouched material constants, that is c_{44}^E, e_{15} and ε_{11}^S, and all the Q-factors have been varied in an attempt to correct this. Given the sheer amount of variable parameters this has so far been deemed inconclusive.

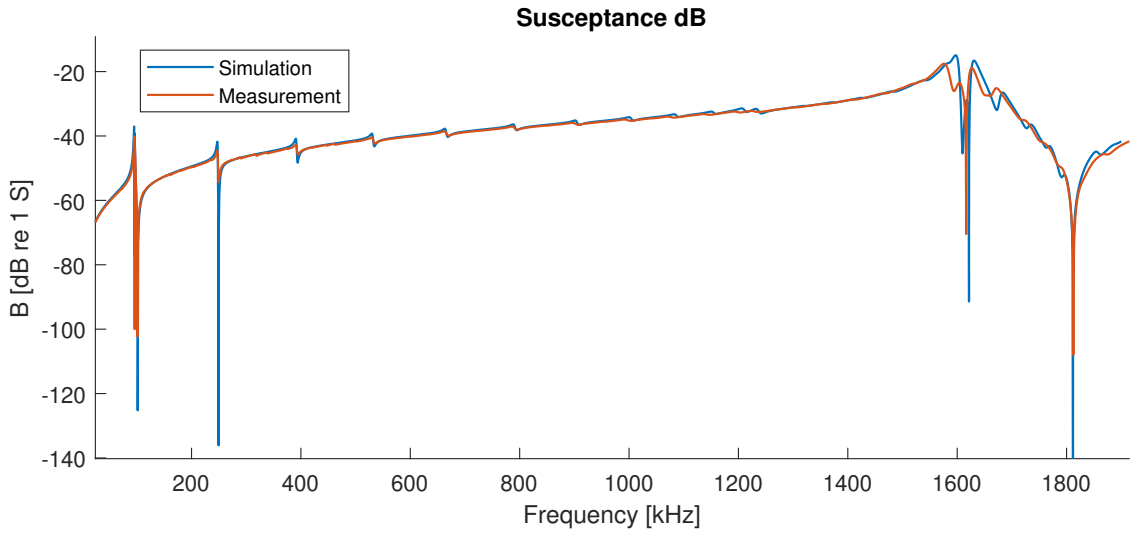

Figure 5.48: Measurement and curve-fitted simulation of Pz37-disc with thickness $t = 0.88mm$ and radius $a = 9.53mm$. Frequency resolution $= 0.05kHz$ for both.

Chapter 6

Conclusion and Further Work

In this thesis the material constants used for simulating in FEMP have been altered, and the resulting changes have been quantified and compared with earlier work done on another piezoceramic PZT-5A [7]. The objective of this thesis was to conduct a solid analysis for Pz37HD. Large amounts of data have been attained which can hopefully be used in further work on the same material.

Due to poor time management a satisfactory analysis for the material constants' influence in FEMP simulations have not been achieved. Similar variation-responses have been conducted for all Q-factors, but have not been discussed for the same reasons as above. The objective of developing a systematic procedure for fine-adjusting material constants was not either achieved.

Further work may be developing a systematic method for fine-adjusting the material constants in FEMP. From the analysis in Section 5 starting with curve-fitting the TE1 mode in both G and R domain seems to be a step in the right direction.

Appendices

Appendix A

GitHub-repository

Due to the large amount of data and MATLAB-scripts a GitHub-repository have
been created where the scripts in this thesis can be accessed: https://github.com/philiptraetteberg/M

Appendix B

FEMP-files

This section describes, and gives examples of the 2 user-configured files for setting up the simulation of a piezoelectric disc in vaccuum.

B.1 material.dat-file

The file MATERIAL.DAT is a TXT file (with extension .DAT) specifying the material class and a reference number in the header, then follows numerical values for the materials properties. This entails the materials density and its material constants, as well as eventual Q-factors. The piezoelectric elements can be modeled by assuming a hexagonal crystal structure of symmetry class 6mm, specified as 'piezo' in material.dat file, which allows for the following structure of the material matrices $\mathbf{c^E}, \mathbf{e}$ and $\varepsilon^{\mathbf{S}}$ [17].

$$\left[\begin{array}{ccc|ccc|ccc} c_{11}^E & c_{12}^E & c_{13}^E & 0 & 0 & 0 & 0 & 0 & e_{11} \\ c_{12}^E & c_{11}^E & c_{13}^E & 0 & 0 & 0 & 0 & 0 & e_{11} \\ c_{13}^E & c_{13}^E & c_{33}^E & 0 & 0 & 0 & 0 & 0 & e_{31} \\ \hline 0 & 0 & 0 & c_{44}^E & 0 & 0 & 0 & e_{15} & 0 \\ 0 & 0 & 0 & 0 & c_{44}^E & 0 & e_{15} & 0 & 0 \\ 0 & 0 & 0 & 0 & 0 & c_{66}^E & 0 & 0 & 0 \\ \hline 0 & 0 & 0 & 0 & e_{15} & 0 & \varepsilon_{11}^S & 0 & 0 \\ 0 & 0 & 0 & e_{15} & 0 & 0 & 0 & \varepsilon_{11}^S & 0 \\ e_{11} & e_{11} & e_{31} & 0 & 0 & 0 & 0 & 0 & \varepsilon_{33}^S \end{array}\right]$$

Which corresponds to the following material constant matrices:

$$\begin{bmatrix} c_{11}^E & c_{12}^E & c_{13}^E & 0 & 0 & 0 \\ c_{12}^E & c_{11}^E & c_{13}^E & 0 & 0 & 0 \\ c_{13}^E & c_{13}^E & c_{33}^E & 0 & 0 & 0 \\ 0 & 0 & 0 & c_{44}^E & 0 & 0 \\ 0 & 0 & 0 & 0 & c_{44}^E & 0 \\ 0 & 0 & 0 & 0 & 0 & c_{66}^E \end{bmatrix}$$

where $c_{66}^E = \left(c_{11}^E - c_{12}^E\right)/2$.

$$\begin{bmatrix} 0 & 0 & 0 & 0 & e_{15} & 0 \\ 0 & 0 & 0 & e_{15} & 0 & 0 \\ e_{31} & e_{31} & e_{33} & 0 & 0 & 0 \end{bmatrix}$$

$$\begin{bmatrix} \varepsilon_{11}^S & 0 & 0 \\ 0 & \varepsilon_{11}^S & 0 \\ 0 & 0 & \varepsilon_{33}^S \end{bmatrix}$$

B.2 ∼.inn-file

'.INN'-file is a .TXT file saved with the .INN-extension, and is the overordnet file specifying the work-flow of the simulation by calling on the included commands. A documentation containing usable commands for the FEMP can be found in the bibliography [2].

```
# FEMP 5 INPUT-FILE, DISK 1
set
t,0.87908e-3
a,9.531395e-3
material_number,1
end

materialfile
4
end

meshingtype
elementsperwavelength,2000e3
end

viewmesh
1
end

order
2
end

piezodiskphilip
a,t,3,3,material_number
end

directharmonicanalysis
0e3,.05e3,2000e3,complex_loss
end

admittance
0,0,0
end

save
admittance,admittance_f
end
```

Figure B.1: Example contents of an INN-file.

The 'SET'-command is used to declare variables, i.e. in Figure B.1 the thickness t, radius a, and material reference number are declared directly.

'ELEMENTSPERWAVELENGTH' decides at what frequency the elements per wavelength are calculated at.

'VIEWMESH' enables a figure illustrating the cross-section of the current project.

'ORDER' inputting 2 here results in finite elements defined by 8 nodes.

'PIEZODISKPHILIP' initializes the structure for the project, see section **??**.

'DIRECTHARMONICANALYSIS' does the FEMP stuff and solves by the direct harmonic analysis method. The first three arguments defines "START, STEP, STOP"-frequencies for the frequency vector.

'ADMITTANCE' calculates the total admittance.

For descriptions of the remaining commands and more see the inn-fil guide [2].

Appendix C

Extended Sensitivity Analysis

Relative variation in electrical quantity (row) due to a 1% INCREASE in a single material constant (column)

	c_11	Qc_11	c_12	Qc_12	c_13	Qc_13	c_33	Qc_33	c_44	Qc_44	e_31	Qe_31	e_33	Qe_33	e_15	Qe_15	eps_11	Qeps_11	eps_33	Qeps_33
1kHz:R	0.2075%	-0.0967%	0.1201%	-0.0558%	-0.7321%	0.3336%	0.9266%	-0.4316%	0.0000%	0.0000%	0.0620%	0.0000%	-1.1408%	0.0000%	0.0000%	0.0000%	0.0000%	0.0000%	-0.4557%	-0.7393%
1kHz:G	-0.0966%	-0.0967%	-0.0560%	-0.0558%	0.3438%	0.3335%	-0.4285%	-0.4316%	0.0000%	0.0000%	-0.0289%	0.0000%	0.5378%	0.0000%	0.0000%	0.0000%	0.0000%	0.0000%	0.7470%	-0.7395%
1kHz:B/omega	-0.1519%	0.0000%	-0.0880%	0.0000%	0.5405%	-0.0001%	-0.6737%	0.0001%	0.0000%	0.0000%	-0.0454%	0.0000%	0.8455%	0.0000%	0.0000%	0.0000%	0.0000%	0.0000%	0.6022%	0.0000%
R1:R	-1.2477%	1.0129%	-0.8602%	0.3786%	3.5528%	-0.8739%	-2.0577%	0.3593%	0.0000%	0.0000%	-0.2332%	0.0000%	0.6486%	0.0000%	0.0000%	0.0000%	0.0000%	0.0000%	-1.2071%	0.1327%
R1:G	-0.3891%	1.1875%	-0.5448%	0.4922%	3.2619%	-1.3346%	-2.7205%	0.6831%	0.0000%	0.0000%	-0.3235%	0.0000%	2.3360%	0.0000%	0.0000%	0.0000%	0.0000%	0.0000%	0.0006%	-0.0006%
R1:fs	0.5889%	0.0000%	0.2471%	0.0000%	-0.6888%	0.0000%	0.3365%	0.0000%	0.0000%	0.0000%	0.0000%	0.0000%	0.0000%	0.0000%	0.0000%	0.0000%	0.0000%	0.0000%	0.0000%	0.0000%
R1:BWs	0.0000%	-1.0638%	0.0000%	0.0000%	-1.0638%	1.0638%	0.0000%	-1.0638%	0.0000%	0.0000%	0.0000%	0.0000%	0.0000%	0.0000%	0.0000%	0.0000%	0.0000%	0.0000%	0.0000%	0.0000%
R1:fp	0.5408%	0.0000%	0.2034%	0.0000%	-0.4813%	0.0000%	0.1935%	0.0000%	0.0000%	0.0000%	-0.0149%	0.0000%	0.0893%	0.0000%	0.0000%	0.0000%	0.0000%	0.0000%	-0.0347%	0.0000%
R1:BWp	0.0000%	-0.9346%	0.0000%	-0.9346%	0.0000%	0.9346%	-0.9346%	-0.9346%	0.0000%	0.0000%	-0.9346%	0.0000%	0.0000%	0.0000%	0.0000%	0.0000%	0.0000%	0.0000%	-0.9346%	-0.9346%
R2:R	-2.0091%	1.4205%	-0.1233%	0.0581%	3.7896%	-0.9769%	-2.3696%	0.4920%	0.0000%	0.0000%	-0.3015%	0.0000%	1.0096%	0.0000%	0.0000%	0.0000%	0.0000%	0.0000%	-1.3457%	0.0168%
R2:G	-0.6261%	1.4581%	-0.0513%	0.0602%	2.8025%	-1.0390%	-2.5365%	0.5384%	0.0000%	0.0000%	-0.3151%	0.0000%	2.3189%	0.0000%	0.0000%	0.0000%	0.0000%	0.0000%	0.0049%	-0.0048%
R2:fs	0.7271%	0.0000%	0.0306%	0.0000%	-0.5392%	0.0000%	0.2696%	0.0000%	0.0000%	0.0000%	0.0000%	0.0000%	0.0000%	0.0000%	0.0000%	0.0000%	0.0000%	0.0000%	0.0000%	0.0000%
R2:BWs	0.8230%	-1.6461%	0.0000%	0.0000%	-0.8230%	0.8230%	0.0000%	-0.8230%	0.0000%	0.0000%	0.0000%	0.0000%	0.0000%	0.0000%	0.0000%	0.0000%	0.0000%	0.0000%	0.0000%	0.0000%
R2:fp	0.7172%	0.0000%	0.0304%	0.0000%	-0.5105%	0.0000%	0.2492%	0.0000%	0.0000%	0.0000%	-0.0020%	0.0000%	0.0142%	0.0000%	0.0000%	0.0000%	0.0000%	0.0000%	-0.0061%	0.0000%
R2:BWp	0.8097%	-1.2146%	0.0000%	0.0000%	0.0000%	1.2146%	0.4049%	-0.4049%	0.0000%	0.0000%	0.0000%	0.0000%	0.0000%	0.0000%	0.0000%	0.0000%	0.0000%	0.0000%	0.4049%	0.0000%
R3:R	-1.9974%	1.4509%	-0.0474%	0.0229%	3.7316%	-1.0098%	-2.3919%	0.5337%	0.0000%	0.0000%	-0.2950%	0.0000%	0.9941%	0.0000%	0.0000%	0.0000%	0.0000%	0.0000%	-1.3406%	-0.0018%
R3:G	-0.5216%	1.4663%	-0.0172%	0.0232%	2.6298%	-1.0353%	-2.5018%	0.5534%	0.0000%	0.0000%	-0.3006%	0.0000%	2.2906%	0.0000%	0.0000%	0.0000%	0.0000%	0.0000%	0.0117%	-0.0111%
R3:fs	0.7383%	0.0000%	0.0117%	0.0000%	-0.5410%	0.0000%	0.2803%	0.0000%	0.0000%	0.0000%	0.0000%	0.0000%	0.0000%	0.0000%	0.0000%	0.0000%	0.0000%	0.0000%	0.0000%	0.0000%
R3:BWs	0.5195%	-1.5584%	0.0000%	0.0000%	-0.5195%	1.0390%	0.2597%	-0.5195%	0.0000%	0.0000%	0.0000%	0.0000%	0.0000%	0.0000%	0.0000%	0.0000%	0.0000%	0.0000%	0.0000%	0.0000%
R3:fp	0.7344%	0.0000%	0.0129%	0.0000%	-0.5289%	0.0000%	0.2728%	0.0000%	0.0000%	0.0000%	0.0000%	0.0000%	0.0065%	0.0000%	0.0000%	0.0000%	0.0000%	0.0000%	-0.0013%	0.0000%
R3:BWp	0.7752%	-1.0336%	0.2584%	0.0000%	-0.2584%	1.2920%	0.5168%	-0.5168%	0.0000%	0.0000%	0.2584%	0.0000%	0.2584%	0.0000%	0.0000%	0.0000%	0.0000%	0.0000%	0.2584%	0.0000%
TE1:R	-0.5955%	0.2702%	0.0065%	0.0001%	-4.7233%	-0.1824%	-0.0128%	0.4737%	3.9013%	0.0657%	-0.1092%	0.0000%	-0.8807%	0.0000%	1.2983%	0.0000%	-0.4100%	0.0267%	-1.3951%	0.2858%
TE1:G	5.8288%	-0.0617%	0.0042%	0.0000%	4.5556%	0.0416%	6.5473%	0.6169%	3.7415%	0.0009%	-0.1355%	0.0000%	2.7340%	0.0000%	-0.4084%	0.0000%	-0.0919%	-0.0049%	0.0307%	0.0466%
TE1:fs	-0.0048%	-0.0006%	0.0000%	0.0000%	0.4271%	0.0000%	0.9263%	-0.0010%	0.0103%	-0.0003%	0.0003%	0.0000%	0.0397%	0.0000%	-0.0035%	0.0000%	0.0013%	0.0000%	-0.0195%	-0.0003%
TE1:BWs	-14.7593%	0.1441%	0.0000%	0.0000%	-9.3399%	-0.0865%	-10.9542%	-0.3747%	-1.4702%	0.0288%	-0.0288%	0.0000%	0.0577%	0.0000%	0.7783%	0.0000%	-0.2018%	0.0288%	-0.2018%	-0.0288%
TE1:fp	0.1863%	0.0000%	0.0000%	0.0000%	-0.1321%	0.0000%	0.2931%	0.0000%	0.0996%	0.0000%	-0.0033%	0.0000%	0.1767%	0.0000%	0.0173%	0.0000%	-0.0096%	0.0000%	-0.0859%	0.0000%
TE1:BWp	0.0458%	-0.3665%	0.0458%	0.0000%	0.0916%	0.2749%	1.0078%	-0.5039%	-0.4581%	-0.0916%	0.0000%	0.0000%	1.1452%	0.0000%	0.0000%	0.0000%	0.0000%	0.0000%	-0.3665%	-0.2749%

Table C.1: Sensitivity analysis for the supplemented material constants from the manufacturer for a 1% increase in a specific material constant. Blue indicates a negative difference, while red a positive. Intensity of the color indicates the magnitude of the deviation.

Relative variation in electrical quantity (row) due to a 1% DECREASE in a single material constant (column)

	c_11	Qc_11	c_12	Qc_12	c_13	Qc_13	c_33	Qc_33	c_44	Qc_44	e_31	Qe_31	e_33	Qe_33	e_15	Qe_15	eps_11	Qeps_11	eps_33	Qeps_33
1kHz:R	-0.2113%	0.0986%	-0.1214%	0.0569%	0.7127%	-0.3403%	-0.9428%	0.4403%	0.0000%	0.0000%	-0.0620%	0.0000%	1.1531%	0.0000%	0.0000%	0.0000%	0.0000%	0.0000%	0.4594%	0.7544%
1kHz:G	0.0988%	0.0986%	0.0567%	0.0569%	-0.3303%	-0.3403%	0.4436%	0.4403%	0.0000%	0.0000%	0.0289%	0.0000%	-0.5321%	0.0000%	0.0000%	0.0000%	0.0000%	0.0000%	-0.7470%	0.7546%
1kHz:B/omega	0.1553%	0.0000%	0.0891%	0.0000%	-0.5192%	0.0001%	0.6974%	-0.0001%	0.0000%	0.0000%	0.0455%	0.0000%	-0.8365%	0.0000%	0.0000%	0.0000%	0.0000%	0.0000%	-0.6022%	0.0000%
R1:R	1.2718%	-1.0126%	0.8707%	-0.3833%	-3.4402%	0.9076%	2.1106%	-0.3639%	0.0000%	0.0000%	0.2275%	0.0000%	-0.6760%	0.0000%	0.0000%	0.0000%	0.0000%	0.0000%	1.2243%	-0.1351%
R1:G	0.3905%	-1.1830%	0.5464%	-0.4972%	-3.1656%	1.3993%	2.8301%	-0.6874%	0.0000%	0.0000%	0.3241%	0.0000%	-2.3090%	0.0000%	0.0000%	0.0000%	0.0000%	0.0000%	-0.0006%	0.0006%
R1:fs	-0.5941%	0.0000%	-0.2471%	0.0000%	0.6783%	0.0000%	-0.3470%	0.0000%	0.0000%	0.0000%	0.0000%	0.0000%	0.0000%	0.0000%	0.0000%	0.0000%	0.0000%	0.0000%	0.0000%	0.0000%
R1:BWs	-1.0638%	1.0638%	-1.0638%	1.0638%	1.0638%	-1.0638%	0.0000%	1.0638%	0.0000%	0.0000%	0.0000%	0.0000%	0.0000%	0.0000%	0.0000%	0.0000%	0.0000%	0.0000%	0.0000%	0.0000%
R1:fp	-0.5458%	0.0000%	-0.2034%	0.0000%	0.4713%	0.0000%	-0.1935%	0.0000%	0.0000%	0.0000%	0.0149%	0.0000%	-0.0893%	0.0000%	0.0000%	0.0000%	0.0000%	0.0000%	0.0347%	0.0000%
R1:BWp	-0.9346%	0.9346%	-0.9346%	0.0000%	0.0000%	-0.9346%	-0.9346%	0.0000%	0.0000%	0.0000%	0.0000%	0.0000%	-0.9346%	0.0000%	0.0000%	0.0000%	0.0000%	0.0000%	0.0000%	0.0000%
R2:R	2.0794%	-1.4085%	0.1226%	-0.0592%	-3.6495%	1.0169%	2.4536%	-0.4970%	0.0000%	0.0000%	0.3015%	0.0000%	-1.0306%	0.0000%	0.0000%	0.0000%	0.0000%	0.0000%	1.3732%	-0.0171%
R2:G	0.6408%	-1.4447%	0.0509%	-0.0613%	-2.7408%	1.0829%	2.6292%	-0.5433%	0.0000%	0.0000%	0.3156%	0.0000%	-2.2922%	0.0000%	0.0000%	0.0000%	0.0000%	0.0000%	-0.0049%	0.0049%
R2:fs	-0.7333%	0.0000%	-0.0306%	0.0000%	0.5290%	0.0000%	-0.2757%	0.0000%	0.0000%	0.0000%	0.0000%	0.0000%	0.0000%	0.0000%	0.0000%	0.0000%	0.0000%	0.0000%	0.0000%	0.0000%
R2:BWs	-0.8230%	1.6461%	0.0000%	0.0000%	0.4115%	-0.8230%	0.0000%	0.8230%	0.0000%	0.0000%	0.0000%	0.0000%	0.0000%	0.0000%	0.0000%	0.0000%	0.0000%	0.0000%	0.0000%	0.0000%
R2:fp	-0.7212%	0.0000%	-0.0304%	0.0000%	0.5024%	0.0000%	-0.2553%	0.0000%	0.0000%	0.0000%	0.0020%	0.0000%	-0.0142%	0.0000%	0.0000%	0.0000%	0.0000%	0.0000%	0.0061%	0.0000%
R2:BWp	-0.4049%	1.6194%	0.4049%	0.4049%	0.4049%	-0.8097%	0.0000%	0.8097%	0.0000%	0.0000%	0.4049%	0.0000%	0.4049%	0.0000%	0.0000%	0.0000%	0.0000%	0.0000%	0.0000%	0.0000%
R3:R	2.0709%	-1.4374%	0.0473%	-0.0233%	-3.5930%	1.0520%	2.4788%	-0.5385%	-0.0001%	0.0000%	0.2956%	0.0000%	-1.0139%	0.0000%	0.0000%	0.0000%	0.0000%	0.0000%	1.3685%	0.0019%
R3:G	0.5352%	-1.4522%	0.0170%	-0.0236%	-2.5774%	1.0791%	2.5917%	-0.5582%	-0.0004%	0.0000%	0.3011%	0.0000%	-2.2643%	0.0000%	0.0000%	0.0000%	0.0000%	0.0000%	-0.0117%	0.0113%
R3:fs	-0.7447%	0.0000%	-0.0130%	0.0000%	0.5320%	0.0000%	-0.2867%	0.0000%	0.0000%	0.0000%	0.0000%	0.0000%	-0.0013%	0.0000%	0.0000%	0.0000%	0.0000%	0.0000%	0.0000%	0.0000%
R3:BWs	-0.7792%	1.5584%	0.0000%	0.0000%	0.5195%	-1.0390%	-0.5195%	0.5195%	0.0000%	0.0000%	0.0000%	0.0000%	0.0000%	0.0000%	0.0000%	0.0000%	0.0000%	0.0000%	0.0000%	0.0000%
R3:fp	-0.7383%	0.0000%	-0.0116%	0.0000%	0.5224%	0.0000%	-0.2780%	0.0000%	0.0000%	0.0000%	0.0013%	0.0000%	-0.0052%	0.0000%	0.0000%	0.0000%	0.0000%	0.0000%	0.0026%	0.0000%
R3:BWp	-0.5168%	1.5504%	0.0000%	0.2584%	0.7752%	-1.0336%	0.0000%	1.0336%	0.0000%	0.0000%	0.2584%	0.0000%	0.2584%	0.0000%	0.0000%	0.0000%	0.0000%	0.0000%	0.2584%	0.2584%
TE1:R	-1.2833%	-0.2736%	-0.0066%	-0.0001%	3.6314%	0.1871%	-0.8729%	-0.4785%	-2.8083%	-0.0669%	0.1084%	0.0000%	-0.7719%	0.0000%	-1.3862%	0.0000%	0.4024%	-0.0272%	0.9870%	-0.2899%
TE1:G	13.0627%	0.0630%	-0.0042%	0.0000%	2.1049%	-0.0425%	8.7221%	-0.6189%	-1.1808%	-0.0008%	0.1368%	0.0000%	-2.6630%	0.0000%	0.4560%	0.0000%	0.0999%	0.0050%	-0.0311%	-0.0474%
TE1:fs	0.3903%	0.0003%	0.0000%	0.0000%	-0.0125%	-0.0003%	-0.4630%	0.0010%	0.4983%	0.0003%	-0.0003%	0.0000%	-0.0394%	0.0000%	0.0032%	0.0000%	-0.0013%	0.0000%	0.0195%	0.0000%
TE1:BWs	-19.8040%	-0.1153%	0.0000%	0.0000%	2.7962%	0.0865%	-8.2445%	0.4036%	-0.4324%	0.0000%	0.0288%	0.0000%	-0.0865%	0.0000%	-0.7783%	0.0000%	0.2306%	0.0000%	0.1730%	0.0288%
TE1:fp	-0.1871%	0.0000%	0.0000%	0.0000%	0.1211%	-0.0003%	-0.2911%	0.0000%	-0.0537%	0.0000%	0.0033%	0.0000%	-0.1778%	0.0000%	-0.0176%	0.0000%	0.0094%	0.0000%	0.0870%	0.0000%
TE1:BWp	0.0000%	0.4123%	0.0000%	0.0000%	0.0000%	-0.2290%	-0.5497%	0.5497%	1.7865%	0.1374%	0.0000%	0.0000%	-0.7787%	0.0000%	0.0458%	0.0000%	0.0458%	0.0458%	0.5497%	0.3207%

Table C.2: Sensitivity analysis for the supplemented material constants from the manufacturer for a 1% decrease in a specific material constant. Blue indicates a negative difference, while red a positive. Intensity of the color indicates the magnitude of the deviation.

Appendix D

Fardals Sensitivty Analysis Tables

Tables fetched from Fardals master thesis [7]. Used for comparison in Section 5.

Tabell 5.15: *Relativ variasjon i serie- og parallellresonansfrekvensene ved de to første radielle modene og første tykkelsesmode, og verdiene av henholdsvis G og R ved disse frekvensene når real- og Q–verdien til c^E_{11} økes 1%.*

		Rel diff [%]	
	Originalverdi	c^E_{11}+1%	Q (c^E_{11}) +1%
R1:fs [Hz]	50323,1	0,660929076	0
R2:fs [Hz]	129794	0,811285576	0
TE1:fs [Hz]	984830	0,022338881	0
R1:BWs [Hz]	490	0,102040816	-0,755102041
R2:BWs [Hz]	1321,5	0,075671585	-0,908059024
TE1:BWs [Hz]	6230	4,173354735	0
R1:G [S]	0,056751	0,111141745	0,76617235
R2:G [S]	0,017523	-0,055736374	0,9008337
TE1:G [S]	0,471229	-6,166385654	0,033333146
R1:fp [Hz]	58885,5	0,537993224	0
R2:fp [Hz]	133078	0,773982176	0
TE1:fp [Hz]	1084260	0,00922288	0
R1:BWp [Hz]	348,7	0,057355893	-1,03240608
R2:BWp [Hz]	1248,5	0,200240288	-0,921105326
TE1:BWp [Hz]	5880	1,020408163	0
R1:R [S]	25881,94	-0,50261287	1,029078453
R2:R [S]	1454,788	-1,542397961	0,932722279
TE1:R [S]	996,3294	-3,656418046	0,02363024

(a)

Tabell 5.17: *Relativ variasjon i serie- og parallellresonansfrekvensene ved de to første radielle modene og første tykkelsesmode, og verdiene av henholdsvis G og R ved disse frekvensene når real- og Q–verdien til c^E_{12} økes 1%.*

		Rel diff [%]	
	Originalverdi	c^E_{12}+1%	Q (c^E_{12})+1%
R1:fs [Hz]	50323,1	0,295689256	0
R2:fs [Hz]	129794	0,036596453	0
TE1:fs [Hz]	984830	0	0
R1:BWs [Hz]	490	-0,142857143	-0,12244898
R2:BWs [Hz]	1321,5	-0,037835793	0
TE1:BWs [Hz]	6230	0	0
R1:G [S]	0,056751	-0,210956952	0,128693006
R2:G [S]	0,017523	-0,0065089	0,015098068
TE1:G [S]	0,471229	-0,007748737	9,09393E-05
R1:fp [Hz]	58885,5	0,16778324	0
R2:fp [Hz]	133078	0,033439036	0
TE1:fp [Hz]	1084260	0	0
R1:BWp [Hz]	348,7	0,200745627	-0,114711787
R2:BWp [Hz]	1248,5	0	0
TE1:BWp [Hz]	5880	0	0
R1:R [S]	25881,94	-0,895004822	0,120045447
R2:R [S]	1454,788	-0,128586046	0,015028775
TE1:R [S]	996,3294	-0,003634635	-4,17462E-05

(b)

Figure D.1

Tabell 5.19: *Relativ variasjon i serie- og parallellresonansfrekvensene ved de to første radielle modene og første tykkelsesmode, og verdiene av henholdsvis G og R ved disse frekvensene når real- og Q–verdien til c^E_{13} økes 1%.*

		Rel diff [%]	
	Originalverdi	c^E_{13}+1%	Q (c^E_{13})+1%
R1:fs [Hz]	50323,1	-0,931580129	0
R2:fs [Hz]	129794	-0,718831379	0
TE1:fs [Hz]	984830	-0,027415899	0
R1:BWs [Hz]	490	1,12244898	0,469387755
R2:BWs [Hz]	1321,5	0,870223231	0,378357927
TE1:BWs [Hz]	6230	0,321027287	0
R1:G [S]	0,056751	0,434677157	-0,469730863
R2:G [S]	0,017523	0,384931423	-0,34769731
TE1:G [S]	0,471229	3,162913388	-0,013712593
R1:fp [Hz]	58885,5	-0,510821849	0
R2:fp [Hz]	133078	-0,654127654	0
TE1:fp [Hz]	1084260	0,001844576	0
R1:BWp [Hz]	348,7	0,60223688	0,401491253
R2:BWp [Hz]	1248,5	0,760913096	0,360432519
TE1:BWp [Hz]	5880	-1,870748299	0
R1:R [S]	25881,94	1,29608195	-0,424327921
R2:R [S]	1454,788	1,722183969	-0,343217104
TE1:R [S]	996,3294	3,026790105	0,009047524

(a)

Tabell 5.21: *Relativ variasjon i serie- og parallellresonansfrekvensene ved de to første radielle modene og første tykkelsesmode, og verdiene av henholdsvis G og R ved disse frekvensene når real- og Q–verdien til c^E_{33} økes 1%.*

		Rel diff [%]	
	Originalverdi	c^E_{33}+1%	Q -(c^E_{33})+1%
R1:fs [Hz]	50323,1	0,456251702	0
R2:fs [Hz]	129794	0,357874786	0
TE1:fs [Hz]	984830	0,462008672	0
R1:BWs [Hz]	490	-0,551020408	-0,571428571
R2:BWs [Hz]	1321,5	-0,416193719	-0,454029512
TE1:BWs [Hz]	6230	-0,321027287	-0,963081862
R1:G [S]	0,056751	-0,847268973	0,576217408
R2:G [S]	0,017523	-0,830727369	0,430721321
TE1:G [S]	0,471229	1,248579649	0,890203261
R1:fp [Hz]	58885,5	0,202087101	0
R2:fp [Hz]	133078	0,315980102	0
TE1:fp [Hz]	1084260	0,360614613	0
R1:BWp [Hz]	348,7	-0,286779467	-0,4301692
R2:BWp [Hz]	1248,5	-0,320384461	-0,400480577
TE1:BWp [Hz]	5880	1,020408163	-1,020408163
R1:R [S]	25881,94	-0,692832883	0,418460405
R2:R [S]	1454,788	-1,026831028	0,41227554
TE1:R [S]	996,3294	-0,550242814	0,814823337

(b)

Figure D.2

Tabell 5.23: *Relativ variasjon i serie- og parallellresonansfrekvensene ved de to første radielle modene og første tykkelsesmode, og verdiene av henholdsvis G og R ved disse frekvensene når real og Q–verdien til c^E_{33} økes 1%.*

		Rel diff [%]	
	Originalverdi	c^E_{44}+1%	Q –(c^E_{44})+1%
R1:fs [Hz]	50323,1	0	0
R2:fs [Hz]	129794	0	0
TE1:fs [Hz]	984830	0,014215651	0
R1:BWs [Hz]	490	0	0
R2:BWs [Hz]	1321,5	0	0
TE1:BWs [Hz]	6230	0,963081862	0
R1:G [S]	0,056751	3,53903E-07	2,09594E-07
R2:G [S]	0,017523	5,04359E-06	1,90241E-06
TE1:G [S]	0,471229	-1,58067727	0,052269674
R1:fp [Hz]	58885,5	0	0
R2:fp [Hz]	133078	0	0
TE1:fp [Hz]	1084260	0,038736097	0
R1:BWp [Hz]	348,7	0	0
R2:BWp [Hz]	1248,5	0	0
TE1:BWp [Hz]	5880	0,340136054	-0,340136054
R1:R [S]	25881,94	8,62052E-07	3,74363E-07
R2:R [S]	1454,788	4,26519E-06	1,84568E-06
TE1:R [S]	996,3294	-1,425783251	0,17285459

(a)

Tabell 5.25: *Relativ variasjon i serie- og parallellresonansfrekvensene ved de to første radielle modene og første tykkelsesmode, og verdiene av henholdsvis G og R ved disse frekvensene når real- og Q–verdien til e_{31} økes 1%.*

		Rel diff [%]	
	Originalverdi	Real e_{31}+1%	Q e_{31} +1%
R1:fs [Hz]	50323,1	0	0
R2:fs [Hz]	129794	0	0
TE1:fs [Hz]	984830	0,001015404	0
R1:BWs [Hz]	490	0	0
R2:BWs [Hz]	1321,5	0	0
TE1:BWs [Hz]	6230	0,160513644	0
R1:G [S]	0,056751	0,741367557	-2,61052E-06
R2:G [S]	0,017523	0,734362979	-1,06859E-05
TE1:G [S]	0,471229	-0,407821601	-0,002683608
R1:fp [Hz]	58885,5	0,087627684	0
R2:fp [Hz]	133078	0,017658817	0
TE1:fp [Hz]	1084260	-0,001844576	0
R1:BWp [Hz]	348,7	-0,114711787	0,17206768
R2:BWp [Hz]	1248,5	0	0,040048058
TE1:BWp [Hz]	5880	0,170068027	0
R1:R [S]	25881,94	0,490997141	-0,176826767
R2:R [S]	1454,788	0,694222303	-0,02239007
TE1:R [S]	996,3294	-0,282092094	0,002768475

(b)

Figure D.3

Tabell 5.27: *Relativ variasjon i serie- og parallellresonansfrekvensene ved de to første radielle modene den første tykkelsesmoden, og verdiene av G og R henholdsvis ved disse frekvensene Når real og Q–verdien til e_{33} økes 1%.*

		Rel diff [%]	
	Originalverdi	e_{33}+1%	Q - (e_{33})+1%
R1:fs [Hz]	50323,1	0	0
R2:fs [Hz]	129794	0	0
TE1:fs [Hz]	984830	0,031477514	0
R1:BWs [Hz]	490	0	0
R2:BWs [Hz]	1321,5	0	0
TE1:BWs [Hz]	6230	0,160513644	0
R1:G [S]	0,056751	1,263750534	-2,86772E-05
R2:G [S]	0,017523	1,269296988	-0,000387671
TE1:G [S]	0,471229	2,000636806	-0,04594767
R1:fp [Hz]	58885,5	0,098326413	0
R2:fp [Hz]	133078	0,019913134	0
TE1:fp [Hz]	1084260	0,149410658	0
R1:BWp [Hz]	348,7	-0,08603384	0,114711787
R2:BWp [Hz]	1248,5	0	0,040048058
TE1:BWp [Hz]	5880	1,700680272	0,340136054
R1:R [S]	25881,94	0,081597109	-0,153396763
R2:R [S]	1454,788	0,346216501	-0,020001935
TE1:R [S]	996,3294	2,500588804	-0,260302407

(a)

Tabell 5.29: *Relative variasjonen serie- og parallellresonansfrekvensene ved de to første radielle modene og ved den første tykkelsesmoden og verdiene av henholdsvis G og R ved disse frekvensene når real og Q–verdien til e_{15} økes 1%.*

		Rel diff [%]	
	Originalverdi	Real e_{15}+1%	Q e_{15}+1%
R1:fs [Hz]	50323,1	0	0
R2:fs [Hz]	129794	0	0
TE1:fs [Hz]	984830	0,007107826	0
R1:BWs [Hz]	490	0	0
R2:BWs [Hz]	1321,5	0	0
TE1:BWs [Hz]	6230	0,321027287	0
R1:G [S]	0,056751	-2,89328E-09	2,60225E-10
R2:G [S]	0,017523	-2,92188E-06	2,24344E-07
TE1:G [S]	0,471229	-1,30195935	-0,01110966
R1:fp [Hz]	58885,5	0	0
R2:fp [Hz]	133078	0	0
TE1:fp [Hz]	1084260	0,007378304	0
R1:BWp [Hz]	348,7	0	0
R2:BWp [Hz]	1248,5	0	0
TE1:BWp [Hz]	5880	0,510204082	0
R1:R [S]	25881,94	-7,11587E-10	9,51651E-10
R2:R [S]	1454,788	-3,21536E-06	2,99452E-07
TE1:R [S]	996,3294	-1,611980371	-0,012060849

(b)

Figure D.4

Tabell 5.31: *Relative variasjonen serie- og parallellresonansfrekvensene ved de to første radielle modene og ved den første tykkelsesmoden, og verdiene av henholdsvis G og R ved disse frekvensene når real og Q–verdien til ε^S_{11} økes 1%.*

		Rel diff [%]	
	Originalverdi	Real ε^S_{11}+1%	Q ε^S_{11} +1%
R1:fs [Hz]	50323,1	0	0
R2:fs [Hz]	129794	0	0
TE1:fs [Hz]	984830	-0,004061615	0
R1:BWs [Hz]	490	0	0
R2:BWs [Hz]	1321,5	0	0
TE1:BWs [Hz]	6230	0	0
R1:G [S]	0,056751	-6,93097E-09	2,19111E-09
R2:G [S]	0,017523	-2,23081E-06	7,12125E-07
TE1:G [S]	0,471229	0,573058664	0,018018927
R1:fp [Hz]	58885,5	0	0
R2:fp [Hz]	133078	0	0
TE1:fp [Hz]	1084260	-0,000922288	0
R1:BWp [Hz]	348,7	0	0
R2:BWp [Hz]	1248,5	0	0
TE1:BWp [Hz]	5880	-0,510204082	0
R1:R [S]	25881,94	-2,71909E-08	9,01132E-09
R2:R [S]	1454,788	-2,37077E-06	8,82628E-07
TE1:R [S]	996,3294	0,792561649	0,007852644

(a)

Tabell 5.33: *Relative variasjoner i serie- og parallellresonansfrekvensene ved de to første radielle modene og ved den første tykkelsesmoden, og verdiene av henholdsvis G og R ved disse frekvensene når real og Q–verdien til ε^S_{33} økes 1%.*

		Rel diff [%]	
	Originalverdi	ε^S_{33}+1%	Q (ε^S_{33})+1%
R1:fs [Hz]	50323,1	0	0
R2:fs [Hz]	129794	0	0
TE1:fs [Hz]	984830	-0,018277266	0
R1:BWs [Hz]	490	0	0
R2:BWs [Hz]	1321,5	0	0
TE1:BWs [Hz]	6230	0	0
R1:G [S]	0,056751	0,000109707	-0,000110664
R2:G [S]	0,017523	0,000850618	-0,000908272
TE1:G [S]	0,471229	0,248820806	0,032876716
R1:fp [Hz]	58885,5	-0,092722317	0
R2:fp [Hz]	133078	-0,018410256	0
TE1:fp [Hz]	1084260	-0,075627617	0
R1:BWp [Hz]	348,7	0,08603384	-0,229423573
R2:BWp [Hz]	1248,5	0,040048058	0
TE1:BWp [Hz]	5880	0	-0,340136054
R1:R [S]	25881,94	-1,27889133	0,191623339
R2:R [S]	1454,788	-1,505721977	0,023479432
TE1:R [S]	996,3294	-2,769806054	0,17552241

(b)

Figure D.5

Bibliography

[1] (2017). *Data Sheet: Low acoustic impedance PZT Type Pz37*. Meggit Ferroperm.

[2] Aanes, M. (2011). *A Guide to "inn-files" to FEMP 5*. University of Bergen, Department of Physics and Technology - Acoustic Group.

[3] Aanes, M. (2013). *Interaction of piezoelectric transducer excited ultrasonic pulsed beams with a fluid-embedded viscoelastic plate*. PhD thesis, University of Bergen.

[4] Atterås, F. (1998). Materialkonstantar for piezokeramiske elementer. Master's thesis, University of Bergen.

[5] C., A., A.M., G., L., P., B., J., F., C., and J., M. (1995a). Automatic determination of complex constants of piezoelectric lossy materials in the radial mode. *Journal of Physics*, 28:945–956.

[6] C., A., L., P., B., J., F., C., J., M., and A.M., G. (1995b). Automatic iterative evaluation of complex constants in piezoelectric ceramics. *Journal of Physics*, 27:148–155.

[7] Fardal, R. (2002). Endelig element analyse av elektriske egenskaper til piezoelektriske skiver. Master's thesis, University of Bergen.

[8] Ferroperm (2017). Pz37 low acoustic impedance pzt. www.meggittferroperm.com. Accessed: 2021-12-26.

[9] Ferroperm (2019). Meggit Ferroperm, data for modelling. www.meggittferroperm.com. Accessed: 2021-05-27.

[10] Holland, R. (1967). Representation of dielectric, elastic, and piezoelectric losses by complex coefficients. *IEEE Transactions on Sonics and Ultrasonics*, 14(1):18–20.

[11] IEEE (1988). 176-1987 - ieee standard on piezoelectricity webpage. https://ieeexplore.ieee.org. Standard withdrawn at January 1st 1988.

[12] Institute of Electrical and Electronics Engineers (1978). IEEE standard on piezoelectricity. *ANSI/IEEE Std 176-1978*, pages 1–58.

[13] Institute of Electrical and Electronics Engineers (1988). IEEE Standard on Piezoelectricity. *ANSI/IEEE Std 176-1987*.

[14] International Electrotechnical Commission (1976). Guide to Dynamic Measurements of Piezoelectric Ceramics with High Electromechanical Coupling. *IEC Standard*, 483.

[15] Kinsler, L., Kinsler, ., Kinsler, L., Frey, A., Coppens, A., and Sanders, J. (2000). *Fundamentals of Acoustics*. Wiley.

[16] Knappskog, V. (2007). Radiellmode svingninger i piezoelektriske ultralydtransdusere for luft. målinger og endelig element analyser. Master's thesis, University of Bergen.

[17] Kocbach, J. (2000). *Finite Element Modeling of Ultrasonic Piezoelectric Transducers*. PhD thesis, University of Bergen.

[18] Kocbach, J. and Sæther, M. (2002). Femp. Special curriculum at UiB based on Jan Kocbach's dr. scient. thesis, and taught by Mathias Sæther.

[19] Lohne, K. D. (2005). Undersøkelse og utnyttelse av svingemoder i ultralyd transduserkonstruksjoner. Master's thesis, University of Bergen.

[20] Lunde, P. and Vestrheim, M. (1991). Piezoelectric Transducer Modelling Part 1: Basic Equations For Poled Ferroelectric Ceramics. *CMI Tech Report*, CMI-91-A10010.

[21] Ringgaard, E. and Trætteberg, P. (2021). Personal Communication.

[22] Sherrit, S., Gauthier, N., Wiederick, H. D., and Mukherjee, B. K. (1991). Accurate evaluation of the real and imaginary material constants for a piezoelectric resonator in the radial mode. *Ferroelectrics*, 119(1):17–32.

[23] Sherrit, S., Wiederick, H., and Mukherjee, B. (1992). Non-iterative evaluation of the real and imaginary material constants of piezoelectric resonators. *Ferroelectrics*, 134:111–119.

[24] Vestrheim, M. (2013a). Akustiske målesystemer. Compendium for the course PHYS373: Acoustic Measurement Systems at UiB, written by Magne Vestrheim and taught by Mathias Sæther.

[25] Vestrheim, M. (2013b). Akustiske transdusere. Compendium for the course PHYS272: Acoustic Transducers at UiB, written by Magne Vestrheim and taught by Marianne Solberg.